Critical Deflagration Waves that Lead to the Onset of Detonation

by

Jenny Chao

Department of Mechanical Engineering
McGill University
Montréal, Québec, Canada

October 2006

A thesis submitted to the
Faculty of Graduate Studies and Research
in partial fulfillment of the requirements for the degree of
Doctor of Philosophy
in
Mechanical Engineering

© Jenny Chao 2006

Library and Archives Canada

Published Heritage Branch

395 Wellington Street
Ottawa ON K1A 0N4
Canada

Bibliothèque et Archives Canada

Direction du Patrimoine de l'édition

395, rue Wellington
Ottawa ON K1A 0N4
Canada

Your file Votre référence
ISBN: 978-0-494-27762-1
Our file Notre référence
ISBN: 978-0-494-27762-1

NOTICE:
The author has granted a non-exclusive license allowing Library and Archives Canada to reproduce, publish, archive, preserve, conserve, communicate to the public by telecommunication or on the Internet, loan, distribute and sell theses worldwide, for commercial or non-commercial purposes, in microform, paper, electronic and/or any other formats.

The author retains copyright ownership and moral rights in this thesis. Neither the thesis nor substantial extracts from it may be printed or otherwise reproduced without the author's permission.

AVIS:
L'auteur a accordé une licence non exclusive permettant à la Bibliothèque et Archives Canada de reproduire, publier, archiver, sauvegarder, conserver, transmettre au public par télécommunication ou par l'Internet, prêter, distribuer et vendre des thèses partout dans le monde, à des fins commerciales ou autres, sur support microforme, papier, électronique et/ou autres formats.

L'auteur conserve la propriété du droit d'auteur et des droits moraux qui protège cette thèse. Ni la thèse ni des extraits substantiels de celle-ci ne doivent être imprimés ou autrement reproduits sans son autorisation.

In compliance with the Canadian Privacy Act some supporting forms may have been removed from this thesis.

While these forms may be included in the document page count, their removal does not represent any loss of content from the thesis.

Conformément à la loi canadienne sur la protection de la vie privée, quelques formulaires secondaires ont été enlevés de cette thèse.

Bien que ces formulaires aient inclus dans la pagination, il n'y aura aucun contenu manquant.

Canada

Abstract

The conditions that are required for DDT are studied in the present thesis by focusing on the final phase of the onset of detonation. A series of experiments were carried out where high speed turbulent deflagrations were generated downstream of a perforated plate by reflecting a CJ detonation upstream from the plate. Four different detonation tubes were used to investigate scaling effects. Four different fuels (acetylene, hydrogen, propane, and ethylene) were used with either pure oxygen or air as an oxidizer to investigate the effect of mixture sensitivity on the onset of detonation. In some cases, fuel-oxygen mixtures were diluted with either nitrogen or argon. Perforated plates with various hole diameters and hole spacings were used in order to control the turbulence parameters in the reacting downstream flow. A theoretical study was also carried out to determine the various flow fields as well as the ignition processes via turbulent mixing.

It is found that a high speed turbulent deflagration traveling at about the CJ deflagration speed of the mixture (around 800 to 1200 m/s, depending on the given mixture) is required for the onset of detonation in a smooth tube. This critical velocity is found to be rather insensitive to boundary conditions, which supports the conclusion that critical deflagrations are driven by the expansion of the combustion products (similar to a CJ detonation) and are dependent on the energetics of the mixture rather than on transport rates. The ignition mechanism in a critical deflagration differs from that of a CJ detonation and is effected by the turbulent mixing

of combustion products with the unburned mixture. Therefore, intense turbulence is required in the reaction zone. Since the initial plate generated turbulence decays, the sustained propagation of a critical deflagration wave in a smooth tube relies on "flame generated turbulence" where the high temperature sensitivity of the mixture can mantain the turbulence in the reaction zone. It is also found that the critical deflagration is comprised of a leading shock wave followed closely by an extended turbulent reaction zone rather than the conventional shock wave followed by a distinct thin flame.

Once a critical deflagration wave is established, the onset of detonation requires the generation of transverse waves that couple to the reactions and are sustained by the chemical energy release as in a cellular detonation. The onset of detonation can be effected by the amplification (via the Rayleigh criterion) of repeatedly reflected transverse waves resonating with the reaction zone in a confined tube. It can also occur via the formation of a local explosion centre where an overdriven detonation bubble and the accompanying retonation wave is formed in the turbulent reaction zone.

Résumé

Les conditions nécessaires à la transition de déflagrations en détonations (en anglais Detonation to Deflagration Transition ou DDT) sont étudiées dans la présente thèse. L'emphase est placée sur la phase finale de la génération de l'onde de détonation. Une série d'expériences ont été réalisées dans lesquelles des déflagrations turbulentes à haute vitesse ont été générées en aval d'une plaque perforée par la réflection d'une détonation de type CJ en amont de la plaque. Quatre différents tubes ont été utilisés dans le but d'étudier les effets de la dimension globale du phénomène. Quatre différents gaz (acétylène, hydrogène, propane et éthylène) ont été utilisés avec de l'oxygène ou de l'air comme oxidant, ce qui a permis d'étudier les effets de la sensibilité du mélange sur la génération de l'onde de détonation. Dans certains cas, des mélanges de comburant-oxygène ont été dilués avec de l'argon ou de l'azote. Des plaques perforées avec des trous de grosseur et d'espacement variés ont été utilisées, permettant le contrôle des paramètres de turbulence dans l'écoulement réactif en aval de la plaque. Une étude théorique a aussi été menée pour déterminer les differents écoulements résultants de la réflection d'une détonation sur une plaque perforée. De plus, les différents processus d'ignition qui peuvent survenir par brassage turbulent ont également été étudiés théoriquement.

Les résultats montrent que la présence d'une onde rapide de déflagration turbulente se déplaçant environ à la vitesse de déflagration CJ (environ 800 à 1200 m/s, selon le mélange utilisé) est nécessaire à la génération d'une onde de détonation dans

un tube lisse. De plus, cette vitesse de propagation critique est indépendante des conditions limites, ce qui implique que les déflagrations critiques sont supportées énergétiquement par l'expansion des produits de combustion, similairement aux détonations de type CJ. Le mécanisme d'ignition diffère de celui des détonations CJ, et est affecté par le brassage turbulent, initialement généré par la plaque perforée et ensuite, alors que la perturbation de la plaque perd en importance, par la turbulence inhérente à la flamme. Il apparaît aussi que la déflagration critique est composée d'une onde de choc suivi de près d'une zone de réaction turbulente étendue, plutôt que l'image classique d'une déflagration où l'onde de choc et la zone de réaction forment deux fronts minces et distincts.

Lorsqu'une déflagration critique se propage, la génération d'une détonation nécessite la création d'ondes de choc transverses qui sont couplées aux réactions chimiques et sont soutenues par l'émission d'énergie, comme dans une détonation cellulaire. La génération de la détonation peut survenir via l'amplification (par le critère de Rayleigh) d'ondes de choc transverses réfléchies de maintes fois dans un tube rigide. Cette génération d'ondes de détonation peut aussi survenir via la formation d'une bulle de détonation à partir d'un centre d'explosion local, comme ce fut observé dans les études de Oppenheim.

Acknowledgements

I would like to first thank my thesis supervisor, Prof. John H.S. Lee, who had the patience to guide me through this journey. He has been a great mentor from whom I have learned a lot–not just about science but also about problem solving, character development, and marathon training (especially of the mental variety). I am grateful for the many opportunities that being his graduate student has given to me.

I would also like thank everyone who has been a part of the SWPG for the last decade as they have each made my experience in this research group extremely rewarding. Dr. Nicolas Ponchaut and Charles Kiyanda were very helpful for proof reading and translating the abstract. I am particularly indebted to Dr. Hoi Dick Ng for helping me so much along the way. I would also like to thank Dr. K. Ramamurthi, Matthew Walker, Graham Noble, Teruhito Otsuka, Yujian Zhu and David DeKonninck for their assistance in the lab.

The assistance from the technicians in the Measurement Lab and in the Machine Tool Lab is greatly appreciated. Gary Savard & John Boisvert in the Mechanical Lab and Steve Kecani & Eddie del Campo in the Physics Machine Shop were very helpful with the fabrication of different aspects of the experimental apparatus.

I would like to thank my parents for their love and support. As well, I would like to thank John, my husband-to-be, for being my best friend and my teammate.

Contents

List of Figures

List of Figures

List of Figures

List of Tables

Glossary

A	Exit area (cross-sectional area of the tube)
A^*	Open throat area (total area of the holes)
A_k	Pre-exponential constant
c	speed of sound
c_p	Specific heat at constant pressure
d	Hole diameter
D	Tube diameter; Mass diffusivity
D_H	Hydraulic diameter
e	Specific internal energy
E_a	Activation energy
F	Force
f	Friction factor
h	Enthalpy of the mixture
k	Pressure drop coefficient
K	Heat conductivity
D_o, K_o	Transport coefficients
l	Hole spacing
L	Characteristic length
Le	Lewis number
M	Mach number

p	Pressure
Q, q	Chemical energy release
R	Universal gas constant
R_s	Specific gas constant
Re	Reynolds number
$\dot{R}_f$	Flame speed
T	Temperature
T_f	Adiabatic flame temperature
t	Time
u	Particle velocity
V	Wave speed
x	Distance along x-coordinate direction
Y	Species mass fraction
z	Mixing fraction

Acronyms

CJ	Chapman-Jouguet
DDT	Deflagration to Detonation Transition
HMI	Homogeneous Mixing Ignition
LOCA	Loss of Coolant Accident
RUD	Run-up Distance
SWACER	Shock Wave Amplification by Coherent Energy Release
ZND	Zel'dovich - von Neumann - Döring

Greek symbols

α	Diffusivity
β	Nitrogen to oxygen ratio
ϵ	Porosity of porous media
ϕ	Equivalence ratio
γ	Ratio of specific heats
Γ	Turbulence factor
λ	Detonation cell size; reaction progress variable
$\dot{\omega}$	Reaction rate
ρ	Density

Subscripts

CJ	Chapman-Jouguet detonation
D	Detonation
f	Flame
o	Initial condition, unburnt mixture properties
p	Product
r	Reactant
R	Reflected
T	Transmitted

Chapter 1

Introduction

1.1 Overview

When a combustible mixture is ignited, either a deflagration wave or a detonation wave will begin to propagate away from the ignition source depending on how much and on how quickly the ignition energy is released into the mixture. A detonation is relatively difficult to initiate and generally requires that a large amount of energy is deposited "instantaneously" in a small localized volume. For example, 4.2 MJ–which is equivalent to about a gram of solid explosive (e.g., TNT)–is required to directly initiate a detonation in stoichiometric hydrogen-air mixture at standard conditions. On the other hand, a deflagration wave (or a propagating flame) can be easily ignited by a weak spark that releases only fractions of a millijoule of energy. In general, propagating flames are unstable. With appropriate boundary conditions, the flame can accelerate rapidly from its initial velocity of a few metres per second to hundreds of metres per second and undergo an abrupt transition to a detonation (that typically propagate at a velocity of the order of 1800 m/s for the common hydrocarbon-air mixtures).

Deflagration to detonation transition (or DDT) is an important but as yet unresolved problem in detonation theory. It is still not possible, even semi-empirically, to determine a priori whether or not DDT can occur in an explosive mixture for given initial and boundary conditions. Initial conditions refer to the composition of the mixture, the initial thermodynamic properties of the mixture, and the fluid mechanic properties of the unburned mixture ahead of the flame. Boundary conditions refer to whether or not there is a confining vessel, the geometry of the confining vessel (if any), and the details of the tube wall roughness or of the obstacles configuration placed in the path of the propagating flame. A comprehensive theory for DDT will be extremely complex since almost all of the transport, thermodynamic, fluid mechanic and gasdynamic processes of combustion are involved (see Dorofeev 2002 for a concise discussion).

DDT is a problem of great practical interest since it is the most probable way in which a detonation can be formed in industrial accident scenarios. For example, a "loss of coolant accident" (LOCA) in a nuclear reactor can result in the generation of hydrogen from the interaction of molten fuel rods with water, forming an explosive hydrogen-air mixture inside the containment building. As well, the accidental release of a combustible gas or vapour into the atmosphere in chemical plants, on offshore oil platforms or during the transport of liquified natural gas in tankers or in pipelines can generate a large combustible vapour cloud. A flame can easily be ignited by a weak ignition source, and the subsequent rapid acceleration can lead to the eventual transition to detonation. Considering the potential for the loss of life, severe injuries to personnel, and the tremendous structural damages associated with detonations, there has been an intensive and continued interest in developing the ability to predict DDT.

The current trend in risk assessment is to use various commercial computer codes (e.g., FLACS, REAGAS, COBRA, etc.) that have been developed to asses industrial

hazards (Popat *et al.* 1996, Dharmavaram *et al.* 2005). These codes are used to qualitatively estimate the overpressures from flame acceleration as well as the potential for DDT. Empirical constants are chosen to fit existing experimental data and, as such, these codes have very little predictive capabilities outside the range of conditions in which the empirical parameters are fitted. Experimentally, industrial safety research programs usually focus on large-scale experiments in complicated geometries in an effort to simulate prototypical accident scenarios in industrial settings. In large-scale experiments, diagnostics are somewhat limited, and comprehensive information on the combustion processes is difficult to obtain and to interpret.

Well-designed laboratory-scale experiments that are more fundamental in nature have also been conducted over the last several decades, testing a wide range of initial and boundary conditions. In general, long circular tubes with and without obstacles are used. However, a general criterion for successful DDT (even in a simple geometry such as a circular tube) has yet to be formulated. Numerical simulations are also difficult since the codes have to describe non-steady, compressible, turbulent and chemically reactive flows. Progress in the understanding of DDT has been made from past experimental and numerical work (see Nettleton 2002 for a review); however, the knowledge that has been accumulated to date on DDT is not well-synthesized since there is a multitude of combustion and gasdynamic processes that are involved in the DDT phenomenon.

DDT can essentially be considered to consist of two separate phases: an initial flame acceleration phase and the final phase of the "onset of detonation." Assuming that ignition is effected by a weak spark, the flame acceleration phase describes the growth of a small flame kernel that eventually reaches some maximum critical supersonic velocity. The final onset of detonation is when this supersonic deflagration wave undergoes an abrupt transition to a detonation.

In previous studies, the "run-up distance" was generally used to characterize the

entire DDT process from the initial flame acceleration to the final onset of detonation. The turbulent flame acceleration phase of DDT involves almost all aspects of combustion phenomena and, thus, a single parameter such as the run-up distance cannot adequately characterize DDT.

A self-propagating flame is generally unstable and there are numerous instability mechanisms (e.g. thermo-diffusion instabilities, acoustic instabilities, Richtmyer-Meshkov-Markstein instabilities, Taylor instabilities, etc.) that can cause an increase in the flame area and, hence, an increase in the burning rate. The relative importance of each instability mechanism varies depending on the initial and boundary conditions. In addition to instabilities, there exist positive feedback loops between the displacement flow ahead of the propagating flame (due to the specific volume increase across the flame) and the burning rate. As well, the acoustic pressure waves that are generated can return to excite the flame, which also promotes flame acceleration. A thorough discussion of the different positive feedback flame acceleration mechanisms can be found in Lee & Moen (1980).

Flame acceleration essentially refers to the increase in the rate of energy release (or the burning rate). The burning rate of a flame depends on its surface area as well as the local burning velocity. Therefore, any mechanism that can increase the surface area of a flame can be defined as a flame acceleration mechanism. Since the various flame acceleration mechanisms are sensitive to initial and boundary conditions, it does not appear that a simple universal criterion (such as the run-up distance) can be found to describe the flame acceleration phase of DDT.

On the other hand, it appears to be possible to formulate a theory that describes the final phase of DDT since only the mechanism responsible for the onset of detonation is involved. In the final onset of detonation, the deflagration wave is usually observed to travel at some quasi-steady critical velocity for some duration prior to an abrupt formation of the detonation. This critical velocity corresponds to about

half the theoretical Chapman-Jouguet detonation velocity (Lee *et al.* 1969). In the study of Eder & Brehm (2001), the critical deflagration velocity was found to correspond to the sound speed of the combustion products, which is also of the order of half the theoretical CJ detonation velocity ($\frac{1}{2}V_{CJ}$). In a recent analysis by Vasil'ev (2006), the critical shock strength of a deflagration for transition to detonation was estimated to be around $\frac{1}{2}M_{CJ}$. It turns out that the $\frac{1}{2}V_{CJ}$ value also corresponds closely to the CJ deflagration velocity of the given mixture, which suggests that the critical deflagration velocity just prior to the onset of detonation is also the maximum possible deflagration velocity for the given mixture.

It is interesting to note that when a CJ detonation fails due to the dampening of its transverse waves, the resulting deflagration velocity is also of the order of $\frac{1}{2}V_{CJ}$ (Dupré *et al.* 1988, Teodorczyk *et al.* 1995, Radulescu & Lee 2002). A self-luminous streak photograph from Radulescu & Lee is shown in Fig.1.1. The acoustic damping section is indicated by the horizontal arrow. The established CJ detonation enters the damping section and fails, and a critical deflagration wave continues to propagate at about $\frac{1}{2}V_{CJ}$ for the remainder of the field of view. Under appropriate conditions, the critical deflagration wave will transit back to a detonation downstream of the damping section.

Other detonation phenomena also seem to demonstrate that a deflagration wave propagating at $\frac{1}{2}V_{CJ}$ is common prior to the onset of detonation. For example, in near-limit "galloping" detonations in "unstable" mixtures, the low velocity phase of the galloping cycle is found to propagate at about $\frac{1}{2}V_{CJ}$ (see Fig. 1.2). The quasi-steady low velocity phase of galloping detonations has been observed to persist for over a hundred tube diameters (in small diameter tubes) before a rapid re-acceleration to detonation, thus starting another galloping cycle (St. Cloud *et al.* 1972, Edwards & Morgan 1977, Lee *et al.* 1995). In direct blast initiation, it is found both experimentally and numerically that, in the critical energy regime,

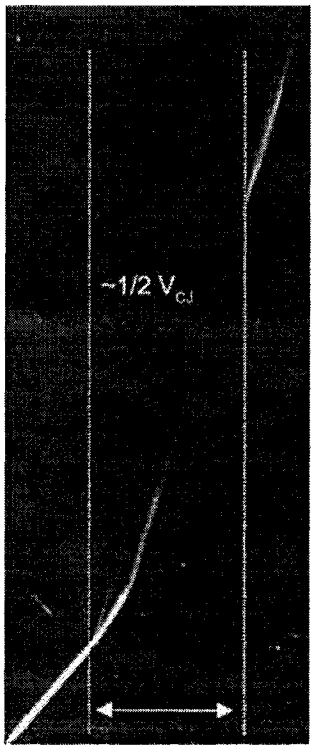

Figure 1.1. Self-luminous streak photograph of a CJ detonation entering a damping section in stoichiometric acetylene-oxygen (P_o = 2.2 kPa). Arrow indicates the length of the damping section (l = 454 mm) (Radulescu & Lee 2002).

the initially overdriven blast wave first decays to a $\frac{1}{2}V_{CJ}$ wave and propagates for a certain quasi-steady period before amplifying to a detonation (Lee & Higgins 1999).

Therefore, it appears that the $\frac{1}{2}V_{CJ}$ deflagration velocity is a common feature as the prelude to the onset of detonation. When the maximum possible deflagration velocity is reached, the onset of detonation generally occurs. Deflagration waves that travel in excess of the $\frac{1}{2}V_{CJ}$ value are usually not observed during the final pre-detonation phase of DDT; those that travel below the critical velocity are either observed to accelerate up to $\frac{1}{2}V_{CJ}$ or eventually decay. It should be noted that it may be possible for deflagration waves at sub-critical velocities to transit to a

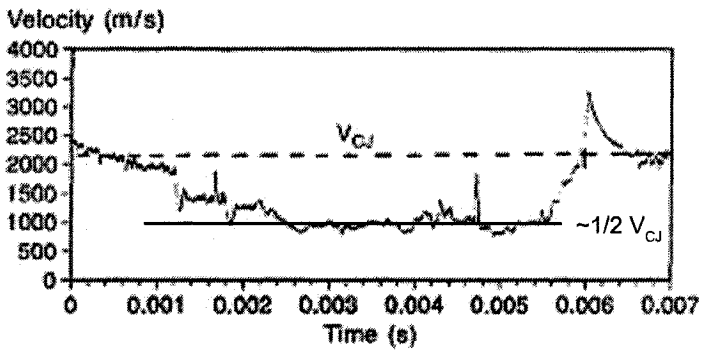

Figure 1.2. Velocity history of a galloping detonation in stoichiometric propane-oxygen at $P_o = 8$ torr (Lee *et al.* 1995).

detonation but would require a major perturbation to the reaction zone (such as a large obstacle). At the critical velocity, only minor perturbations are sufficient to bring about the onset of detonation.

It is not surprising that the critical velocity corresponds to the CJ deflagration velocity since the tangency solution of the lower branch of the Hugoniot (i.e., the CJ deflagration solution) gives the maximum theoretical velocity in the deflagration regime. In general, the velocity of a deflagration is controlled by transport rates (which depend on boundary conditions) since the precursor shock wave associated with the deflagration is too weak to cause auto-ignition. However, the CJ deflagration velocity (like the CJ detonation velocity) is only a function of the chemical energy release and does not depend on boundary conditions due to the sonic condition behind the CJ deflagration. (The sonic condition presents the closure criterion that permits the CJ deflagration speed to be found from the Rankine-Hugoniot equations across the deflagration.)

Experimentally, critical deflagration velocities of the final pre-detonation phase are found to fall within a narrow range about the $\frac{1}{2}V_{CJ}$ value even though back boundary conditions and tube geometries varied significantly depending on the ex-

periment. The observed independence of the pre-detonation velocity on boundary conditions may be a consequence of a sonic condition behind the wave. It also suggests that the critical deflagration is energetically driven (rather than being transport rate dependent) and is, essentially, a CJ deflagration. Therefore, it seems reasonable to assume that in order for DDT to occur, a flame must first accelerate to the maximum possible deflagration velocity (i.e., the CJ deflagration velocity). The subsequent onset of detonation is then represented by a sudden jump from the lower tangency point of the Hugoniot to the upper tangency point of the Hugoniot. (As pointed out previously, DDT can also occur for sub-critical deflagrations but will require a major perturbation to cause the onset of detonation.)

The experiments of Oppenheim and his co-workers over the years have shown that once the CJ deflagration velocity is reached, the genesis of the detonation usually occurs at a local hot spot in the turbulent flame brush of the deflagration wave (an "explosion within an explosion" as coined by Urtiew & Oppenheim 1965). The blast wave generated by this localized explosion then propagates into the mixture preconditioned by the precursor shock wave and accelerates rapidly to form a "detonation bubble" within the reaction zone. The detonation bubble eventually expands and catches up with the precursor shock, forming a fully established detonation wave.

It is important to note that the precursor shock wave of the pre-detonation deflagration is of the order of $M \approx 3$ and is relatively weak. Although it may contribute to the adiabatic heating of the unburned mixture ahead of the turbulent flame brush, auto-ignition of the mixture does not occur via the precursor shock as demonstrated by Meyer *et al.* (1970). This implies that a mechanism other than adiabatic shock heating is responsible for ignition in the mixture. In their study, Meyer *et al.* postulated that auto-ignition could be due to heat or mass transfer in the turbulent zone behind the precursor shock wave.

The turbulent mixing of combustion products with a unburned mixture can re-

sult in auto-ignition without the presence of strong shock waves. This was first demonstrated by Knystautas *et al.* (1979). However, even if auto-ignition at a local hot spot occurs via turbulent mixing, the maximum pressure rise is still only of the order of the constant volume explosion pressure. The resulting shock wave is about $M \approx 2.5$, which is far below the $M \approx 5 - 6$ value for a detonation. Therefore, the subsequent formation of a detonation from the explosion centre still requires an amplification mechanism since the blast wave from a constant volume explosion is insufficient to effect auto-ignition. Lee *et al.* (1978) proposed that if an appropriate induction time gradient is present, resonant coupling between the chemical energy release and the blast wave can be achieved via the SWACER (shock wave amplification by coherent energy release) mechanism. Hence, the growth of the detonation bubble from the explosion centre that leads to the eventual onset of detonation may be due to SWACER as this appears to be the most plausible mechanism for the onset of detonation from auto-ignition via turbulent mixing.

Since the final pre-detonation phase appears to be crucial in the understanding of the mechanism for DDT, the present thesis is devoted only to the study of this final phase of DDT. The initial flame acceleration phase deals with a wide spectrum of turbulent combustion and flame instability mechanisms and is, thus, too broad in scope to be considered in this investigation.

1.2 General Considerations

Since the classical experiments of Berthelot & Vieille (1882) and of Mallard & Le Chatelier (1883), there has been a plethora of studies on DDT. Relatively little focus, however, has been placed on the final phase of DDT. In most of the previous work, the final onset of detonation (once the maximum deflagration velocity has been obtained) is lumped together with the flame acceleration phase. As a result,

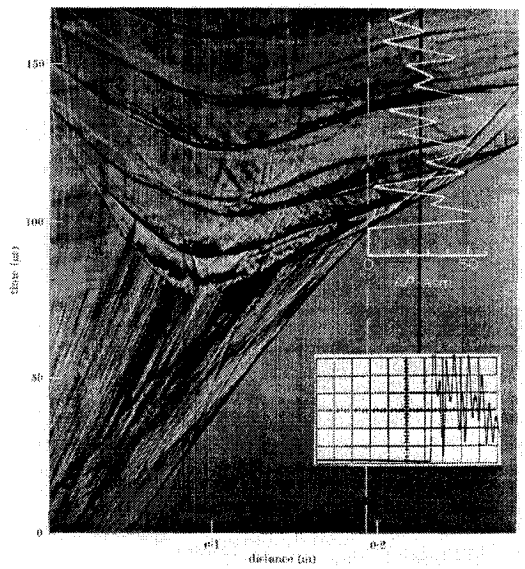

Figure 1.3. Streak schlieren photograph of the final onset of detonation in stoichiometric hydrogen-oxygen at $P_o = 1$ atm (Urtiew & Oppenheim 1966).

it is difficult to establish what are the critical conditions for the successful onset of detonation. Nevertheless, there are a number of relevant studies that have been done in the past, and it is worthwhile to analyze the relevant work in order to summarize the current understanding of the final phase of DDT.

Perhaps the most didactic contribution to the understanding of the onset of detonation has been made by A.K. Oppenheim and his co-workers through their seminal studies in the 1960's and the 1970's. To illustrate the general phenomenon of the final phase of DDT, a classic streak schlieren photograph taken by Urtiew & Oppenheim (1966) of the onset of detonation is shown in Fig. 1.3. The critical deflagration wave is shown to propagate at a velocity of about 1480 m/s (or of the order of $\frac{1}{2}V_{CJ}$) prior to the onset of detonation, which is characterized by the standard local explosion that occurs within the deflagration wave.

From this photograph, several intriguing questions arise concerning the final phase

of DDT. What is the critical deflagration wave? Is it truly a CJ deflagration, and if so, by what mechanism is the final onset of detonation effected?

In an attempt to address these questions, a systematic study of the propagation of high speed turbulent flames at the onset of detonation was conducted in obstacle filled tubes by Lee *et al.* (1984a) and by Peraldi *et al.* (1986). It was previously demonstrated in the pioneering studies of Lafitte (1923), Chapman & Wheeler (1926), and Schelkhin (1940) that the presence of obstacles in the path of a deflagration can promote very rapid flame acceleration and can greatly reduce the length and the time to DDT compared to a smooth tube. This was exploited by Lee *et al.* and by Peraldi *et al.* to bypass the slow initial flame acceleration phase of DDT where numerous flame acceleration mechanisms are involved, complicating the onset phenomenon of interest. Extensive studies were thus carried out on the transition to detonation in obstacle filled tubes of different diameters using various obstacle configurations, combustible mixtures, and mixture sensitivities.

In general, the DDT process in rough tubes was observed to begin with a rapid initial acceleration until the flame reached some final steady state velocity. Typical flame velocities that were obtained by Lee *et al.* are shown in Fig. 1.4 for a range of acetylene-air mixtures. It can be seen from the figure that there are three distinct regimes of steady state flame velocities in the rough tubes, depending on the sensitivity of the mixture.

For a mixture composition of 3% acetylene-air, a steady state flame velocity of 100 m/s is observed. However, if the mixture is made slightly more sensitive (3.5% acetylene-air), a sudden jump in the steady state flame velocity to 600 m/s occurs. In the figure, steady state velocities in this regime can be seen to increase gradually to 800 m/s with increasing mixture sensitivity. This regime is called the "choking" regime, and the observed steady state velocities (in the fixed laboratory frame) correspond very closely to the sound speed of the combustion products (and

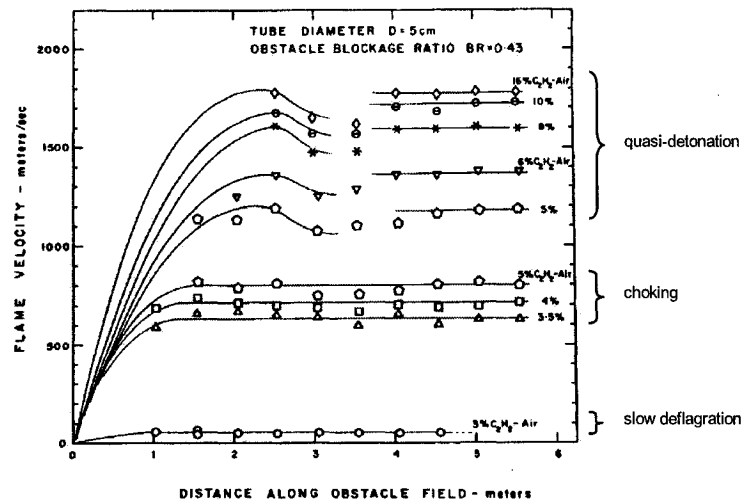

Figure 1.4. Flame velocity as a function of distance for various acetylene-air mixtures ($P_o = 1$ atm). Figure taken from Lee *et al.* (1984).

to the CJ deflagration velocity of the given mixture).

A second critical composition limit is reached at about 5% acetylene-air where another sudden jump in the final steady state velocity occurs. At this critical mixture composition, either a velocity of 800 m/s (in the choking regime) or a velocity of 1200 m/s is obtained. As the mixture sensitivity is increased even further, the steady state velocities increase gradually. In this final regime, called the "quasi-detonation" regime, the observed velocities generally range from about 0.6 V_{CJ} to the actual theoretical CJ detonation velocity for the mixture, depending on the boundary condition. The observed velocity deficit from the theoretical CJ value is attributed to severe momentum losses to the obstacles (Zel'dovich *et al.* 1988).

The terminal flame velocities are shown again in Fig. 1.5 as a function of mixture composition. Results that were obtained by Lee *et al.* in a larger diameter tube (15 cm compared to 5 cm) are also shown for comparison. It can be seen that the sudden jump from the choking regime to the quasi-detonation regime occurs at a

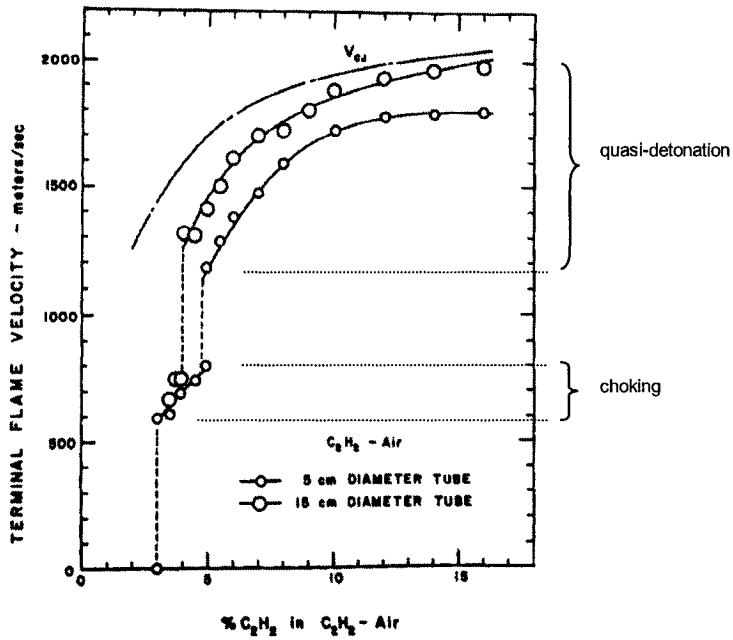

Figure 1.5. Terminal flame velocities as a function of mixture sensitivity (P_o = 1 atm). Figure taken from Lee *et al.* (1984).

less sensitive mixture composition in the larger diameter tube. However, the change in the boundary condition has very little effect on the terminal flame velocity in the choking regime. In the quasi-detonation regime where momentum losses to the obstacles and the tube wall are significant, there is a noticeable difference in the final steady state quasi-detonation velocity when the boundary condition is varied.

In the choking regime, the chemical length scale of the mixture (denoted by λ, the characteristic detonation cell size) is large compared to the characteristic dimension of the obstacles, d. As a result, the mechanisms that permit the propagation of a detonation cannot be established in the rough tube. However, the obstacles do provide enough turbulence (through the generation of vorticity at the surfaces of the obstacles and also by the reflection of transverse shock waves from the obstacles) that promotes rapid mixing and burning and, therefore, provides the mechanism for

the propagation of a deflagration wave at the maximum possible deflagration velocity of $\frac{1}{2}V_{CJ}$ (or the CJ deflagration velocity). Only when the sensitivity of the mixture is further increased such that $d \approx \lambda$ can the mechanism for detonation propagation take effect in a rough tube. Therefore, the sudden jump to the choking regime (where the maximum possible deflagration velocity is obtained) represents the transition to a detonation (in a smooth tube) but is prevented by the presence of the obstacles. If the obstacles were removed, the onset of detonation from the critical deflagration wave should be possible.

This was demonstrated by Lee *et al.* (1984b) and by Knystautas *et al.* (1986) where the choking regime was first established in an obstacle section and then the critical deflagration wave was transmitted into a smooth tube section. A typical velocity history profile from Knystautas *et al.* is shown in Fig. 1.6 for a critical mixture composition of 4% acetylene-air. Within the obstacle field, a steady state velocity of 700 m/s is established. In the smooth tube, it was found that the critical deflagration velocity either decayed to a few hundred metres per second or accelerated to transit to a detonation. It can be seen from the figure that the run-up from the critical deflagration wave exiting the obstacle section to the final onset of detonation is rather long (about 6 m or 120 tube diameters). It seems that this is a period during which the proper conditions for the onset of detonation are being generated.

A summary of the results obtained by Knystautas *et al.* in a 5 cm diameter tube are shown in Table 1.1. It can be seen that the critical limit was found to be $\lambda \approx D$ (where λ is the characteristic detonation cell size) for a range of combustible mixtures, indicating that the characteristic chemical length scale of the explosive mixture (λ) should correspond to the characteristic dimension of the tube (D) in order for DDT to be successful. In the study of Lee *et al.*, the critical limit was found to be πD, which also corresponds to the criterion for a single-headed spin detonation in a tube. The results of these two studies suggest that the proper conditions for the onset of

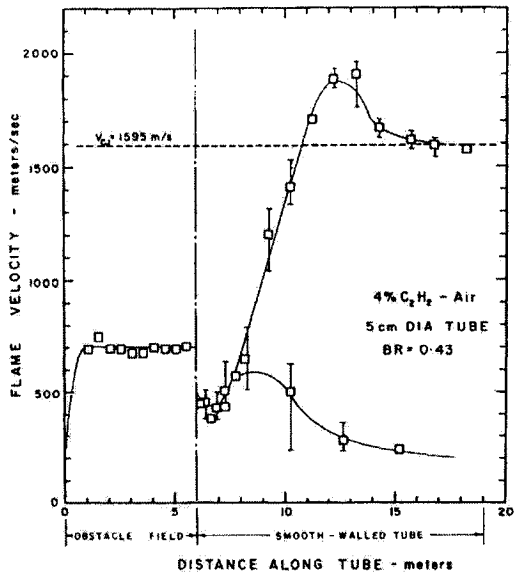

Figure 1.6. Flame velocity as a function of distance in an obstacle section followed by a smooth tube. Figure taken from Knystautas *et al.* (1986).

detonation can be achieved when the chemical energy release (characterized by λ) becomes coupled to the fundamental acoustic modes of the tube (represented by D and by πD). Therefore, it appears that the lifetime of the critical deflagration wave is a period in which the chemical energy release and the acoustic fluctuations are becoming re-coupled in order to trigger the eventual onset of detonation.

In the studies of Dupré *et al.*, of Teodorczyk *et al.*, and of Radulescu & Lee on the failure mechanism of CJ detonations, acoustic absorbing walls or porous tube bundles were used to dampen out the transverse waves that are inherent to the cellular structure of a CJ detonation. Once the transverse wave structure was destroyed, the CJ detonation failed and a deflagration travelling at about $\frac{1}{2}V_{CJ}$ emerged into a smooth tube section and continued to propagate at a relatively constant velocity.

It was conclusively demonstrated in these studies that the periodic transverse waves that sweep across the leading detonation front are absolutely necessary in the

Mixture	D (cm)	λ (mm)	λ/D
4% C_2H_2-air	5	58.3	1.18
5% C_2H_4-air	5	65.1	1.32
10% C_2H_4-air	5	39.1	0.80
4% C_3H_8-air	5	52.2	1.06
5% C_3H_8-air	5	59.0	1.19
20% H_2-air	5	55.4	1.12
51% H_2-air	5	52.5	1.06

Table 1.1. Critical Conditions for Transition in the Smooth Walled Section (Knystautas *et al.* 1986).

propagation of a detonation. In essence, self-sustained detonations propagate as a consequence of the resonant coupling that exists between the chemical energy release and the acoustic fluctuations (manifested by the existence of the transverse waves). When the resonant coupling is destroyed, the propagation of a detonation is no longer possible. Therefore, it seems reasonable to assume that since detonations can fail into a critical deflagration wave when their transverse waves are destroyed, then the transition to detonation from a critical deflagration wave requires the re-creation of transverse waves, thereby re-establishing the resonant coupling between the chemical energy release and the acoustic fluctuations.

1.3 Objective of Present Investigation

There is compelling evidence from previous studies indicating that in order for DDT to occur, the deflagration velocity must reach a critical value of $\frac{1}{2}V_{CJ}$. This is a common condition for all DDT processes in the final phase. Once a critical deflagration is established, it seems that in order to achieve the eventual onset of detonation, the resonant coupling between the chemical energy release and the transverse acoustic

fluctuations must be established. Presently, there exists only a general picture of critical deflagration waves and how they transit to detonations, and it is not clear what exactly the critical deflagration wave is. Therefore, the objective of the present research is to determine the structure and the propagation mechanism of critical deflagration waves. In doing so, an attempt can be made to elucidate the process through which the resonant coupling of the chemical reactions and the pressure fluctuations is achieved. Ultimately, this may clarify the critical conditions that are required for the successful onset of detonation.

In order to experimentally generate a critical deflagration wave, an established CJ detonation is reflected from a perforated plate. The structure of the incident detonation is completely destroyed upon its collision with the perforated plate. The detonation products flow through the holes of the perforated plate and ignite the unburned downstream mixture via turbulent mixing. The turbulence scales in the reaction zone can be controlled via the geometry of the perforated plate while the turbulence intensities are related to the velocity at which the detonation products are transmitted downstream (which corresponds to the sound speed of the combustion products since the flow through the holes of the perforated plate is choked). By varying the mixture sensitivity and turbulence characteristics, the conditions under which critical deflagrations are generated and propagate can be readily studied.

Chapter 2

Theoretical Considerations

To help understand the different phenomena that occur subsequent to the reflection of a CJ detonation from a perforated plate, simple idealized cases are considered theoretically in this chapter. A one-dimensional analysis of possible steady wave configurations is first performed in order to verify the flow fields that are observed experimentally. This is followed by a simple analysis of the ignition processes that can occur when combustion products are mixed with reactants at the interface.

2.1 Steady One-Dimensional Flow Fields

The wave processes following the reflection of a CJ detonation from a perforated plate are unsteady and multi-dimensional. High pressure detonation products flow through the holes of the perforated plate subsequent to the reflection of the CJ detonation, and each individual turbulent jet of combustion products that emerges downstream drives a blast wave. Transverse shock waves and Mach stems are generated as the blast waves interact with each other, and the near field immediately downstream of the perforated plate is a rather complex ensemble of interacting shock waves. The

blast waves do eventually coalesce at some distance downstream of the perforated plate to form a planar shock front. However, the periodic transverse wave structure can persist for a long duration as the transverse waves reflect from each other and the tube wall. A series of oblique shock waves are also generated in the overexpanded jets of combustion products since the holes of the perforated plate are essentially choked orifices (Dosanjh 1955, Franks 1957). Furthermore, considerable turbulent mixing occurs at the head of the jets, which can result in ignition and chemical energy release.

It can be seen that the downstream flow field is unsteady and multi-dimensional. Nevertheless, an idealized one-dimensional analysis of possible steady wave processes will be useful to provide a reference that can guide the interpretation of the experimental results. In a steady one-dimensional wave analysis, the conservation equations across each discontinuity are solved. Upstream and downstream flows are matched at the interface. The pressure drop across a given perforated plate is not known *a priori*, and a separate model has to be used to describe the flow across the perforated plate.

In the previous studies of Dosanjh and of Franks where shock waves were reflected from perforated plates in air, the perforated plates were modelled as two-dimensional isentropic converging-diverging nozzles that were choked at the throat. A similar model was used by Soloukhin (1974) in his study of ignition processes subsequent to the reflection of a shock wave from a perforated plate in a combustible mixture. In all of these cases where a two-dimensional isentropic area change model was used, the incident shock strength and the blockage of the plate were both relatively high, resulting in choked flow through the holes of the perforated plate. Knowing A/A^*, the ratio of the exit area (the cross-sectional area of the tube) to the open throat area (the total area of the holes), the properties of the flow upstream and downstream of the perforated plate were determined from isentropic flow relations. Since the flow

downstream of the 2D model is supersonic and overexpanded, a backwards facing shock had to be introduced immediately downstream of the perforated plate in order to raise the pressure and reduce the flow velocity such that the conditions across the interface were satisfied. Experimentally, the observation of a backward facing shock is a consequence of the local condition immediately downstream of the perforated plate as each individual hole is a choked orifice and each jet from the holes is overexpanded.

Although the previous theoretical model of Dosanjh, of Franks and of Soloukhin was compared to experimental results with some success, it is not clear that a two-dimensional isentropic area change model is entirely appropriate in the present case. The expansion of the flow downstream of choked orifice is governed by the back pressure and not by an area ratio. As well, stagnation pressure losses occur only across the backward facing shock wave when the isentropic nozzle model is used. In reality, there is also total pressure loss that occurs in the turbulent wakes behind the perforated plate. Thus, the previous model used to describe the flow across the perforated plate may not be adequate.

It should be noted that the global one-dimensional model that is used for the wave interactions is not valid immediately downstream of the perforated plate. Therefore, within a one-dimensional framework, distances sufficiently far from the perforated plate should be considered where a quasi-one-dimensional flow is regained. In this manner, the local three-dimensional flow near the perforated plate is not considered and any appropriate one-dimensional physical model can be used instead, provided that the conditions across the interface are satisfied. Ergun (1952) developed a friction factor, f, to describe steady flow through porous media:

$$f = a + b\frac{1-\epsilon}{Re}$$

where ϵ is the porosity of the media, a and b are empirial constants, and Re is the Reynolds number based on the particle diameter. Ergun estimated $a = 1.75$ and $b = 150$, although values of $a = 1.8$ to 4.0 (for a range of particle roughness)

and $b = 180$ that were based on a wide range of experimental data have also been reported (Macdonald 1979). Ergun's correlation has also been previously used to model the attenuation of a shock wave through porous media and perforated plate (Zloch 1976, Medvedev *et al.* 1990, Bakken *et al.* 2003). In the present study, the flow across the perforated plate is modelled in a similar manner by simply choosing an appropriate pressure drop coefficient (or friction factor) to describe the effect of the perforated plate on the downstream flow. The pressure drop coefficient is determined empirically.

2.1.1 Non-Reacting Downstream Flow Fields

If the downstream mixture is unreactive, the interface drives a transmitted shock wave downstream. The corresponding one-dimensional steady wave diagram is shown in Fig. 2.1. Upon the collision of the incident detonation with the perforated plate, a shock wave is reflected. The reflected shock wave is formed in order to slow the flow behind the detonation such that the velocity matches that of the flow through the perforated plate. The strength of the reflected shock wave depends on the pressure drop across the perforated plate, which is determined by the amount of flow blockage that is provided by the plate. The high pressure combustion products behind the reflected shock wave flow through the holes of the perforated plate and expand downstream. The interface that separates the detonation products from the downstream gas acts as a piston that drives a transmitted shock wave ahead of it.

Referring to the wave diagram in Fig. 2.1, the properties of the flow in region (1) can be determined by solving the one-dimensional steady conservation equations

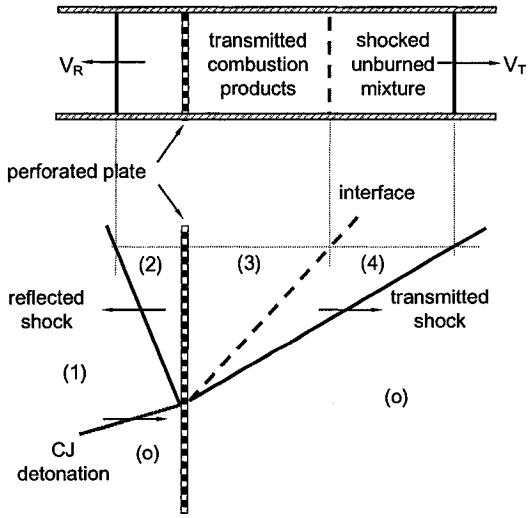

Figure 2.1. Steady 1D wave diagram subsequent to the reflection of a CJ detonation from a perforated plate; no chemical reactions occur downstream of the perforated plate.

across the CJ detonation:

$$\rho_o V_D = \rho_1 (V_D - u_1) \tag{2.1}$$

$$p_o + \rho_o V_D^2 = p_1 + \rho_1 (V_D - u_1)^2 \tag{2.2}$$

$$\frac{\gamma_o p_o}{(\gamma_o - 1)\rho_o} + \frac{{V_D}^2}{2} + Q = \frac{\gamma_1 p_1}{(\gamma_1 - 1)\rho_1} + \frac{(V_D - u_1)^2}{2} \tag{2.3}$$

The flow behind the incident detonation is assumed to be uniform. The Taylor wave behind the detonation is assumed to be of negligible gradient, i.e., the detonation is initiated far from the perforated plate. Also, the heat release, Q, and the ratios of specific heats, γ_1 and γ_o, are assumed to be constant. The value of γ_1 is not the same as γ_o in order to account for the difference in mixture composition between the reactants and the products. The values of the two different γ's can be calculated by fitting the Hugoniot curve to an exact equilibrium calculation (using an equilibrium code like STANJAN or CEA). This procedure is described by Lee & Guirao (1981).

Assuming that $\gamma_1 = \gamma_2$ (since the mixture composition does not change much

across the reflected shock wave), the conservation equations across the reflected shock,

$$\rho_1(V_R + u_1) = \rho_2(V_R + u_2) \tag{2.4}$$

$$p_1 + \rho_1(V_R + u_1)^2 = p_2 + \rho_2(V_R + u_2)^2 \tag{2.5}$$

$$\frac{\gamma_1 p_1}{(\gamma_1 - 1)\rho_1} + \frac{(V_R + u_1)^2}{2} = \frac{\gamma_2 p_2}{(\gamma_2 - 1)\rho_2} + \frac{(V_R + u_2)^2}{2} \tag{2.6}$$

can be manipulated to yield:

$$\frac{p_2}{p_1} = \frac{2\gamma_1 {M_R}^2 - (\gamma_1 - 1)}{\gamma_1 + 1} \tag{2.7}$$

$$\frac{T_2}{T_1} = \frac{(2 + (\gamma_1 - 1){M_R}^2)(2\gamma_1 {M_R}^2 - (\gamma_1 - 1)}{(\gamma_1 + 1)^2 {M_R}^2} \tag{2.8}$$

$$M_2 = \frac{2 + (\gamma_1 + 1)M_1 M_R - 2{M_R}^2}{\sqrt{(2 + (\gamma_1 - 1){M_R}^2)(2\gamma_1 {M_R}^2 - (\gamma_1 - 1))}} \tag{2.9}$$

From Eq. 2.9, it can be seen that the strength of the reflected shock, M_R, depends on γ_1, M_1, and M_2. The value of M_2 is controlled by the pressure drop across the perforated plate, and once it is known, the strength of the reflected shock–and subsequently, all of the flow properties in region (2)–can be calculated.

The conservation equations across the perforated plate can be written as:

$$\rho_2 u_2 = \rho_3 u_3 \tag{2.10}$$

$$p_2 + \rho_2 {u_2}^2 = p_3 + \rho_3 {u_3}^2 + \frac{F}{A} \tag{2.11}$$

$$\frac{\gamma_2 p_2}{(\gamma_2 - 1)\rho_2} + \frac{{u_2}^2}{2} = \frac{\gamma_3 p_3}{(\gamma_3 - 1)\rho_3} + \frac{{u_3}^2}{2} \tag{2.12}$$

where $\frac{F}{A}$ in the momentum equation (Eq. 2.11) represents the total pressure loss across the perforated plate. A pressure drop coefficient, k, can be defined as:

$$k = \frac{\frac{F}{A}}{\frac{1}{2}\rho_2 {u_2}^2}$$

which is equivalent to the non-dimensional friction factor, $\frac{4fL}{D_H}$, in quasi-one-dimensional Fanno flow. The conservation equations across the perforated plate (Eqs. 2.10 to 2.12) can be manipulated to yield a similar set of equations to the Fanno flow relations.

The conservation equations across the transmitted shock wave downstream are given by:

$$\rho_o V_T = \rho_4 (V_T - u_4) \tag{2.13}$$

$$p_o + \rho_o {V_T}^2 = p_4 + \rho_4 (V_T - u_4)^2 \tag{2.14}$$

$$\frac{\gamma_o p_o}{(\gamma_o - 1)\rho_o} + \frac{{V_T}^2}{2} = \frac{\gamma_4 p_4}{(\gamma_4 - 1)\rho_4} + \frac{(V_T - u_4)^2}{2} \tag{2.15}$$

and can be expressed as the usual normal shock relations when $\gamma_4 \approx \gamma_o$:

$$\frac{p_4}{p_o} = \frac{2\gamma_o {M_T}^2 - (\gamma_o - 1)}{\gamma_o + 1} \tag{2.16}$$

$$\left(\frac{c_4}{c_o}\right)^2 = \frac{T_4}{T_o} = \frac{(2 + (\gamma_o - 1){M_T}^2)(2\gamma_o {M_T}^2 - (\gamma_o - 1))}{(\gamma_o + 1)^2 {M_T}^2} \tag{2.17}$$

$$u_4 = c_o \left(M_T - \frac{c_4}{c_o} \sqrt{\frac{2 + (\gamma_o - 1){M_T}^2}{2\gamma_o {M_T}^2 - (\gamma_o - 1)}} \right) \tag{2.18}$$

The strength of the transmitted shock is determined by matching the pressure and the particle velocity across the interface between the products and the shocked mixture behind the transmitted shock ($p_3 = p_4$ and $u_3 = u_4$). The particle velocity in region (3) depends on the blockage and geometry of the holes and on the pressure drop across the perforated plate. An appropriate model must be used to analyze the flow across the perforated plate.

Pressure Drop Across Perforated Plate

In the present investigation, the pressure drop coefficient for a given perforated plate was determined empirically. Experiments were conducted where an incident shock

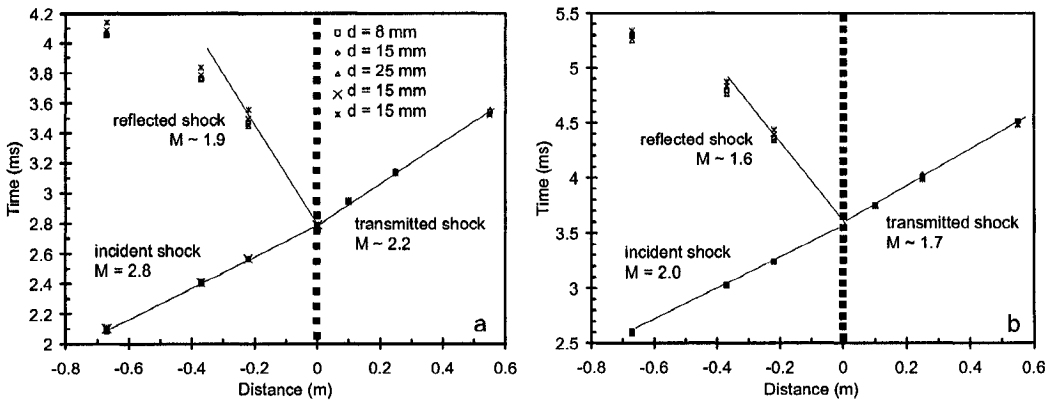

Figure 2.2. Experimental flow field obtained subsequent to the reflection of a a) $M = 2.8$ and a b) $M = 2.0$ shock from various perforated plates with $\sim$ 64% blockage; x and * represent plates with countersunk holes facing downstream and upstream, respectively.

wave in air was reflected from the different perforated plates that were used in the present study. Typical flow fields for an incident shock strength of $M = 2.8$ is shown in Fig. 2.2a for a range of perforated plates with different holes diameters but with the same hole spacing to hole diameter ratios (and, therefore, the same amount of blockage that is provided to the flow). The flow fields for a weaker incident shock of $M = 2.0$ is shown in Fig. 2.2b for the same perforated plates. It can be seen that for a given incident shock strength, the same flow field is obtained regardless of the perforated plate that was used (provided that there is the same amount of blockage to the flow). It is also interesting to note that in the two cases that were tested with the $d = 15$ mm countersunk holes (facing towards and facing away from the flow), the resulting flow field does not change compared to the perforated plates with the straight holes. This is different from objects in steady flow where the drag force on an object varies depending on its orientation to the flow.

The flow fields for perforated plates with a greater amount of blockage (79%) is shown in Figs. 2.3a and b for an incident shock of $M = 1.8$ and of $M = 1.4$, respectively. Once again, the flow fields for a given incident shock strength remains

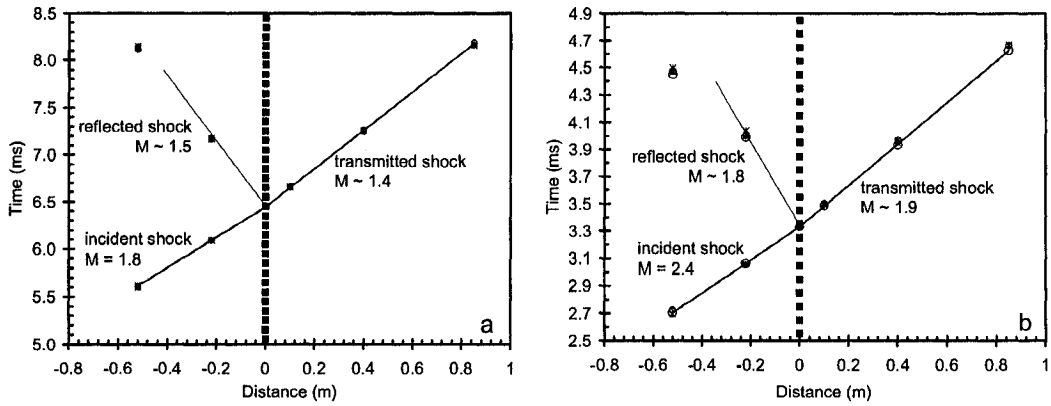

Figure 2.3. Experimental flow field obtained subsequent to the reflection of a a) $M = 1.8$ and b) $M = 1.4$ shocks from various perforated plates with $\sim 78\%$ blocakge.

invariant for perforated plates with the same blockage, which indicates that the pressure drop across a perforated plate is controlled solely by the amount of blockage that the perforated plate provides to the flow.

In order to determine the value of k, the experimental results were compared to the calculated values of the transmitted shock strength and of the reflected shock strength (shown as functions of k in Figs. 2.4a and b for an incident shock strength of $M = 2.8$ and of $M = 2.0$, respectively). When compared to the transmitted shock strengths and the reflected shock strengths obtained experimentally in Fig. 2.2, it can be seen that for perforated plates with 64% blockage, the experimental results correspond to a pressure drop coefficient of about $k = 40$.

2.1.2 Chemical Reactions Downstream

When the downstream mixture is reactive, the interface will ignite it. In a one-dimensional theoretical model, a reaction front will begin to propagate away from the interface as required by the conservation of mass. However, instead of a thin

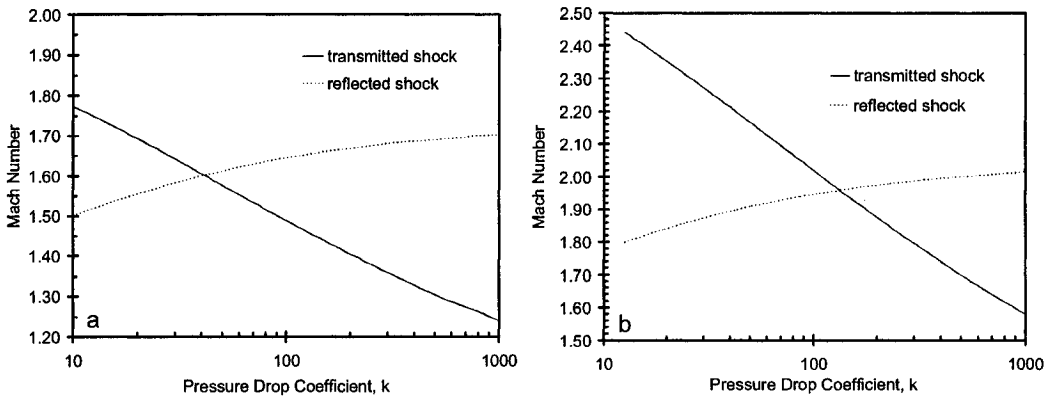

Figure 2.4. Transmitted and reflected shock strengths calculated as a function of the pressure drop coefficient for a) $M = 2.0$ and b) $M = 2.8$ incident shocks.

reaction front, a more realistic downstream scenario may be that the interface ignites an extended mixing reaction zone. The leading edge of the reaction zone could be found immediately behind the transmitted shock, and the trailing edge could be at the interface. Nonetheless, the simpler case where a deflagration wave consists of two separate discontinuities (i.e., a leading shock wave and a thin reaction front) will be considered here. A schematic of the one-dimensional flow field using a thin reaction front is shown in Fig. 2.5. The interface now separates the detonation products (that were originally upstream) from the combustion products behind the reaction front. This reacting flow field is solved in a similar manner to the previous non-reacting case. The same steady conservation laws across the incident CJ detonation, the reflected shock, the perforated plate and the transmitted shock are used in the present case. Across the reaction front (assuming a constant heat release, Q, and constant ratios of specific heats, γ_5 and γ_4), the conservation equations are:

$$\rho_5(\dot{R}_f - u_5) = \rho_4(\dot{R}_f - u_4) \tag{2.19}$$

$$p_5 + \rho_5(\dot{R}_f - u_5)^2 = p_4 + \rho_4(\dot{R}_f - u_4)^2 \tag{2.20}$$

$$\frac{\gamma_5 p_5}{(\gamma_5 - 1)\rho_5} + \frac{(\dot{R}_f - u_5)^2}{2} + Q = \frac{\gamma_4 p_4}{(\gamma_4 - 1)\rho_4} + \frac{(\dot{R}_f - u_4)^2}{2} \tag{2.21}$$

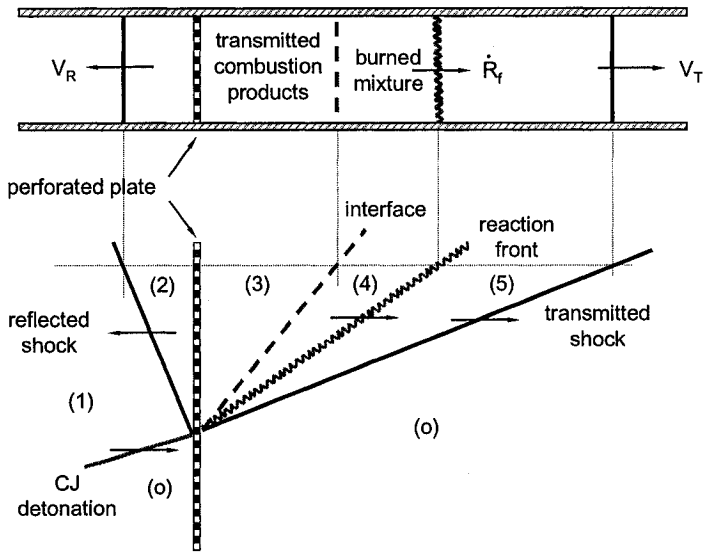

Figure 2.5. Steady 1D wave diagram subsequent to the reflection of a CJ detonation from a perforated plate; the interface ignites a flame front in the combustible mixture downstream.

The value of γ_4 is not equal to that of γ_5 due to the difference in mixture composition between the combustion products and the shocked unburned mixture.

From the conservation of mass (Eq. 2.19) and momentum (Eq. 2.20), an expression for the Rayleigh line can be obtained:

$$\left(\frac{\dot{R}_f - u_5}{c_5}\right)^2 = \frac{1}{\gamma_5}\left(\frac{y-1}{1-x}\right) \tag{2.22}$$

where

$$y = \frac{P_4}{P_5} \qquad \text{and} \qquad x = \left(\frac{\rho_5}{\rho_4}\right) = \left(\frac{\dot{R}_f - u_4}{\dot{R}_f - u_5}\right).$$

By eliminating the velocity term from the conservation of energy (Eq. 2.21), an expression can be obtained for the Hugoniot in the form:

$$(x-\alpha)(y+\alpha) = \beta \tag{2.23}$$

where

$$\alpha = \frac{\gamma_4 - 1}{\gamma_4 + 1} \qquad \text{and} \qquad \beta = \alpha \left[\frac{\gamma_o + 1}{\gamma_0 - 1} + \frac{2\gamma_o Q}{{c_5}^2} - \alpha \right].$$

The Hugoniot represents the locus of all possible states behind the reaction front, given a shocked state (p_o,v_o) and a chemical energy release, Q. It should be noted that the Hugoniot is a function of the initial state and that, depending on the precursor (or transmitted) shock velocity (and hence the initial state (P_5, v_5) ahead of the reaction front), the Hugoniot curve will vary for a given combustible mixture. The value of γ_5 and γ_4 (or α) are not significantly influenced by the initial state, even for strong shocks. The value of β can vary significantly as the sound speed in the shocked gas, c_5, increases with the shock strength. A procedure for determining the values of α and β is outlined in Lee and Guirao.

An expression for $\dot{R}_f$ can be obtained by using the Hugoniot (Eq. 2.23) to eliminate x from the conservation of mass (Eq. 2.19):

$$\dot{R}_f = \frac{\beta u_5 + \alpha u_5 (y + \alpha) - u_4 (y + \alpha)}{\beta + (\alpha - 1)(y + \alpha)} \tag{2.24}$$

The pressure ratio across the flame can be found by solving the Hugoniot for x. This form of the Hugoniot and Eq. 2.24 are then substituted into the Rayleigh line Eq. 2.22 to obtain:

$$y = \frac{B \pm \sqrt{B^2 + 4(\alpha - 1)C}}{2(1 - \alpha)} \tag{2.25}$$

where

$$B = \beta + (\alpha - 1)^2 + \gamma_5 \left(\frac{u_5 - u_4}{c_5} \right)^2$$

and

$$C = \beta + \alpha(\alpha - 1) - \alpha\gamma_5 \left(\frac{u_5 - u_4}{c_5} \right)^2.$$

Although the pressure drop across the perforated plate can be determined empirically, the conservation laws and the matching conditions across the interface (of continuous pressure and particle velocity) are not sufficient to solve the reacting flow field. Knowledge of the propagation mechanism of the reaction front is also required to solve the flow field. If the reaction front were a laminar flame that propagates via molecular transport, then the laminar burning velocity of the mixture is known from experiments or from theoretical computations with specified transport properties and kinetic rate constants of the elementary reactions. If the reaction front were a turbulent flame, then the flame velocity will depend on the turbulence characteristics of the unburned mixture ahead of it. Furthermore, since the sound speed of the combustion products is generally rather high, the flow is subsonic behind the reaction front and the back boundary can influence the front. Therefore, a range of different solutions can exist for a flame propagating steadily behind a shock wave.

One procedure for solving the flow field is to prescribe a back boundary condition (i.e., the interface velocity), choose a value for the shock velocity, and then iterate for a flame velocity, $\dot{R}_f$, such that the back boundary condition is satisfied. For example, if the interface were a solid wall (and the flow behind the flame were uniform), then $u_4 = 0$. A value of M_T is chosen arbitrarily, and the properties of the shocked gas in region (5) can be computed from the normal shock relations. The pressure ratio across the reaction front and the reaction front velocity can now be found with $u_4 = 0$ from Eqs. 2.25 and 2.24, respectively. The same procedure can be followed for different back boundary conditions; for example, if the interface were a piston traveling at a finite value of u_4 (also assuming uniform flow behind the reaction front).

A range of precursor shock and reaction front velocities are shown as functions of the Mach number of the flow behind the reaction front for two different cases (i.e., $u_4 = 0$ and $u_4 = 500$ m/s) in Fig. 2.6. In each case, the minimum deflagration

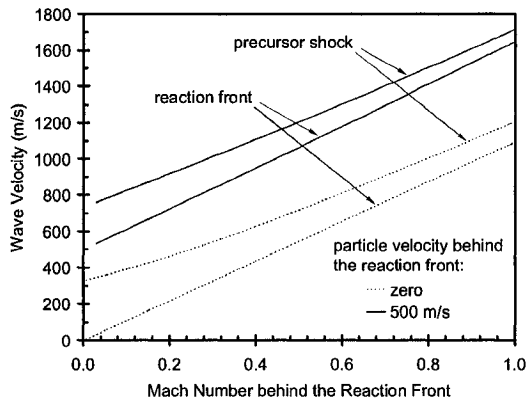

Figure 2.6. Precursor shock and reaction front velocities as a function of the Mach number of the flow behind the reaction front in stoichiometric acetylene-oxygen at $P_o = 1$ kPa.

velocity that was computed corresponds to a precursor shock of $M = 1$. It can be seen that as the reaction front velocity increases, the flame drives a faster shock ahead of it. The maximum deflagration velocity corresponds to the CJ deflagration solution where the flow behind the reaction front becomes choked (i.e., $\dot{R}_f - u_5 = c_5$). This was denoted by Taylor & Tankin (1958) as the "first critical flame speed."

CJ Deflagrations and Detonations

Once the sonic condition behind the deflagration is achieved, information from the back boundary no longer reaches the front. Therefore, for flame speeds that are equal to or greater than the critical value, the back boundary condition can be relaxed without affecting the properties of the flow immediately behind the deflagration front. The procedure to determine the CJ deflagration solution is similar to that of a regular deflagration; however, one must now iterate for the shock velocity (given a value of u_4) such that $\dot{R}_f - u_4 = c_4$. For the calculation shown in Fig. 2.7a, a range of particle velocities is assumed and the corresponding precursor shock and reaction front velocities are calculated.

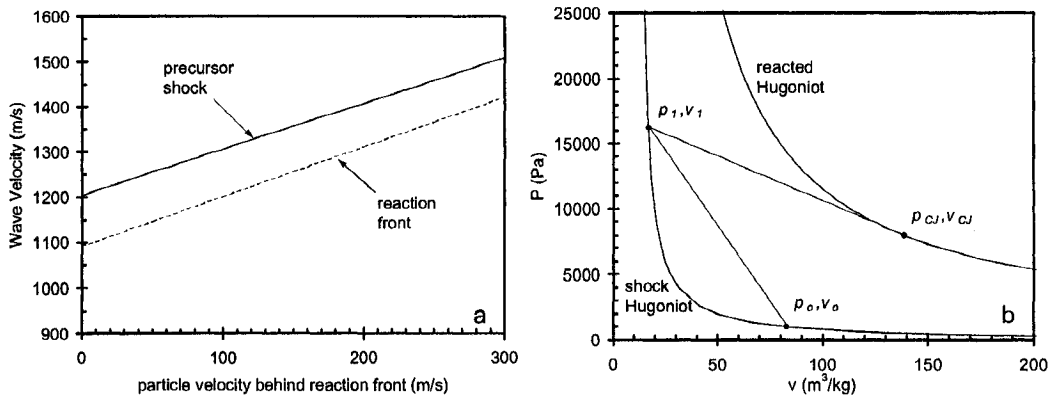

Figure 2.7. a) CJ deflagration solutions as a function of the particle velocity behind the reaction front in stoichiometric acetylene-oxygen at $P_o = 1$ kPa; b) CJ deflagration solution with zero particle velocity behind the reaction front.

It can be seen that, at most, the precursor shock velocity is roughly 10% faster than the reaction front velocity. Therefore, it appears that the precursor shock wave and the reaction front of a CJ deflagration propagate at nearly the same velocity, giving the impressions that the two waves may be coupled and propagate together as a steady precursor shock-reaction front complex like a ZND detonation wave. The CJ deflagration solution that most closely matches the critical deflagration velocity of $\frac{1}{2}V_{CJ}$ corresponds to the case with zero particle velocity behind the reaction front and is represented in Fig. 2.7b on a $p - v$ diagram. Similar results were obtained previously in the study of Chue *et al.* (1993) where CJ deflagration velocities were calculated for different mixtures (assuming zero particle velocity behind the reaction front) and were found to match the experimental results of Dupré *et al.*.

Although only CJ deflagration solutions are shown in Fig. 2.7a up to precursor shock and reaction front velocities of 1500 m/s and 1400 m/s, respectively, greater CJ deflagration velocities can be obtained up to the "second critical flame speed" where the precursor shock wave and the reaction front propagate at identical velocities (Taylor & Tankin). This critical velocity has been found to correspond very closely

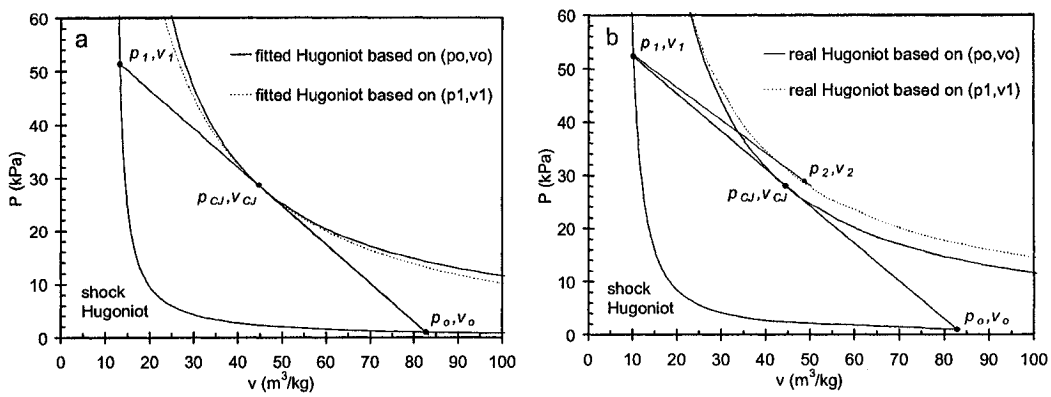

Figure 2.8. a) Fitted and b) real Hugoniots for stoichiometric acetylene-oxygen at P_o = 1 kPa.

to the CJ detonation velocity. In fact, Courant & Friedrich (1948) demonstrated that for stoichiometric acetylene-oxygen (assuming perfect gas with constant heat release, Q, and constant ratios of specific heats, γ), the CJ detonation solution is equivalent to the CJ deflagration solution when the precursor shock and reaction front velocities are the same.

The equivalence of these two solutions are shown in Fig. 2.8a for a stoichiometric mixture of acetylene-oxygen at $P_o = 1$ kPa and $v_o = 82.64$ m^3/kg. The Hugoniot (Eq. 2.23) based on the initial state is shown as the solid line and is constructed by fitting the parameters α and β (see Lee and Guirao for the fitting procedure). The CJ detonation solution is located at $P_{CJ} = 28.63$ kPa and $v_{CJ} = 44.75$ m^3/kg. From the Rayleigh line, the CJ detonation velocity is found to be 2216 m/s. For the equivalent CJ deflagration solution, the mixture initially at (p_o, v_o) is compressed by a shock wave travelling at 2216 m/s to $P_1 = 51.45$ kPa and $v_1 = 13.25$ m^3/kg. A new Hugoniot is constructed based on this shocked state and is shown in the figure as the dotted line. It can be seen that the Hugoniot based on (p_1, v_1) is slightly different than the Hugoniot based on (p_o, v_o). However, at the CJ point, the two curves are tangent, indicating that a CJ detonation is equivalent to a CJ deflagration with a

shock wave and reaction front that travel at identical velocities.

This equivalence, however, is a fortuitous artifact of the assumptions made by Courant & Friedrich (i.e., perfect gas, constant Q, constant γ, no dissociation). The CJ detonation and CJ deflagration solutions for a real gas are shown in Fig. 2.8b where the Hugoniots are computed using thermodynamic equilibrium code (such as STANJAN or CEA). The same mixtures with the same initial state used in Fig. 2.8a is used in this case. The Hugoniot based on (p_o, v_o) for a real gas is shown in the figure as the solid line. The CJ detonation solution is found at the tangency point where $P_{CJ} = 27.99$ kPa and $v_{CJ} = 44.45$ m^3/kg. The CJ detonation velocity is 2185 m/s.

For a 2185 m/s shock wave, the shocked state becomes $P_1 = 52.33$ kPa and $v_1 = 10.16$ m^3/kg. The new Hugoniot based on (p_1, v_1) for a real gas is shown in the Fig. 2.8b as the dashed line. The CJ deflagration solution corresponds to $P_2 = 29.19$ kPa and $v_2 = 47.77$ m^3/kg and does not match the CJ detonation solution. In this case, the reaction front velocity (2166 m/s) is slightly slower than the leading shock velocity (2185 m/s).

Therefore, for a real gas, a CJ detonation is not equivalent to a CJ deflagration where the shock and the flame speeds are identical. This is not surprising since auto-ignition for a CJ detonation is controlled by adiabatic shock compression, which does not correspond to the model of a propagating flame driving a precursor shock wave.

Matching Conditions Across the Interface

If a CJ detonation were formed immediately downstream of the perforated plate, it is clear that it will propagate downstream independently of the interface (provided that the CJ pressure is greater than the interface pressure) since all of the energy that supports the detonation is provided by the combustible gas ahead of it. For

a stoichiometric mixture of acetylene-oxygen at $p_o = 1$ kPa, a CJ detonation will propagate away from the interface at a velocity of 2184 m/s. The pressure and the particle velocity at the sonic plane are 27.4 kPa and 1011 m/s, respectively. Using an empirically determined pressure drop coefficient to model a perforated plate with 64% blockage, the pressure and the particle velocity immediately downstream of the perforated plate is calculated to be 5.94 kPa and 537 m/s. An expansion wave is thus required behind the detonation in order to slow the flow and reduce the CJ pressure such that the matching condition at the interface are satisfied.

If it were assumed that a critical deflagration wave is a CJ deflagration, then a CJ deflagration that is ignited by the interface will propagate in a similar manner to a CJ detonation since it is also controlled by the energetics of the mixture ahead of it. For the CJ deflagration shown in Fig. 2.7b, the pressure and the particle velocity at the sonic plane are 7.97 kPa and 0 m/s, respectively. Once again, the pressure and the particle velocity of the flow is 5.94 kPa and 537 m/s, respectively, immediately downstream of a perforated plate with 64% blockage. A $M = 1.15$ backward facing shock is now required immediately downstream of the perforated plate to raise the pressure and reduce the velocity of the overexpanded flow exiting the perforated plate such that the matching conditions across the interface (and behind the CJ deflagration) are satisfied.

2.2 Ignition at a Turbulent Mixing Interface

To help understand the mechanisms that lead to the onset of detonation in the turbulent mixing reaction zone of the critical deflagration wave, it is important to first study the ignition processes that can occur at the interface downstream of the perforated plate. Ignition at a turbulent mixing interface is rather difficult to model theoretically since both chemical reactions and turbulent mixing are involved si-

multaneously. As well, a detailed quantitative observation of the gasdynamic and chemical processes at the mixing interface is extremely difficult to obtain experimentally. Therefore, it is of value to consider some simple idealized cases that can help elucidate the different possible ignition phenomena due to turbulent mixing.

When high temperature combustion products (initially separated from low temperature reactants by a one-dimensional interface) are mixed with the reactants, different ignition phenomena can occur depending on the chemical reaction rate and on the mixing rate. In the limiting case where the mixing rate is slow (i.e., of the order of molecular transport) compared to the reaction rate, a laminar flame will result. On the other hand, if the mixing rate is infinitely fast compared to the chemical reaction rate, a constant volume explosion can occur. Between these two extremes, the competition between mixing and chemical reactions will control the ignition processes. Under appropriate conditions, it is also possible that auto-ignition can lead to the onset of detonation. A few simple models are considered here to help understand these different cases.

2.2.1 Instantaneous Mixing

The limiting case of an infinitely fast mixing rate at the downstream interface is considered first using a homogeneous mixing ignition (HMI) model (Knikker et al. 2003, Arienti & Shepherd 2003). Initially, the expanded combustion products are separated from the shocked unburned reactants by a one-dimensional interface. The products and the reactants are then mixed instantaneously to form a homogeneous mixture of z kg of combustion products and $(1-z)$ kg of reactants. The ignition delay time after mixing is investigated for different amounts of products and of reactants.

The species mass fraction, Y, and the enthalphy, h, of the mixture are given by:

$$Y_{k,mixture} = zY_{products} + (1-z)Y_{reactants}$$

$$h_{mixture} = zh_{products} + (1-z)h_{reactants}$$

The final temperature of the mixture, $T_{mixture}$, is found from h, Y_k, and the pressure using an iterative Newton-Rhapson method. The ignition delay time is then calculated using a zero-order constant volume explosion code.

The ignition delay time for hydrogen-air as a function of z is shown in Fig. 2.9. The mixture temperature and the final equilibrium temperature are also shown in the figure. For $z = 0.1$ (i.e., a small amount of combustion products in the mixture), the mixture temperature is low (about 834 K) and, accordingly, the ignition delay time is rather long (about 10 ms). As the amount of combustion products in the mixture increases to a value of $z = 0.15$, the mixture temperature increases to about 1100 K, which corresponds to the auto-ignition temperature for H_2-air (Atkinson *et al.* 1980, Westbrook & Urtiew 1982). As a result, a drastic reduction in the ignition delay time is observed to occur. The ignition delay time continues to decrease as more products are added into the mixture. At a value of $z = 0.2$, the ignition delay time is reduced to about 1 μs, which is comparable to the time scale of the experiments. The ignition delay time approaches a value of zero as $z \rightarrow 1$. The final equilibrium temperature after ignition can be seen to depend very weakly on z. However, the important measure of the chemical energy that is released is approximated by the difference between $T_{equilibrium}$ and $T_{mixture}$. Thus, for low values of z, the amount of energy release is rather large. As z increases, the chemical energy release decreases as the amount of reactants in the mixture is reduced.

The results of the HMI model indicate that the temperature of the homogeneous mixture plays an important role in the ignition process. If the amount of combustion products is too small compared to the amount of reactants, the chemical reactions become quenched as $T_{mixture}$ drops below the auto-ignition limit. However, a certain

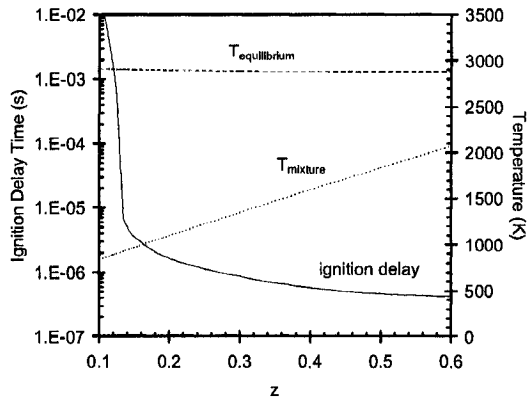

Figure 2.9. Ignition delay time, mixture temperature, and final equilibrium temperature as a function of the mixture composition using the HMI model.

amount of reactants is also required in the homogeneous mixture in order to obtain a large energy release.

2.2.2 Finite Mixing Rate

The HMI model does not take into consideration the finite time during which heat and mass are transported across the interface. A slightly more realistic model is to assume that a mixing layer develops over time from the one-dimensional interface via diffusion. Before chemical reactions are incorporated into the model, the one-dimensional diffusion equation (the solutions to which are well-known) can be used to examine the temperature and species gradients that develop temporally in the mixing layer. A progress variable, λ, is used to denote the amount of reactants and of products (i.e., $\lambda = 1$ corresponds to all reactants whereas $\lambda = 0$ corresponds to all products).

The one-dimensional diffusion equations for the temperature and λ are:

$$\frac{\partial T}{\partial t} = \frac{1}{\rho c_p}\frac{\partial}{\partial x}\left(k\frac{\partial T}{\partial x}\right) \tag{2.26}$$

$$\frac{\partial(\rho\lambda)}{\partial t} = \frac{\partial}{\partial x}\left(\rho D\frac{\partial \lambda}{\partial x}\right) \tag{2.27}$$

For simplicity, ρ is taken to be constant, the Lewis number is assumed to be equal to unity ($Le = \frac{k}{\rho c_p D} = \frac{\alpha}{D} = 1$), and the diffusion rates in the products are equivalent to the those in the reactants ($\alpha = \alpha_{products} = \alpha_{reactants}$ and $D = D_{products} = D_{reactants}$). The interface is located at x = 0.

The analytical solutions are taken from Crank (1975):

$$T(x) = \begin{cases} \frac{1}{2}\mathrm{erfc}\frac{x}{2\sqrt{\alpha t}}(T_p - T_r) + T_r & \text{for } x \geq 0 \\ \frac{1}{2}\left(1 + 2\mathrm{erf}\frac{x}{2\sqrt{\alpha t}}\right)(T_p - T_r) + T_r & \text{for } x \leq 0 \end{cases}$$

$$\lambda(x) = \begin{cases} \frac{1}{2}\left(1 + 2\mathrm{erf}\frac{x}{2\sqrt{Dt}}\right) & \text{for } x \geq 0 \\ \frac{1}{2}\mathrm{erfc}\frac{x}{2\sqrt{Dt}} & \text{for } x \leq 0 \end{cases}$$

where the subscripts "p" and "r" denote "products" and "reactants," respectively.

The results obtained for $\alpha = D = 10^{-5}$ m^2/s (which is of the order of the molecular transport for typical gases) are shown in Figs. 2.10a and b. As expected, a relatively long time is required to develop a mixing layer via molecular transport. For example, to develop gradients in temperature and in species concentration that is about 6 mm long, a mixing time of about 100 ms is required. In comparison with a turbulent diffusivity that is 3 orders of magnitude faster ($\alpha = D = 10^{-2}$ m^2/s), the mixing time that is required to achieve the same mixing layer thickness is reduced significantly to 0.1 ms.

The temperature and species concentration profiles can be used to determine the corresponding reaction rate profile at a given time by using a one-step Arrehenius

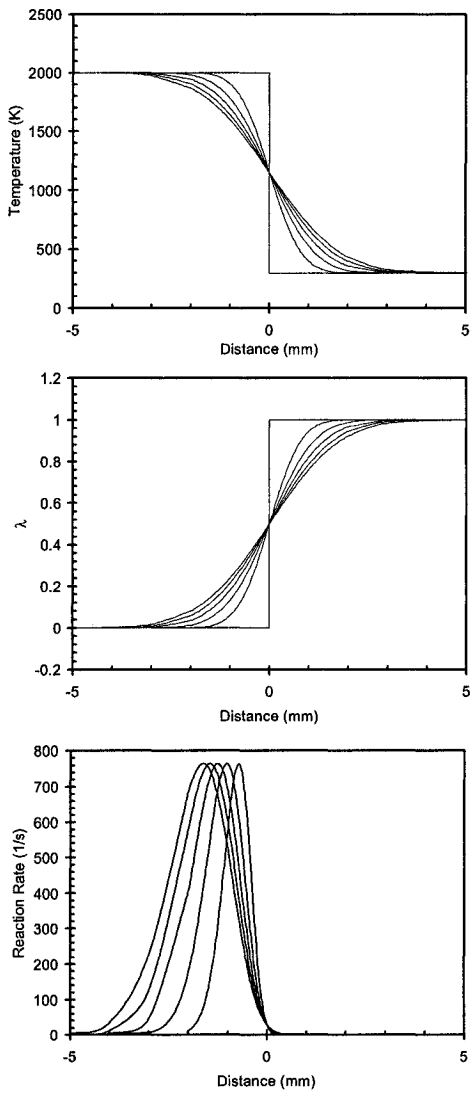

Figure 2.10. a) Temperature b) species concentration and c) reaction rates profiles due to diffusion at $t = 0$, 0.02, 0.04, 0.06, 0.08, 0.1 s ($\alpha = D = 10^{-5}$ m^2/s).

rate law of the form:

$$\dot{\omega} = A_k \lambda \exp\left(-\frac{E_a}{RT}\right)$$

The reaction rate profiles are shown in Fig. 2.10c for $\alpha = D = 10^{-5}$ m^2/s. For $x \geq 0$,

the reaction rates are negligible as the temperature is always low. The peak in the reaction rates always occurs on the left ($x < 0$) where the temperature is high and a certain concentration of reactants have been transported across the original interface. As mixing occurs over time, it can be seen that the peak rate rate shifts towards the left where the temperature remains high and where the is a minimum concentration of reactants. This suggests that if ignition were to occur, it will begin to the left of the interface where the proportion of products is greater than the reactants. It is interesting to note that only a small amount of reactants are required for rapid chemical reactions to occur. This is similar to the results of the HMI model where short ignition delay times were obtained for mixtures with only 20% reactants.

The temperature and reaction rate profiles are shown in Fig. 2.11a when the initial temperature of the combustion products is lowered from 2000 K to 1500 K. The species concentration profile remains the same as the previous case and is not shown. It can be seen that the reduction in the product temperature results in a significant reduction in the reaction rates (by an order of magnitude). On the other hand, when the initial temperature of the reactants is increased to 800 K (which is typically the temperature behind a $M \approx 3$ shock wave), the reaction rates are enhanced (see Fig. 2.11b) as the temperatures in the mixing layer increases.

These results indicate that gradients in temperature and species concentration can be generated via diffusion (i.e., via mixing). As expected, wider mixing layers can be achieved for turbulent transport rates (compared to molecular transport rates). Within the mixing layer, high temperatures and a minimum concentration of reactants are required for rapid chemical reactions to occur.

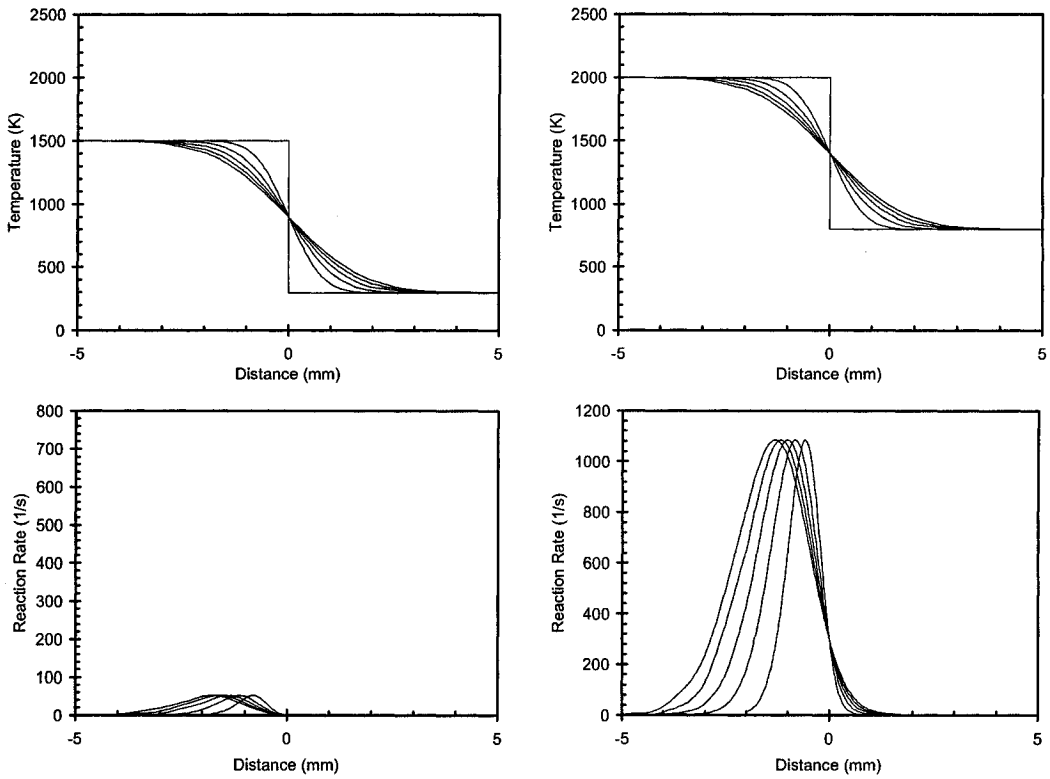

Figure 2.11. Temperature and reaction rates profiles as a result of varying the initial temperature of the a) products and b) reactants at t = 0, 0.02, 0.04, 0.06, 0.08, 0.1 s ($\alpha = D = 10^{-5}$ m^2/s).

2.2.3 Transient Ignition at a Mixing Interface

In order to determine the evolution of the ignition process at a mixing interface, the chemical reactions are coupled to the mixing process by adding a source term for the chemical energy release to the diffusion equations:

$$\frac{\partial T}{\partial t} = \frac{1}{\rho c_p}\frac{\partial}{\partial x}\left(K\frac{\partial T}{\partial x}\right) + \frac{q}{c_p}\dot{\omega} \tag{2.28}$$

$$\frac{\partial(\rho\lambda)}{\partial t} = \frac{\partial}{\partial x}\left(\rho D\frac{\partial \lambda}{\partial x}\right) - \dot{\omega} \tag{2.29}$$

Parameter	Description
$T_o = 293$ K	Initial temperature
$p_o = 101.3$ kPa	Initial pressure
$\rho_o = 1.58 \times 10^{-1}$ kg/m^3	Initial density
$\gamma = 1.25$	Specific heat ratio
$M = 29$	Molecular weight
$A_k = 1.0 \times 10^9$ m^3/kg/s	Pre-exponential constant
$E_a = 29.3RT_o$	Activation energy
$q = 35.0RT_o/M$	Chemical energy release
$K_o = D_o = 1.3 \times 10^{-6}$	Molecular transport coefficient
$T_f = 2340$ K	Adiabatic flame temperature
$\rho_f = 1.98 \times 10^{-2}$ kg/m^3	Density of products

Table 2.1. Chemical and thermodynamic parameters used in the transient computations (Khokhlov & Oran 1999).

where

$$\dot{\omega} = A_k \rho \lambda \exp\left(-\frac{E_a}{RT}\right) \qquad \text{and} \qquad \rho = \frac{p}{R_s T}.$$

The values used for the different parameters (e.g., A_k, $\frac{E_a}{R}$, etc.) are shown in Table 2.1, which are taken from Khokhlov & Oran (1999). The input parameters were selected to model various laminar flame and detonation properties in acetylene-air for a range of initial pressures from 0.1 to 1 atm and at an initial temperature of 293 K. Since gasdynamic effects are not taken into account in this particular model, the pressure remains constant throughout the problem. Initially, the temperature of the combustion products is at 1500 K; the reactants are at 293 K. The interface is located at $x = 0$. There is no analytical solution to the reactive diffusion equation, and the equations are solved numerically using a forward difference method.

The temperature, species concentration, and reaction rate profiles are shown in Figs. 2.12a to c for $\alpha = D = 10^{-5}$ m^2/s. At $t = 10$ μs, the temperature and the λ profiles change mainly as a result of diffusion. Chemical reactions are negligible as

the reaction rates are slow throughout the mixing layer. The peak in the reaction rate occurs just slightly behind the original interface at $x = 0$. At a later time ($t = 50\ \mu s$), the temperature can be seen to increase above 1500 K behind the interface as a result of chemical reactions. The peak in the reaction rates have also shifted towards the left away from $x = 0$ as in the previous non-reacting case. From the species concentration profile, it does not appear that many reactants have been consumed at this time.

As the temperature now increases due to chemical reactions, more heat is transported into the cold reactants ahead, generating a new mixing layer. The temperature in the new mixing layer is greater than the temperature in the previous layer, which results in an increase in the reaction rates. Hence, in this mixing layer, the reactants become consumed more quickly. The energy release from the chemical reactions raises the temperature, and the rate at which the temperature increases also becomes faster. At this point, even more heat is transported into the next mixing layer, which causes another increase in the reaction rates. A positive feedback loop is established, and it can be seen that at $t \geq 100\ \mu s$, the temperature and the reaction rates continually increase as a combustion front propagates into the reactants. Evenutally, a steady state is achieved where the transport rate balances with the reaction rate, and the combustion front reaches a steady velocity that is close to that of a laminar flame.

It should be noted that these processes occur over a very short distance on the order of a mm for slow transport rates. When the diffusivity is increased to a value of $\alpha = D = 10^{-2}$ m^2/s (Figs. 2.13a to c), the mixing rate is much faster, which generates a thicker mixing layer where the gradients in temperature and in species concentration are an order of magnitude longer prior to ignition. If the resonant coupling between the chemical energy release and acoustic waves can be achieved through the gradient field that is generated by turbulent mixing, it may

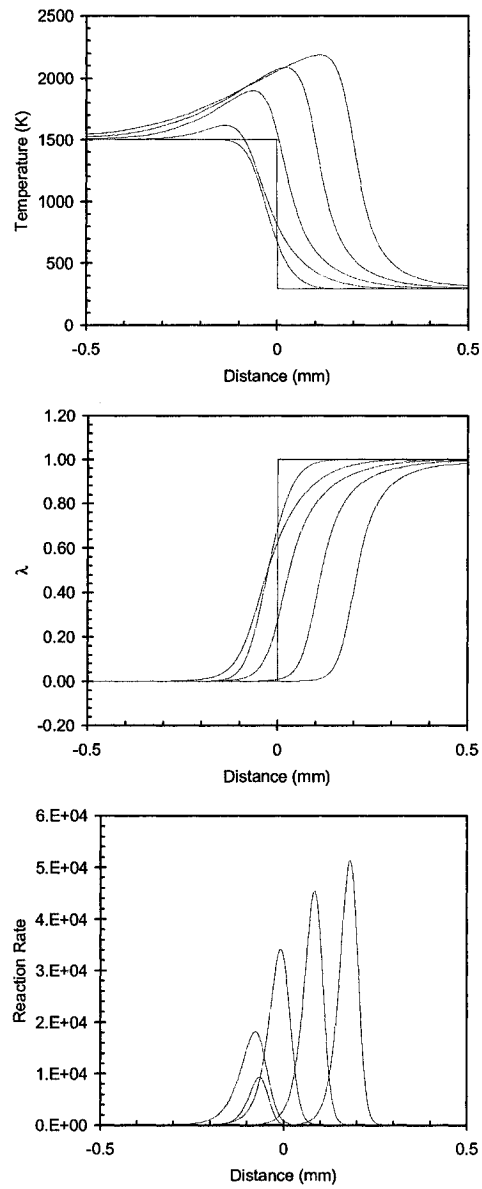

Figure 2.12. a) Temperature b) species concentration and c) reaction rates profiles due to diffusion and chemical energy release at t = 0, 10, 50, 100, 150, 200 μs ($\alpha = D = 10^{-5}$ m^2/s).

be possible that the onset of detonation can be triggered by the transient ignition process in the mixing layer. It was demonstrated by Zel'dovich *et al.* (1970) that a minimum reaction front velocity (about the sound speed of the combustion products or $\approx$ 1000 m/s) is required for successful resonant coupling. However, for the case shown in Fig. 2.13, the reaction front only accelerates up to a steady state velocity less than 100 m/s. Nevertheless, without having taken any gasdynamic effects into account, the results of this simple reactive diffusion model indicate that turbulent mixing can greatly enhance the ignition process.

2.2.4 Gasdynamic Effects

In order to investigate the mixing conditions that are required to achieve the resonant coupling between chemical reactions and pressure waves, gasdynamic effects are incorporated into the simple reactive diffusion model.

Neglecting viscous effects, the governing equations are:

$$\frac{\partial \rho}{\partial t} + \frac{\partial (\rho u)}{\partial x} = 0 \tag{2.30}$$

$$\frac{\partial (\rho u)}{\partial t} + \frac{\partial (\rho u^2 + p)}{\partial x} = 0 \tag{2.31}$$

$$\frac{\partial (\rho e)}{\partial t} + \frac{\partial (u(\rho e + p))}{\partial x} = \frac{\partial}{\partial x}\left(K \frac{\partial T}{\partial x}\right) + \rho q \dot{\omega} \tag{2.32}$$

$$\frac{\partial (\rho \lambda)}{\partial t} + \frac{\partial (\rho u \lambda)}{\partial x} = \frac{\partial}{\partial x}\left(\rho D \frac{\partial \lambda}{\partial x}\right) - \dot{\omega} \tag{2.33}$$

where

$$p = \rho R_s T, \qquad e = \frac{p}{\rho(\gamma - 1)} + \frac{u^2}{2}, \qquad \text{and} \qquad \dot{\omega} = A_k \rho \lambda \exp\left(-\frac{E_a}{RT}\right).$$

The chemico-physical parameters of the system are shown in Table 2.1. Once again, the Lewis number is assumed to be equal to unity. The coefficients for the heat and mass diffusion are temperature dependent and are based on Sutherland's Law:

$$D = D_o \frac{T^n}{\rho} \qquad\qquad \frac{K}{\rho c_p} = K_o \frac{T^n}{\rho}$$

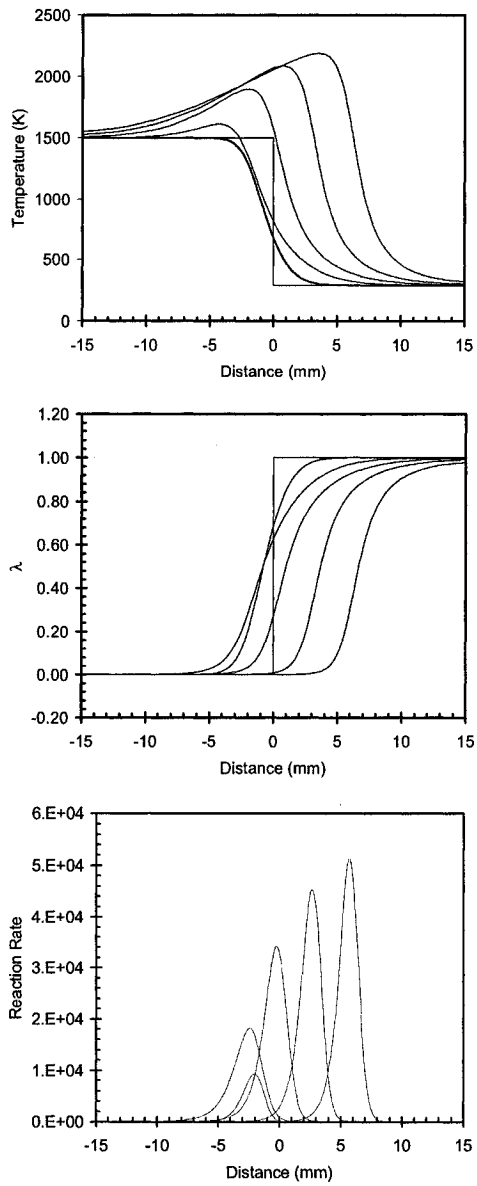

Figure 2.13. a) Temperature b) species concentration and c) reaction rates profiles due to diffusion and chemical energy release at t = 0, 10, 50, 100, 150, 200 μs ($\alpha = D = 10^{-2}$ m^2/s).

where c_p is the specific heat at constant pressure. The index $n = 0.7$ describes the typical temperature dependence of D and K for reactive hydrocarbons. It should be noted that D_o and K_o are transport coefficients that were selected to fit laminar flames and, therefore, account only for molecular transport in laminar flows. In order to account for turbulent transport processes, the transport coefficients are modified by a turbulence factor, Γ, such that the turbulent transport coefficients become:

$$D_T = \Gamma D \qquad\qquad K_T = \Gamma K$$

The initial conditions are described by two thermodynamic states separated by an interface at $x = 2.5$ cm. For $x < 2.5$ cm, the state corresponds to T_f and ρ_f given in Table 2.1. For $x > 2.5$ cm, the state corresponds to the uniform initial properties of the unburned gas. The governing equations are solved numerically using Strang's method of operator splitting, separating the hyperbolic part of the system from the additional chemical and parabolic terms in the model. The hyperbolic Euler equations without the transport effects are approximated using the second-order slope-limiter centered (SLIC) integration scheme (Toro 1999). The additional parabolic terms in the model are treated using explicit second-order finite-difference approximations. Adaptive mesh refinement (AMR) is also adopted as a technique for manipulating the local resolution of the simulation based on a hierarchical series of Cartesian grids (Berger & Oliger 1984).

Temperature and corresponding pressure profiles at equal time intervals for the case where $\Gamma \approx 10$ is shown in Fig. 2.14. It can be seen that changes in pressure are negligible. The process shown in the figure is controlled by molecular transport. As quickly as heat and mass are transported into the mixing layer (which is very thin), chemical reactions occur immediately. As a result, there is an insufficient amount of time to develop a gradient field via mixing prior to ignition, and a laminar flame can be seen to propagate into the reactants.

When the turbulent transport rates are increased such that $\Gamma = 80$, the mixing

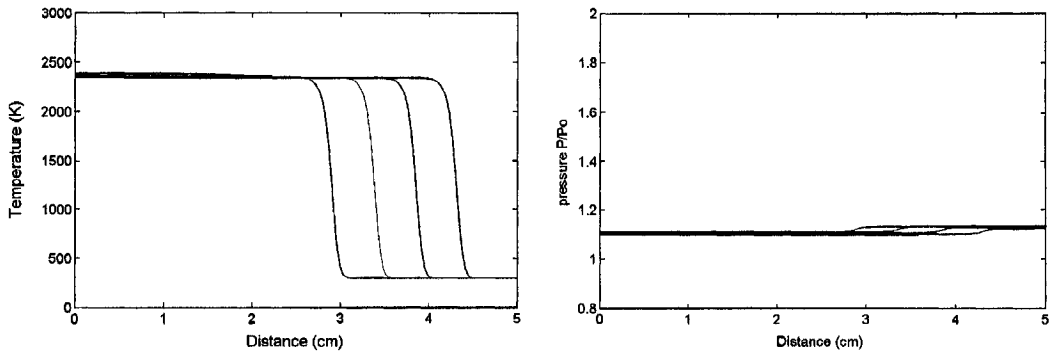

Figure 2.14. Temperature and pressure profiles for $\Gamma = 10$ at $t = 0.1$, 0.2, 0.3, and 0.4 ms.

time decreases compared to the reaction time. The temperature and pressure profiles are shown in Fig. 2.15. The process is now controlled by turbulent transport rates, and the propagation velocity can be seen to increase substantially. From the figure, pressure waves can be seen ahead of the reaction front, which also increases the temperature of the unburned reactants and, hence, of the reaction rates in the mixing layer. The increase in chemical reaction rates can result in a faster propagation velocity and heat release, which can cause the pressure waves to amplify. However, in the present case, the pressure rise never amplifies to a level that is sufficient to achieve auto-ignition via adiabatic shock compression. This suggests that the gradient field that is generated by turbulent mixing is not adequate to establish resonant coupling that can lead to the onset of detonation. This case represents a fast deflagration wave.

When Γ is significantly increased above a value of 250, successful resonant coupling is achieved between the chemical reactions and pressure waves (see Fig. 2.16). Since the mixing time is much shorter than the reaction time, the chemical reactions undergo an induction process during the early stages where temperature and species concentration gradients are being established by rapid turbulent mixing. Once ignition occurs and a reaction front propagates foward, pressure waves are generated.

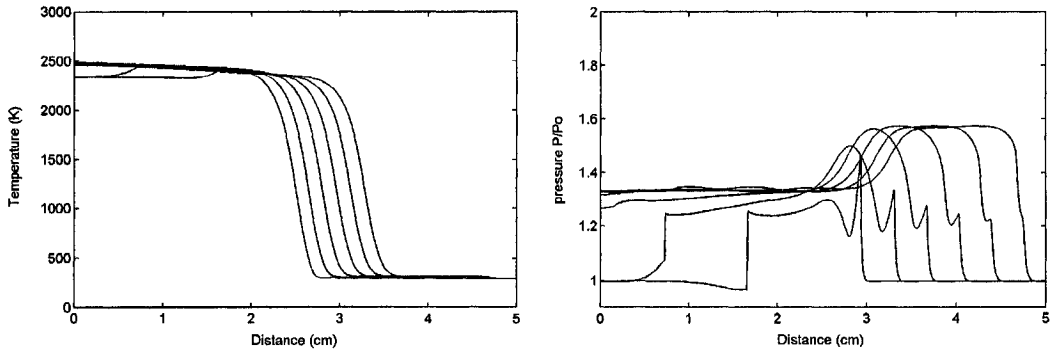

Figure 2.15. Pressure profiles for $\Gamma = 80$ at $t = 10$, 20, 30, 40, 50 and 60 μs.

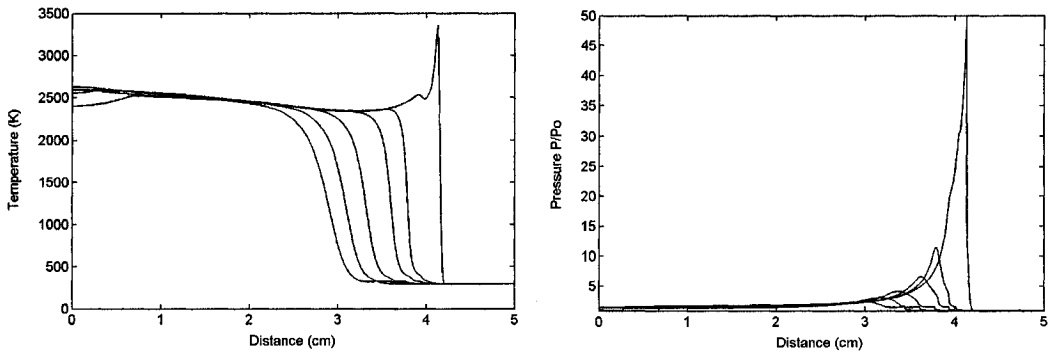

Figure 2.16. a) Temperature and b) pressure profiles for $\Gamma = 280$ at $t = 20$, 24, 28, 32 and 36 μs.

This causes an increase in the temperature of the unburned reactants, which also causes an increase in the reaction rates in the mixing layer. The energy release by the chemical reactions amplify the pressure wave, which raises the temperature in the unburned reactants again. A positive feedback loop is established, and the pressure waves continually amplify as energy is released at a faster rate until the sudden onset of detonation occurs.

It is interesting to note that the present model indicates that the onset of detonation not only requires the proper non-steady coupling between chemical reactions

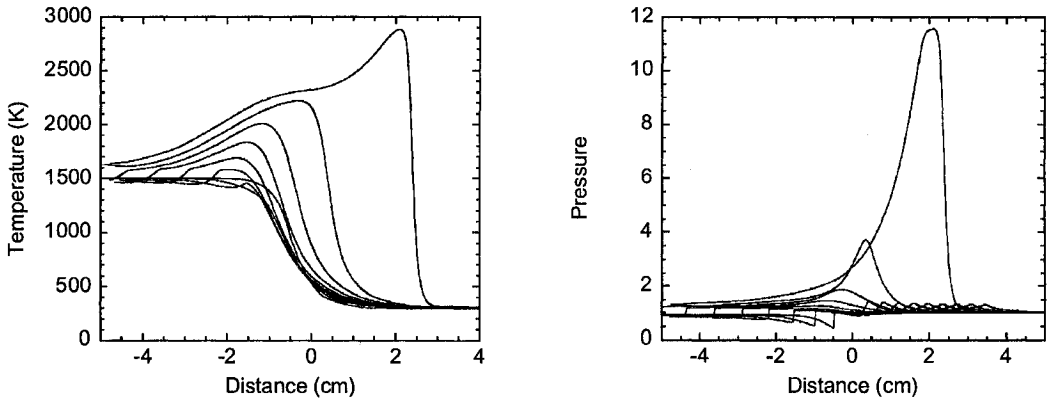

Figure 2.17. a) Temperature and b) pressure profiles for $\alpha = 1.6 \times 10^6$ m^2/s at $t = 10$, 20, 30, 40, 50, 60, 70, 80 and 90 μs.

and pressure wave amplification but also the proper non-steady coupling between turbulent mixing and chemical reactions. When the temperature dependence of the transport rates is removed and a constant value is used for the transport coefficients, the amplification of the pressure waves to values that are required for the onset of detonation is no longer achieved. The temperature and pressure profiles are shown in Figs. 2.17a and b for an unrealistically large value of $\Gamma = 1.3 \times 10^6$. At this value of Γ, a gradient is generated in the mixing layer such that the auto-ignition centre drives a pressure wave that is neither sufficient to result in auto-ignition by adiabatic shock compression nor amplified to the required pressure. It can also be seen that the rise time across the pressure wave is rather long.

This result suggests that turbulent mixing plays an important role in the development of proper temperature and concentration gradients for the successful onset of detonation. In addition to the coupling of the energy release with the pressure waves, another positive feedback loop between the chemical reactions and the turbulent mixing also appears to be required. The energy that is released by chemical reactions increases the temperature of the mixture. This causes an increase in turbulent transport rates and, thus, faster mixing of high temperature products in the

mixing layer. This, in turn, results in faster chemical reactions and a faster increase in temperature, which further increases turbulent mixing rates, etc.

In previous studies on the formation of a detonation in a temperature or a species concentration gradient field, gradient fields were imposed as the initial conditions and the subsequent coupling between the gasdynamics and the chemical reactions was investigated (see review of Bartenev & Gelfand 2000). Using the present mixing model, the gradient field itself is generated by turbulent transport from an initial condition of combustion products separated by a one-dimensional interface from the reactants. Therefore, it appears that rapid turbulent mixing plays an important role in the formation of a detonation via the SWACER mechanism.

Chapter 3

Experimental Details

3.1 Experimental Apparatus

3.1.1 Detonation Tubes

Four different detonation tubes were used in the present investigation:

1. 300 mm by 300 mm square cross-section steel tube
2. 150 mm diameter circular steel tube
3. 65 mm diameter circular steel tube
4. 50 mm diameter circular clear acrylic tube

Schematics of the four different detonation tubes are shown in Figs. 3.1a to d.

In each experiment, the detonation tube was divided into two sections with a perforated plate, and a CJ detonation was established in the section upstream of the plate. The flow field resulting from the reflection of the detonation from the plate was monitored in the downstream test section. Obstacles were placed near the igniter in each tube to ensure the rapid formation of a detonation. The obstacle sections were sufficiently short such that a fully-developed CJ detonation was established in

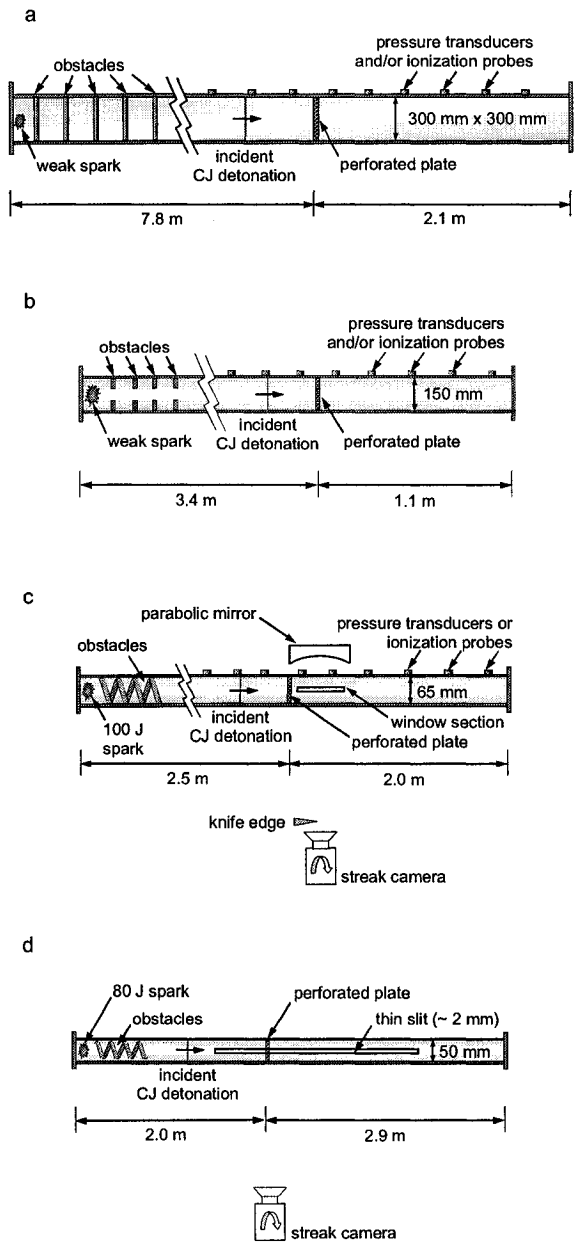

Figure 3.1. a) 300mm by 300 mm steel square tube, b) 150 mm diameter steel tube, c) 65 mm diameter steel tube with double pass schlieren system, and d) 50 mm acrylic tube.

a smooth tube upstream of the perforated plate.

In order to obtain high speed self-luminous streak photographs, the 50 mm diameter acrylic tube was covered with black construction paper, and a thin slit (about 2 mm high) was cut into the black paper along the length of the tube, which allowed light from the tube to escape and to be recorded on film.

For the 65 mm diameter steel tube, a short window section was used for high speed streak schlieren photography. The window section was made by milling two 5 mm by 280 mm long slits (diametrically opposite to each other) in a 300 mm long steel tube. Windows were sealed with o-rings against the slit.

3.1.2 Perforated Plates

A variety of perforated plates with different hole diameters (d) and hole spacings (l) were used. A summary of the perforated plates is shown in Table 3.1. Each plate was perforated throughout its entire cross-section in order to prevent the lateral expansion of the combustion products and the entrainment of the unburned mixture from the sides (and, hence, to establish a quasi-one-dimensional flow field). A photo of a typical perforated plate is shown in Fig. 3.2a. In general, the plates were made out of steel in order to withstand the impact of the detonation; however, in the 65 mm acrylic tube, aluminium perforated plates were used.

A couple of variations that are not listed in Table 3.1 were made to the standard perforated plate configuration. In order to simulate the effect of an "unconfined" jet in the 300 mm by 300 mm square tube, only a small cross-sectional area (165 mm in diameter) was perforated with 10 mm holes that were spaced 5 mm apart. A similar perforated plate was used in the 50 mm acrylic tube (shown in Fig. 3.2b). The dimensions of the holes ($d = 1.6$ mm and $l = 0.8$ mm for 69% blockage) and of the perforated area (30 mm in diameter) were scaled down from the larger plate.

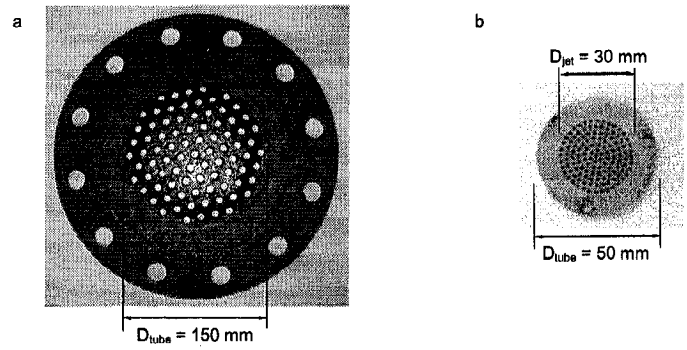

Figure 3.2. a) Typical perforated plate used in the present investigation with holes throughout the entire cross-sectional area of the tube ($d = 15$ mm with 63% blockage); b) perforated plate used in the 50 mm diameter tube with a perforated cross-sectional area 40% smaller than the cross-sectional area of the tube.

The thicknesses of the perforated plates were arbitrarily chosen. However, the holes of one of the perforated plates ($d = 15$ mm; 63% blockage in the 150 mm diameter tube) were countersunk such that the thickness of the plate could be reduced to a few millimeters without sacrificing the strength of the plate. Experiments were conducted with the countersinking facing towards and facing away from the incident detonation. No noticeable difference was observed in the flow field using this plate compared to the plate with straight holes. Skews (2005) also reported an independence of the plate thickness in their study on the reflection of shock waves from porous plates.

3.2 Mixture Selection and Preparation

In total, four different fuels were tested in the present investigation: hydrogen (H_2), acetylene (C_2H_2), propane (C_3H_8) and ethylene (C_2H_4). Both air (O_2 + 3.76 N_2) and oxygen (O_2) were used as oxidizers. For some experiments, fuel-oxygen mixtures were diluted with varying amounts of argon (Ar) or of nitrogen (N_2).

Detonation Tube	d (mm)	l (mm)	l/D	% blockage
300 mm by 300 mm	5	2.5	0.5	69
	5	7.75	1.55	85
	8	4	0.5	69
	15	7.5	0.5	69
	15	22.5	0.5	88
	25	12.5	0.5	60
	25	25	1.0	76
	25	37.5	1.5	84
	50	25	0.5	69
150 mm diameter	8	4	0.5	64
	8	8	1.0	77
	15	7.5	0.5	63
	15	15	1.0	79
	25	12.5	0.5	64
	45	22.5	0.5	65
65 mm diameter	8	4	0.5	61
	8	8	1.0	75
	5	5	1.0	80
50 mm diameter	1.6	0.8	0.5	69
	2.4	1.2	0.5	69

Table 3.1. Summary of the different perforated plates that were tested.

3.2.1 Experiments Conducted at $P_o = 1$ atm

In the two larger detonation tubes (300 mm by 300 mm and 150 mm in diameter), either fuel-air or fuel-oxygen-nitrogen mixtures were tested at an initial pressure of $P_o = 1$ atm. The sensitivity of the fuel-air mixtures was varied by the equivalence ratio (ϕ). For the fuel-oxygen-nitrogen mixtures, a stoichiometric composition was always tested and the sensitivity was varied by the amount of nitrogen dilution (i.e., the ratio of nitrogen to oxygen or β).

In most cases, the entire detonation tube (both sections upstream and down-

stream of the perforated plate) was filled with the same combustible mixture. However, in the 150 mm tube, a series of experiments was performed where a thin diaphragm was used (usually 0.001" thick) in conjunction with a perforated plate in order to have different mixtures in the upstream and downstream sections. The upstream "driver" mixture was fixed (either stoichiometric hydrogen-oxygen or stoichiometric hydrogen-air, both at $P_o = 1$ atm). Downstream, fuel-air mixtures at various equivalence ratios or stoichiometric fuel-oxygen-nitrogen mixtures with different amounts of nitrogen dilution were tested. At times, an inert gas such as nitrogen or air was used downstream in order to establish a non-reacting flow field as a baseline experiment. A summary of the different driver mixtures, test mixtures and sensitivity parameters are summarized in Table 3.2.

For any given experiment, the entire detonation tube was initially evacuated and then filled by the method of partial pressures to obtain the desired concentrations of fuel, of oxidizer, and (in some cases) of nitrogen. The pressure was monitored by a Heise gauge with a rated accuracy of $\pm 0.1\%$ F.S. or ± 1 torr. Once the tube was filled to a total pressure of 1 atm, the mixture was re-circulated through the system using a bellows type re-circulation pump for a sufficient amount of time (about 20 minutes) in order to ensure a homogeneous mixture. A weak spark was used to ignite the mixture.

3.2.2 Experiments Conducted at Low Initial Pressures (0.5 kPa $< P_o <$ 30 kPa)

In the two smaller detonation tubes (65 mm in diameter and 50 mm in diameter), stoichiometric mixtures of acetylene-oxygen, propane-oxygen and hydrogen-oxygen were tested at low initial pressures. Stoichiometric mixtures of acetylene-oxygen with 75% and 80% argon dilution were also tested. In all of these low pressure

Detonation Tube	Driver Mixture	Test Mixture	Sensitivity Parameter
300 mm by 300 mm	H_2-air	same as driver	ϕ
	C_3H_8-air	same as driver	ϕ
	C_2H_4-air	same as driver	ϕ
	C_2H_2-air	same as driver	ϕ
	C_3H_8-O_2-N_2	same as driver	β
	C_2H_4-O_2-N_2	same as driver	β
150 mm diameter	H_2-air	same as driver	ϕ
	C_2H_2-air	same as driver	ϕ
	C_3H_8-O_2-N_2	same as driver	β
	C_2H_4-O_2-N_2	same as driver	β
	H_2-O_2 ($\phi = 1$)	H_2-O_2-N_2	β
	H_2-O_2 ($\phi = 1$)	H_2-air	ϕ
	H_2-air ($\phi = 1$)	H_2-air	ϕ
65 mm diameter	C_2H_2-O_2	same as driver	P_o
	C_3H_8-O_2	same as driver	P_o
	C_2H_2-O_2-80% Ar	same as driver	P_o
50 mm diameter	C_2H_2-O_2	same as driver	P_o
	H_2-O_2	same as driver	P_o
	C_2H_2-O_2-75% Ar	same as driver	P_o

Table 3.2. Summary of driver mixtures, test mixtures and sensitivity parameters that were tested.

experiments, the sensitivities of the mixtures were varied by the changing the initial pressure (rather than by changing the mixture composition).

Each test mixture was prepared beforehand in a separate vessel by the method of partial pressures and allowed to mix for at least 24 hours in order to ensure homogeneity. For any given experiment, the entire tube was initially evacuated to at least 70 Pa and then filled from both ends to the desired initial pressure. The pressure was monitored by an Omega pressure transducer (PX02-I) and a Newport digital meter (IDP). A high energy spark was discharged into the mixture in order to directly initiate a detonation upstream of the perforated plate.

3.3 Diagnostics

3.3.1 Time of Arrival Gauges

For the experiments conducted at $P_o = 1$ atm (in the square tube and in the 150 mm diameter tube), time of arrival measurements were taken using ionization probes and pressure transducers. Ionization probes were used to measure the arrival of regions sufficiently high in ionization (e.g., the arrival of the combustion products). Typically, the ioniziation probes were spaced about one tube diameter apart, although extra ports (spaced about 1/3 of a tube diameter apart) were made in the square tube immediately downstream of the perforated plate in order to obtain better resolution in the time of arrival measurements. Piezoelectric pressure transducers (PCB 113A24) were used to monitor the time of arrival and the pressure rise due to shock waves and detonations. In the square tube, the pressure transducers were placed immediately next to the ionization probes; in the 150 mm diameter tube, the pressure transducers were located diametrically opposite of the ionization probes. This enabled simultaneous measurements of the reaction front and of the shock front to be taken.

Ionization probes and pressure transducers were also used in the 65 mm tube in conjunction with streak schlieren photography. The probes were generally spaced about 4 tube diameters apart from each other.

3.3.2 High Speed Streak Photography

No time of arrival gauges were used in the 50 mm acrylic tube, although a pressure transducer was mounted upstream of the perforated plate to ensure that a CJ detonation was established prior to the reflection from the perforated plate. The wave

processes resulting from the reflection of a detonation from a perforated plate in the acrylic tube were monitored via self-luminous streak photography. The trajectories of luminous wave activity are recorded on film and can be interpreted as an x-t diagram. In general, the shock waves that are generated in the present experiments are not sufficiently strong to illuminate the mixture and, hence, cannot be seen in the streak photographs. A rotating drum streak camera with a constant film velocity of about 0.08 mm/s was used. Depending on the camera lens, a distance up to about 1 m (approximately 20 tube diameters) could be viewed.

For the experiments in the 65 mm diameter steel tube, high speed streak schlieren photographs (using the same rotating drum streak camera described above) were taken in the window section that was mounted immediately downstream of the perforated plate. A double pass schlieren system was used (see Settles 2001 for a description of the setup) and permitted the visualization of density gradients. Therefore, the trajectories of shock waves are visible in the resulting streak photographs.

Chapter 4

Results and Discussion

A large database of experimental results was collected throughout this investigation in four different detonation tubes, using a variety of perforated plates, and testing a range of mixture compositions and sensitivities (see Chapter 3 for specific details). However, only a select amount of results are shown in this chapter and were chosen carefully to represent the entire range of experimental results. Therefore, rather than presenting a description of the results for each apparatus and for each mixture, this chapter is based on the different phenomena that occur when a CJ detonation is reflected from a perforated plate.

4.1 Reflection of a CJ Detonation from a Perforated Plate

Subsequent to the reflection of a CJ detonation from a perforated plate, a shock wave is generated and propagates back upstream in order to slow the flow behind the detonation. A typical self-luminous photograph illustrating this phenomenon is

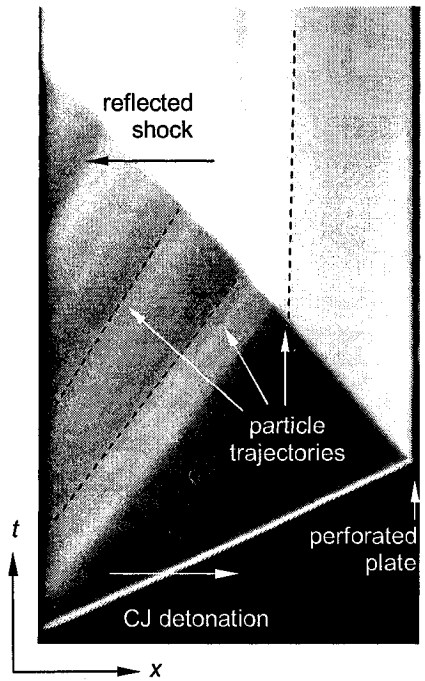

Figure 4.1. Self-luminous streak photograph of the reflection of a detonation from a perforated plate in stoichiometric aceytlene-oxygen at P_o = 10 kPa (D = 50 mm; d = 1.6 mm & 87% blockage).

shown in Fig. 4.1.

The trajectory of the incident detonation (the sharp bright white line with constant slope and luminosity) originates from the bottom left corner of the photograph and propagates towards the perforated plate (the vertical black band on the right hand side of the photograph). The velocity of the incident detonation (about 2280 m/s) is found to correspond very closely to the theoretical Chapman-Jouguet detonation velocity for this particular mixture (2300 m/s).

A typical pressure trace of the incident CJ detonation is shown in Fig. 4.2 for hydrogen-air ($\phi = 0.83$) at $P_o = 1$ atm. The theoretical CJ pressure is shown as the horizontal dashed line. The initial pressure rise corresponds well with the theoretical

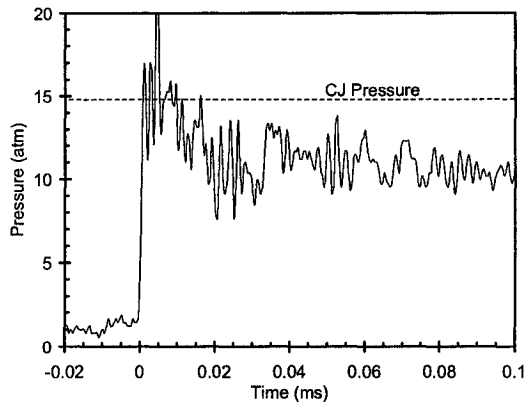

Figure 4.2. Pressure profile of the incident detonation in hydrogen-air ($\phi = 0.83$) at $P_o = 1$ atm ($D = 150$ mm).

value. The pressure can be seen to gradually decrease behind the front as the Taylor wave follows the detonation front. High frequency pressure fluctuations behind the front can be observed with an average period of about 2 μs. This coincides with the natural ringing frequency of the pressure transducer (500 kHz) and appears to be superimposed over lower frequency oscillations with a period of roughly 10 μs. The cell size of this particular mixture is rather large ($\lambda = 17$ mm), which corresponds to a time delay of about 13 μs between successive transverse shock waves (propagating at $M \approx 1.2$ behind the detonation). It is possible that some of these lower frequency fluctuations that are observed in the pressure trace coincide with the arrival of the transverse waves at the pressure transducer.

However, as noted by Edwards *et al.* (1976), the transverse waves behind a detonation decay very rapidly. For example, the transverse waves in hydrogen-oxygen at 100 torr decay completely by 2.5 cell lengths behind the front. This implies that, in the present case, pressure fluctuations due to the transverse waves should not be observed about 40 μs after the arrival of the detonation front. Therefore, the pressure oscillations that persist for longer durations (over 100 μs) after the arrival of the detonation must be attributed to alternative wave phenomena. These pressure

fluctuations may be a result of the interaction of the detonation front with the tube wall, which has been reported previously by Fay (1962), by Edwards *et al.* (1963) and by Desbordes *et al.* (1983). Due to the thermal boundary layer on the tube wall (that acts as a mass sink, producing diverging streamlines), the detonation front becomes curved and the flow behind the front is slightly supersonic. As a result, a series of interacting weak oblique shocks are formed behind the detonation that gives rise to these low frequency oscillations.

It should be noted that for more sensitive mixtures, pressure fluctuations due to transverse waves are generally not observable in the pressure traces. The cell sizes are rather small, and the characteristic frequency of the transverse waves is too high to be recorded by the pressure transducers. For example, the cell size of stoichiometric hydrogen-oxygen at $P_o = 1$ atm is about 1 mm, which corresponds to a frequency of about 1.5 MHz (the frequency response of the pressure transducer is only about 1 MHz). Furthermore, due to the rapid decay of the transverse waves, the accompanying pressure fluctuations should only last a few microseconds behind the detonation front.

Returning to Fig. 4.1, the particle paths behind the incident detonation can be defined by the luminosity of the soot particles, which is sufficiently bright in acetylene-oxygen such that the particle trajectories are visible in the photograph. From their slopes, it can be seen that the particle velocity decreases with increasing distance from the detonation front due to the Taylor expansion fan. The particle trajectories in the Taylor wave behind the incident detonation can be computed and agree with those in the streak photograph.

Since the amount of blockage to the flow that is provided by the perforated plate in the figure is rather large (87% blockage), the flow velocity is almost zero behind the reflected shock wave. For example, at a distance of about 1 tube diameter upstream of the perforated plate, the flow velocity behind the reflected shock wave is reduced

to about 20 m/s from a value of about 800 m/s behind the incident detonation.

The reflected shock wave can also be seen to accelerate slightly in the fixed laboratory frame as it propagates upstream into the Taylor wave of the detonation where the particle velocity is decreasing. The density behind the incident detonation is also decreasing, which will cause the reflected shock wave to amplify. However, the amplitude of the reflected shock wave gradually attenuates as it propagates back into the products as shown in the sequence of pressure profiles in Fig. 4.3. At a distance of about 1.5 tube diameters upstream of the perforated plate, the pressure ratio across the shock wave is about 2.1. Further upstream at 3.5 tube diameters from the perforated plate, it can be seen that the pressure ratio across the reflected shock has decreased to about 1.7. Although the reflected shock wave is seen to accelerate in the laboratory frame, its strength is actually decaying as it propagates into the detonation products. The attenuation of the shock wave formed subsequent to the reflection of a CJ detonation from a solid wall has been previously observed both numerically and experimentally by Shepherd *et al.* (1991). It was found that the reflected shock becomes attenuated due to dissapation mechanisms in the non-ideal flow behind the incident detonation (e.g., multi-dimensional flow due to the transverse shock waves, shock wave/boundary layer interactions, etc.).

4.2 Interface Driven Shock Waves

Following the reflection of the incident detonation from the perforated plate, the combustion products flow through the holes and expand downstream. The simplest case where the downstream gas is inert is considered first and will serve as a reference for the reacting case to be examined later. The idealized steady 1D wave diagram for this case is shown in Fig. 2.1.

Essentially, the interface between the transmitted combustion products and the

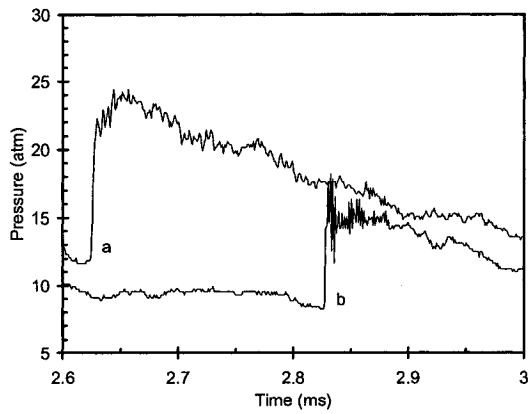

Figure 4.3. Pressure profiles of a reflected shock wave at a) 1.5 and b) 3.5 tube diameters upstream of the perforated plate in hydrogen-air ($\phi = 0.83$) at $P_o = 1$ atm ($D = 150$ mm; $d = 8$ mm & 63% blockage).

downstream gas acts as a piston that drives a precursor shock wave ahead of it. A streak schlieren photograph of the typical non-reacting flow field is shown in Fig. 4.4. A detonation in stoichiometric acetylene-oxygen at $P_o = 3$ kPa is established upstream of the perforated plate (located on the left of the photograph, just out of view). Air (also at $P_o = 3$ kPa) is used downstream of the perforated plate. The precursor shock wave can be clearly seen and is observed to travel at a velocity of about 750 m/s. The interface separating the shocked gas and the combustion products is also clearly visible as a dark band and is found to travel at about 630 m/s. The dark band indicates that there is a steep density gradient across the interface. The pressure and the particle velocity are continuous across the interface, but the temperature and the density are not. The particle trajectories behind the interface can also be seen in the photograph and run roughly parallel to the interface.

Typical measured trajectories of the interface by ionization probes (since there are sufficient ions in the transmitted products to trigger the probes) and the transmitted shock wave by pressure transducers using two different perforated plates are shown in Fig. 4.5. Since the combustion products are the only source of ionization downstream

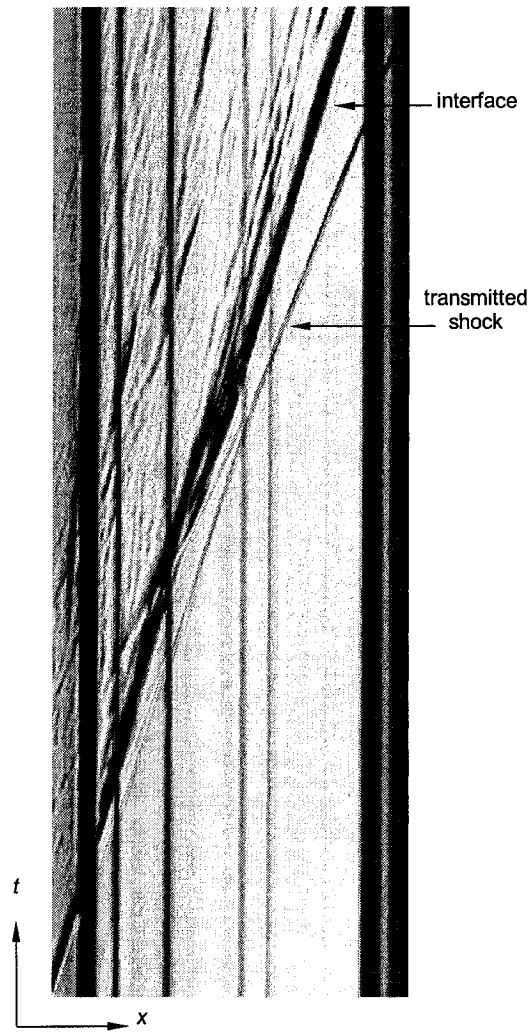

Figure 4.4. Streak schlieren photograph of an interface driving a precursor shock wave in air at $P_o = 3$ kPa ($d = 8$ mm & 61% blockage).

of the perforated plate, the measurements from the ionization probes should coincide with the time of arrival of the interface. It should be noted that mixing at the interface may decrease the ion concentration so that the ionization probe may not indicate the exact location of the interface. The same amount of blockage (64% blockage) is provided by the two different plates although the hole diameters are

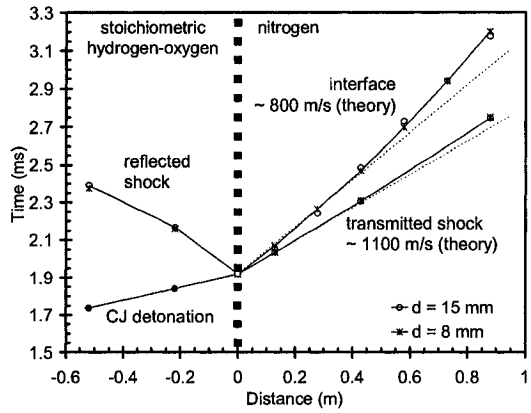

Figure 4.5. Trajectories of the interface and the precursor shock measured by ionization probes and by pressure transducers, respectively (P_o = 1 atm); dotted lines represent theoretical trajectories.

different (d = 8 and 15 mm). The incident detonation in stoichiometric hydrogen-oxygen at P_o = 1 atm is established upstream of the perforated plate (located at $x = 0$) and is found to travel at about 2700 m/s, which is very close to the theoretical CJ value of 2711 m/s. The inert gas that was used downstream of the plate is nitrogen.

It can be seen from the figure that the same flow field is obtained using the two different plates, which indicates that the hole diameter does not affect the pressure drop across the perforated plate (although the turbulence scales in the interface should depend on the details of the hole and spacing configuration). Immediately downstream of the perforated plate in Fig. 4.5, the interface and the precursor shock are found to travel at velocities of 800 m/s and 1100 m/s, respectively. After a distance of about 2.7 tube diameters, both the interface and the precursor shock velocities decay. The expanding combustion products cool by heat loss and by mixing with the cold (albeit shocked) air at the interface; as a result, the interface is less effective as a piston driving the precursor shock, and hence, the precursor shock decays accordingly. When an incident shock wave is reflected from the perforated

plate instead of a CJ detonation, the temperature gradient across the interface is not as severe and the transmitted shock does not decay as rapidly

The theoretical interface and precursor shock trajectories (calculated using an empirical pressure drop coefficient of $k \approx 40$ to model the effect of the perforated plate – see Chapter 2) are shown as the dotted lines in the figure for comparison. It can be seen that the agreement with the experimental results is quite good initially prior to the decay of the two waves, which suggests that the time of arrival measured by the ionization probes coincide with the time of arrival of the interface.

The interface and precursor shock velocities are controlled by the pressure drop across the perforated plate and, hence, by the porosity of the plate. A comparison between the flow fields using two perforated plates with the same hole diameter ($d = 8$ mm) but different porosities (64% and 77% blockage) are shown in Fig. 4.6. The incident detonation velocity in stoichiometric hydrogen-air ($P_o = 1$ atm) is the same for both cases. For the perforated plate with the greater blockage (77% blockage), there is less open area through which the combustion products can flow. As a result, the maximum mass flow rate of the combustion products through the holes of the plate is slower. Correspondingly, both the interface and the precursor shock velocities are noticeably slower at about 550 m/s and 900 m/s, respectively, compared to the case (shown in Fig. 4.5) using the plate with 64% blockage.

It should be noted that the interface is not a one-dimensional boundary that separates the transmitted combustion products from the shocked downstream gas, especially in the near field. From the instantaneous spark schlieren photograph of Skews (2005) shown in Fig. 4.7, the wave processes subsequent to the reflection of a shock wave from a porous plate can be seen. This photograph is taken at an early time after the collision. The interface can be seen driving a precursor shock downstream of the porous plate. It is very clear from the photograph that in the immediate vicinity of the perforated plate, the interface is comprised of individual

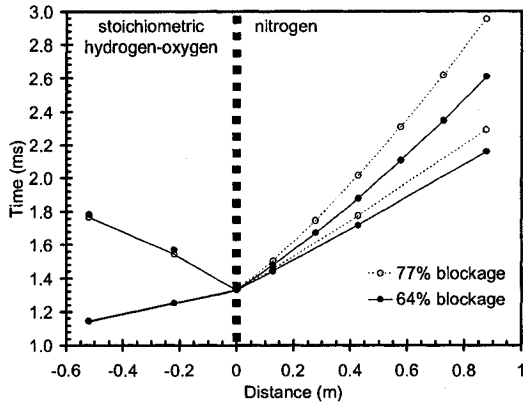

Figure 4.6. The effect of plate porosity on the non-reacting downstream flow field (P_o = 1 atm).

turbulent jets that have characteristic sizes on the order of the hole diameter of the porous plate. At later times, after the turbulent jets have coalesced, the interface becomes diffuse. In the spark schlieren photograph shown in Fig. 4.8, it is clear that the interface is no longer a sharp one-dimensional boundary. The interface, therefore, is actually a turbulent mixing interface where local entrainment and mixing between the transmitted combustion products and the shocked downstream gas occurs.

From the photograph of Skews, it can also be seen that there are significant transverse pressure fluctuations behind the precursor shock wave, which is due to the interaction of the blast waves from the individual holes of the perforated plate. These transverse pressure fluctuations can be observed in the sequence of pressure profiles shown in Fig. 4.9 for different positions downstream of the perforated plate.

In the first pressure trace located at a distance of 0.7 tube diameters from the perforated plate, the initial pressure rise time can be seen to be about 4 μs. This roughly corresponds to the time it takes for the precursor shock wave (traveling at 1100 m/s) to traverse the diameter of the pressure transducer itself. The theoretical pressure rise is indicated by the horizontal dotted line. It can be seen that the initial

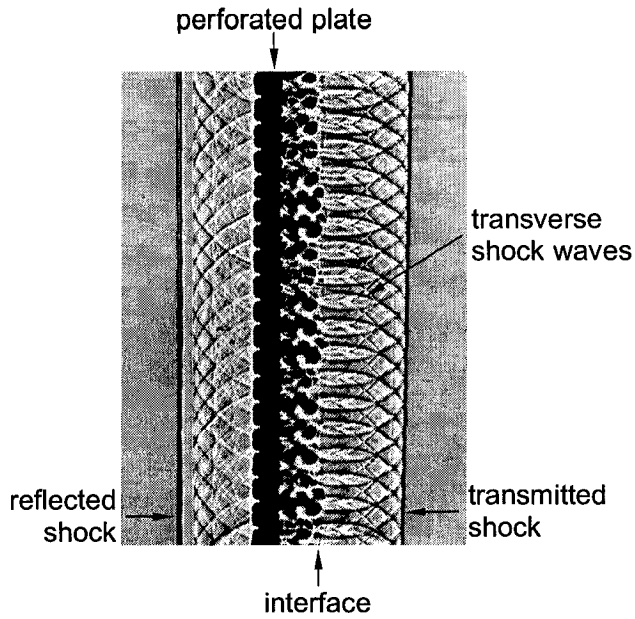

Figure 4.7. Spark schlieren photograph subsequent to the reflection of a shock wave from a porous plate (Skews 2005).

pressure rise corresponds well with the theoretical value. The arrival of the interface as measured by an ionization probe is indicated by the vertical dashed line.

A high frequency oscillation with an average period of about 2-3 μs can be seen, which seems to correspond to the natural frequency of the pressure transducer (500 kHz). A low frequency fluctuation with a period of about 17 μs can be observed between the precursor shock and the interface. For a 1100 m/s shock traveling in nitrogen, the sound speed in the shocked gas is about 600 m/s. Assuming that the transverse waves propagate at the local sound speed and are spaced a hole diameter apart (8 mm in this case), the time between the arrival of successive transverse waves is about 13 μs. Therefore, it appears that these low frequency fluctuation correspond roughly to the arrival of transverse waves generated by the interaction of the blast waves from the individual holes of the perforated plate. The pressure rise due to

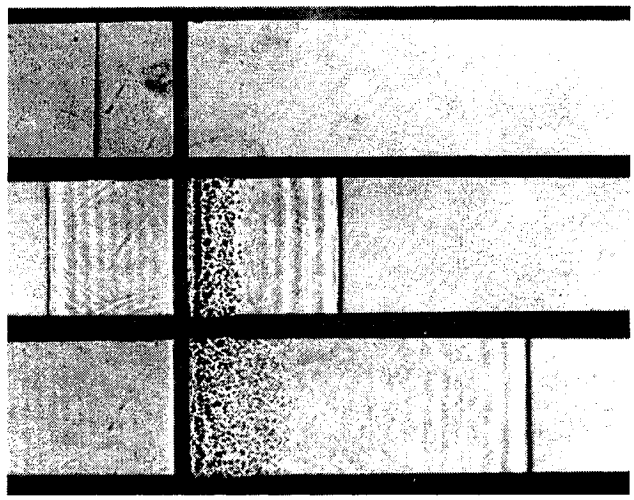

Figure 4.8. Sequence of spark schlieren photographs of the interaction of a shock wave with a porous plate (Reichenbach 1963).

the transverse fluctuations is rather small, indicating that the transverse pressure fluctuations are acoustic waves.

In the next pressure trace located further downstream at a distance of 2.7 tube diameters from the perforated plate, the initial pressure rise can be seen to correspond closely to the theoretical value for a shock traveling at 1100 m/s in nitrogen (denoted by the horizontal dotted line). The arrival of the interface (as measured by ionization probes)is indicated by the vertical dashed line. Pressure fluctuations with a period of about 15 to 30 μs can be observed between the precursor shock and the interface that also seem to correspond to the frequency of the transverse pressure fluctuations generated by the holes of the perforated plate.

By 5.7 tube diameters downstream of the perforated plate, the precursor shock has decayed. The theoretical pressure rise–now for a weaker shock traveling at about 1000 m/s in nitrogen–is indicated by the horizontal dotted line. The pressure rise that is obtained experimentally is well below this theoretical value. It should be

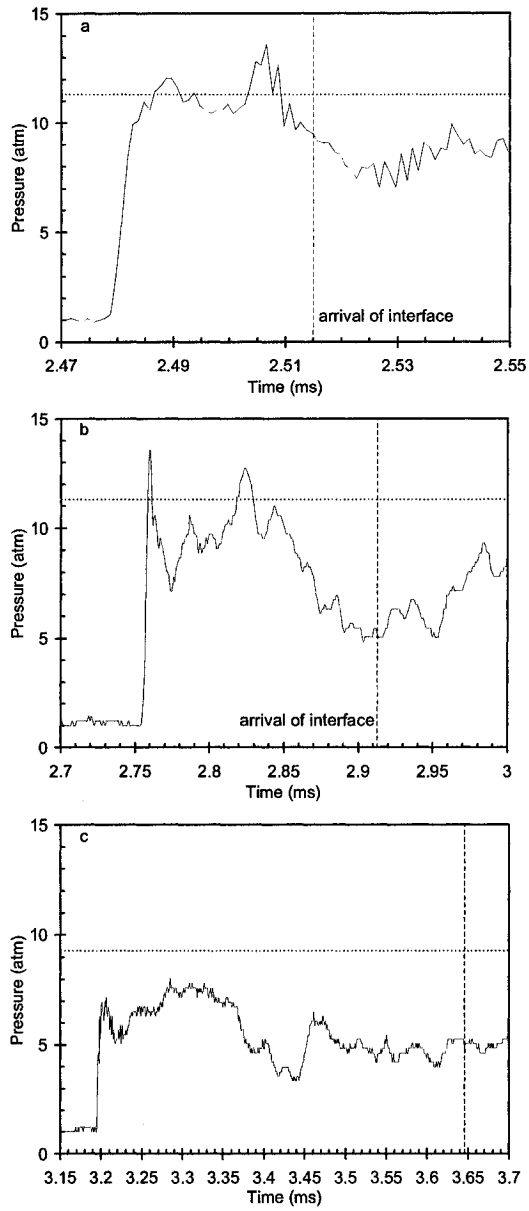

Figure 4.9. Pressure profiles of a precursor shock wave driven by an interface in air at a) 0.7, b) 2.7 and c) 5.7 tube diameters downstream of the perforated plate ($P_o = 1$ atm; $D = 150$ mm; $d = 8$ mm & 64% blockage).

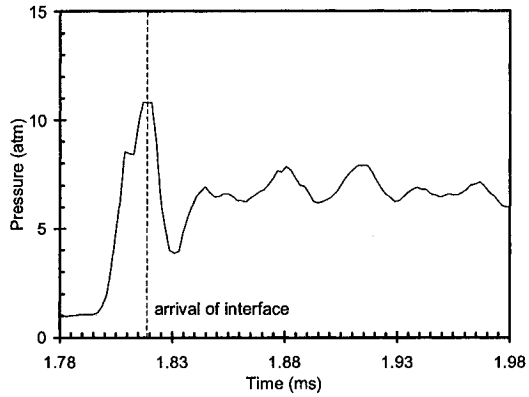

Figure 4.10. Pressure profile of an interface driving a precursor shock wave using a perforated plate with $d = 15$ mm and $l = 15$ mm; transverse wave fluctuations on the order of the dimensions hole spacing of the perforated plate.

noted that the pressure fluctuations behind the precursor shock still persist at such a long distance from the perforated plate, indicating that although the turbulence from the perforated plate may have decayed, the transverse pressure waves that are generated downstream of the perforated plate can still be maintained by reflections from the tube wall.

It is interesting to note that the period of the pressure fluctuations vary depending on the characteristics of the hole diameter and of the hole spacing. For example, a pressure trace is shown in Fig. 4.10 for a perforated plate with larger holes and wider spacing between the holes ($d = 15$ mm and $l = 15$ mm). It can be seen that the period of the fluctuations are now about 30 μs. For a 1000 m/s shock in nitrogen, the sound speed in the shocked gas is about 550 m/s. If the transverse wave spacing is of the order of the hole diameter (15 mm), the time between successive transverse waves is about 27 μs, which corresponds closely to the observed period of the pressure fluctuations.

Therefore, when the gas downstream of the perforated plate is inert, the velocities of the interface and the precursor shock are controlled by the porosity of the

perforated plate. The interface can be considered as a turbulent zone where mixing occurs. In addition to the vorticity from the jets emerging from each hole, the turbulence in the flow includes significant transverse pressure fluctuations that can persist for several tube diameters even as the interface velocity and the precursor shock wave decay.

4.3 Chemical Reactions at the Interface

Prior to investigating the conditions required for the onset of detonation using a detonable mixture downstream of the perforated plate, slightly reactive mixtures are used in an attempt to produce only a small perturbation on the non-reacting flow field where air or nitrogen was used. When a reactive mixture is used downstream, ignition will occur first at the interface as the shocked unburned mixture is entrained and mixed with the combustion products.

For a strictly one-dimensional interface where it is assumed that no mixing occurs, a reaction front (i.e., a flame) will begin to propagate away from the interface at a velocity that is controlled by the propagation mechanism of the flame (an idealized one-dimensional wave diagram is shown of this case in Fig. 2.5). However, the present results indicate that in the slightly reactive case, the interface becomes a highly turbulent three-dimensional reactive "mixing zone," and the idealized picture of an interface with a thin flame front ahead of it is not obtained experimentally. In fact, it is difficult to discern a distinct flame front from the interface itself. The boundary between the transmitted combustion products and the shocked unburned mixture is now a diffuse reacting turbulent mixing zone.

This is confirmed in the streak schlieren photographs shown in Figs. 4.11a and 4.11b where a distinct flame front ahead of the interface cannot be seen. In Fig. 4.11a, only a slightly reactive mixture of stoichiometric acetylene-oxygen diluted with 80%

argon is used (P_o = 20 kPa). The precursor shock wave can be clearly seen and is measured to propagate at about 700 m/s. The interface (the dark band at the back end of the wave structure in the photograph) is found to travel at 450 m/s. This corresponds very closely to the theoretical values calculated for a non-reacting flow field in acetylene-oxygen with 80% argon dilution. In Fig. 4.11b, the mixture is stoichiometric acetylene-oxygen at a very low initial pressure (P_o = 0.6 kPa). A similar flow field as in the case of the non-reacting interface is also observed. The interface and the precursor shock velocities are found to be 500 m/s and 700 m/s, respectively. It can be seen from both of these photographs that even when chemical reactions occur at the interface, a distinct flame front that propagates away from the interface cannot be observed. Instead, only a reacting turbulent interface that drives the precursor shock wave is obtained.

It is interesting to note that even when reactive mixtures are used downstream, the velocity of the reacting turbulent interface does not increase with increasing sensitivity of the downstream mixture. In Fig. 4.12, the upstream mixture is stoichiometric hydrogen-oxygen at P_o = 1 atm for all of the cases shown. Downstream, the black dots represent the non-reacting case where only nitrogen is used. Three other cases of stoichiometric hydrogen-oxygen with varying amounts of nitrogen dilution (all at P_o = 1 atm) are shown for comparison. The nitrogen concentration is denoted by β, which is the ratio of nitrogen to oxygen in the mixture (for hydrogen-air, the value of nitrogen dilution is $\beta = 3.76$).

It can be seen that the interface trajectories for values of $6.1 < \beta < 8.0$ are essentially similar to the non-reacting interface trajectory in pure nitrogen. The reacting interface velocities are still observed to be about 800 m/s. The precursor shock velocities for the reacting case appear to be slightly faster than that for the non-reacting case (about 7% faster). This may be both a gasdynamic effect in addition to the chemical energy that is released at the interface, although the conversion of

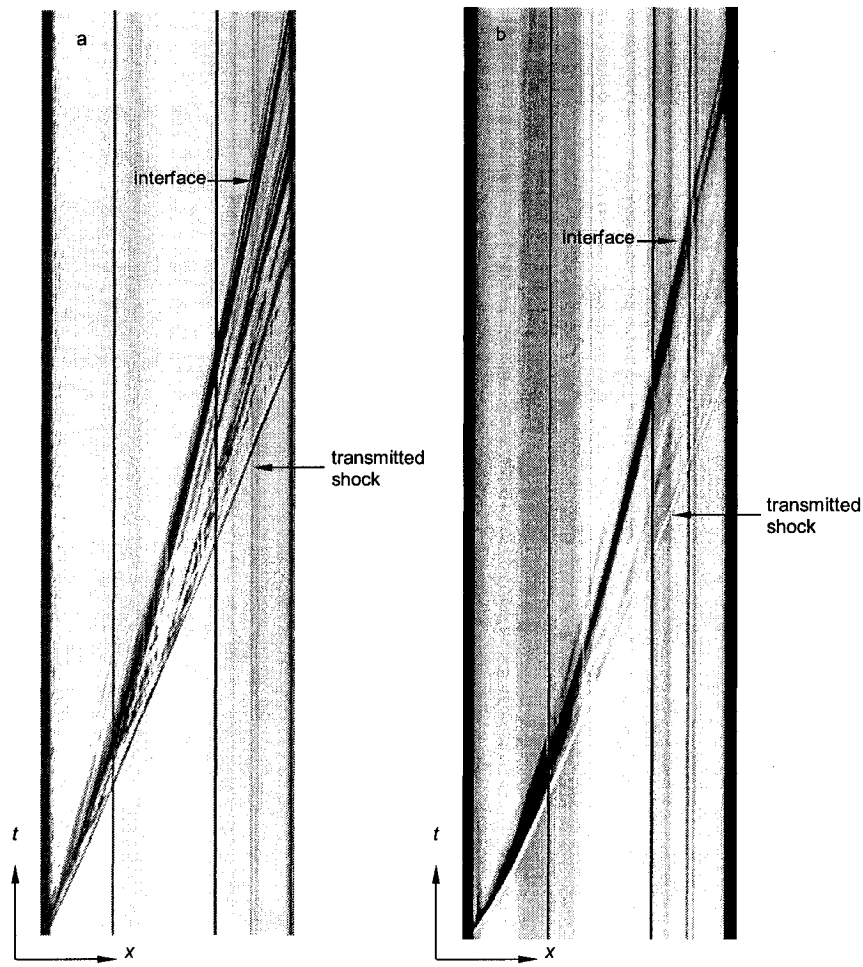

Figure 4.11. Streak schlieren photographs of reacting interfaces driving precursor shock waves in stoichiometric acetylene-oxygen mixtures a) diluted with 80% argon at P_o = 20 kPa and b) at $P_o = 0.6$ kPa.

the chemical energy release to mechanical work of the driving interface is small.

Since pressure is more sensitive than wave velocities, a sequence of pressure profiles for the case of $\beta = 8$ is shown in Fig. 4.13. The arrival of the reacting interface (as measured by ionization probes) in each trace is denoted by the vertical dashed line. In general, the pressure traces are found to be very similar to the non-reacting

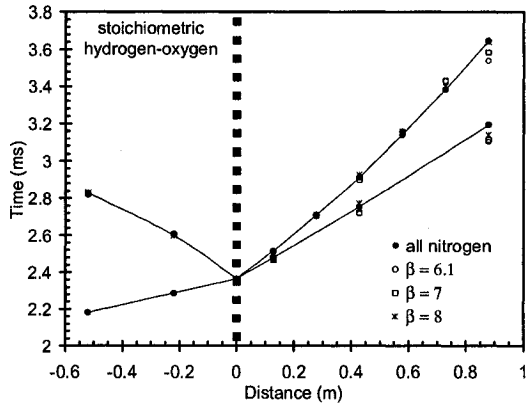

Figure 4.12. Comparison of flow fields using stoichiometric hydrogen-oxygen mixtures downstream of the perforated plate with varying amounts of nitrogen dilution ($d = 8$ mm & 64% blockage).

pressure profiles shown in Fig. 4.9. Even the magnitude of the pressure rise is comparable to the non-reacting case, which indicates that the chemical energy release does not contribute significantly to the gasdynamic flow field of the interface and precursor shock wave.

In the first pressure trace located at 0.7 tube diameters, the arrival of the interface occurs about 20 μs sooner than in the non-reacting case (refer to Fig. 4.9). However, in the second and third pressure traces located at 2.7 and 5.7 tube diameters, the arrival of the interface occurs just slightly later (about 30 to 40 μs) than in the non-reacting case. Since ionization probes are used to detect the time of arrival of the reacting interface (and since the interface is not a planer boundary), there can be some variation in the time at which they are triggered. Nonetheless, this time delay is actually very small and suggests that although there are chemical reactions that occur at the interface, the interface trajectory does not differ much from the non-reacting case.

Pressure fluctuations with about the same frequency as those observed in Fig. 4.9

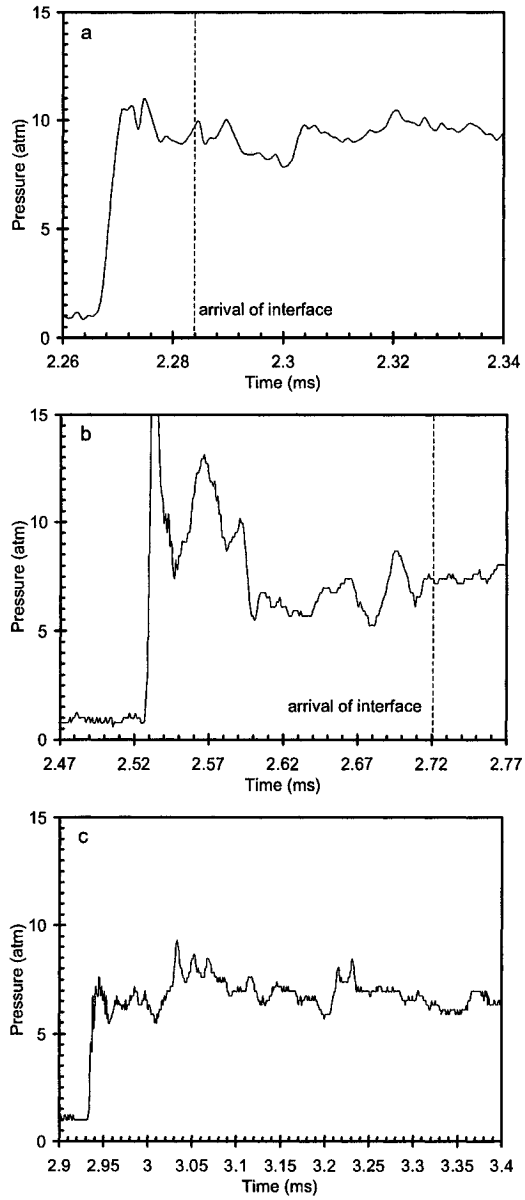

Figure 4.13. Pressure profiles of a reacting interface driving a precursor shock wave in stoichiometric hydrogen-oxygen-nitrogen (β = 6.1) at a) 0.7, b) 3.7 and c) 5.7 tube diameters downstream of the perforated plate (D = 150 mm; d = 8 mm & 64% blockage; P_o = 1 atm.

can be seen in the present pressure profiles, indicating the arrival of transverse pressure fluctuations (generated by the interaction of individual blast waves from each hole of the perforated plate) at the pressure transducer are similar to the non-reacting case. In the pressure profile at 5.7 tube diameters, more distinct pressure fluctuations can be observed compared to the non-reacting case, which suggests that, in addition to the reflection of the transverse waves from the tube wall, the pressure fluctuations may be enhanced by the chemical reactions that occur at the interface.

Thus, it can be seen that for slightly reactive mixtures, the resulting flow field is similar to the that obtained in the non-reacting case (i.e., the velocities of the reacting interface and of the precursor shock wave are essentially the same).

4.4 CJ Deflagration Waves

The flow field of a reacting interface following a precursor shock wave is observed for a wide range of mixture sensitivities until a certain critical mixture composition is obtained downstream. Beyond this critical mixture, a sudden change in the downstream flow field occurs. Instead of a reacting interface, a high speed deflagration is now observed to propagate at a relatively constant velocity of about $\frac{1}{2}V_{CJ}$. In some mixtures, this high speed turbulent deflagration is seen to be able to sustain itself at a steady velocity for a rather long duration.

A comparison between a reacting interface and a high speed turbulent deflagration is shown in Fig. 4.14. In both cases, the same upstream mixture (stoichiometric hydrogen-oxygen at $P_o = 1$ atm) and perforated plate are used. For the case of the reacting interface, the downstream mixture is stoichiometric hydrogen-oxygen-nitrogen with a nitrogen dilution of $\beta = 6.1$. When the amount of nitrogen dilution of the downstream hydrogen-oxygen-nitrogen mixture is decreased slightly to a value of $\beta = 6.0$ to make the mixture slightly more sensitive, a high speed deflagration wave

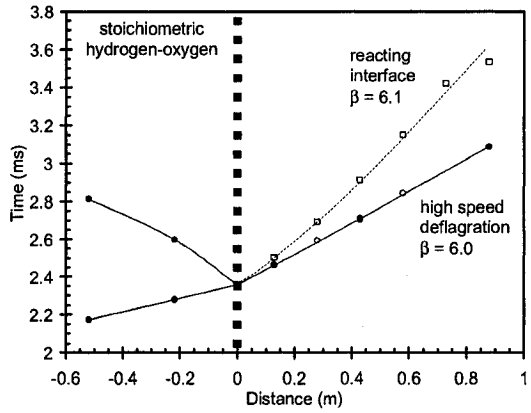

Figure 4.14. Comparison of a reacting interface with a high speed turbulent deflagration in stoichiometric hydrogen-oxygen-nitrogen at $P_o = 1$ atm.

is now observed. Both the reaction zone and the precursor shock of the deflagration wave travel at almost the same velocity of about 1200 m/s, which is roughly the $\frac{1}{2}V_{CJ}$ value for the given mixture.

The deflagration velocity is not observed to increase gradually from the reacting interface velocity to the $\frac{1}{2}V_{CJ}$ value when the mixture sensitivity is increased. Instead, a sudden jump to the $\frac{1}{2}V_{CJ}$ velocity is observed to occur spontaneously, which suggests that there is a sudden switch in the propagation mechanism between a turbulent reacting interface and the high speed deflagration. If the mixture is made more sensitive (by decreasing β in this case), the deflagration velocity does not increase but remains about the $\frac{1}{2}V_{CJ}$ value. In fact, when the sensitivity of the mixture is increased, the sudden transition from a deflagration travelling at $\frac{1}{2}V_{CJ}$ to a detonation occurs after a certain distance.

It appears that the $\frac{1}{2}V_{CJ}$ velocity is the maximum possible deflagration velocity that can be obtained, which also corresponds to the theoretical CJ deflagration velocity. Therefore, it seems that the high speed turbulent deflagrations that are observed in the present investigation are CJ deflagrations, and the driving mechanism

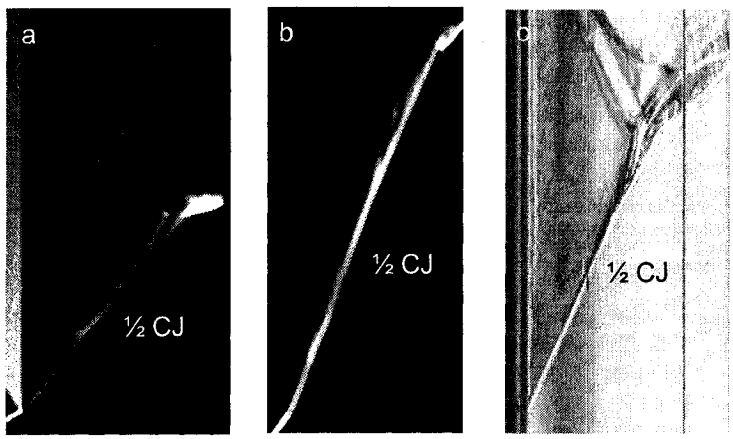

Figure 4.15. CJ deflagration velocities in stoichiometric acetylene-oxygen using different tube dimensions and perforated plate characteristics: a) $D = 50$ mm; $d = 1.6$ mm & 87% blockage; $P_o = 7$ kPa, b) $D = 50$ mm; $d = 2.4$ mm & 69% blockage; $P_o = 2$ kPa and c) $D = 65$ mm; $d = 8$ mm & 75% blockage; $P_o = 3.5$ kPa .

is controlled only by the energetics of the mixture. In other words, the CJ deflagration velocity of $\frac{1}{2}V_{CJ}$ should be observed experimentally regardless of the tube and perforated plate configurations.

Photographs from experiments conducted in stoichiometric acetylene-oxygen at low initial pressures are shown in Fig. 4.15 for different tube dimensions and perforated plate characteristics (hole diameter, hole spacing, and cross-sectional area over which the plate is perforated). For the three cases shown in the figure, it can be seen that a high speed turbulent deflagration wave always propagates at a relatively constant velocity around the $\frac{1}{2}V_{CJ}$ value. The hole diameter and spacing–and, therefore, the turbulent length scales that are generated downstream–are all different for the perforated plates that are shown in the figure. As well, since the amount of blockage that is provided to the flow varies from 69% blockage to 87% blockage, the downstream interface velocities and turbulence intensities also vary from plate to plate (the interface velocities in the non-reacting case range from 300 to 700 m/s). Nevertheless, a deflagration wave propagating at about $\frac{1}{2}V_{CJ}$ is observed regardless

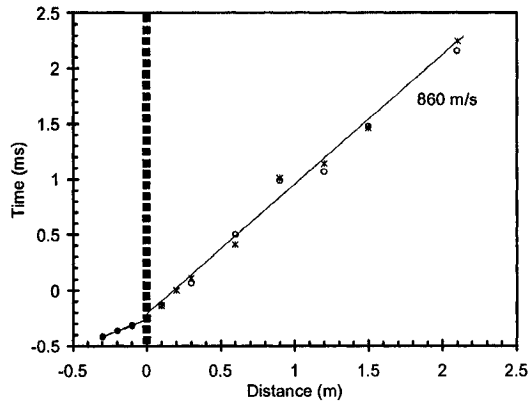

Figure 4.16. CJ deflagration velocity in stoichiometric acetylene-air at $P_o = 1$ atm in the 300 mm by 300 mm square tube ($d = 5$ mm & 69% blockage).

of the turbulence that is generated by the perforated plate and of the back boundary of the interface velocity.

A typical flow field obtained in the 300 mm by 300 mm square detonation tube is shown for stoichiometric acetylene-air in Fig. 4.16. The velocity of the deflagration downstream of the perforated plate is measured to be about 850 m/s. Although this value is lower than the velocities observed in more sensitive mixture fuel-oxygen mixtures, it still corresponds closely to the $\frac{1}{2}V_{CJ}$ value (0.45 V_{CJ} in this particular case).

The CJ deflagration velocity is also obtained even in the case where the incident detonation upstream of the perforated plate is varied. The flow field using an incident stoichiometric hydrogen-oxygen detonation at $P_o = 1$ atm ($V_{CJ} = 2840$ m/s) is shown in Fig. 4.17 and compared to the flow field using a stoichiometric hydrogen-air detonation upstream ($V_{CJ} = 1970$ m/s). The temperature of the detonation products is much greater in hydrogen-oxygen than in hydrogen-air (3680 K compared to 2945 K). As well, the sound speed of the detonation products is also greater in hydrogen-oxygen (1540 m/s compared to 1090 m/s in hydrogen-air). However, a de-

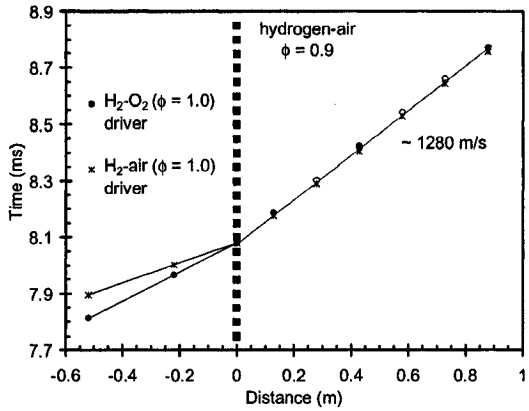

Figure 4.17. Comparison of downstream flow fields in hydrogen-air ($\phi = 0.9$) using a stoichiometric hydrogen-oxygen versus a stoichiometric hydrogen-air driver upstream ($d =$ 8 mm & 77% blockage; $P_o = 1$ atm).

flagration velocity of 1280 m/s is obtained downstream in both cases, indicating that the CJ deflagration velocity is obtained regardless of the thermodynamic properties of the combustion products of the driver mixture and the interface properties.

Based on these results, it seems that the high speed turbulent deflagrations observed in the present study are CJ deflagrations that propagate at the maximum $\frac{1}{2}V_{CJ}$ velocity independently of initial turbulence parameters (from the perforated plate) and of the interface velocity. Turbulent transport rates do not control the propagation velocity of the high speed turbulent deflagrations, which are instead energetically driven at the maximum deflagration velocity (i.e., the expansion of the combustion products drives the deflagration front forward at the $\frac{1}{2}V_{CJ}$ velocity).

The structure of a CJ deflagration wave can be seen in Fig. 4.18 where a typical self-luminous streak photograph of a CJ deflagration is shown in conjunction with a typical streak schlieren photograph. It should be noted that the photographs were not taken from the same experiment; however, the juxtaposition of the two photographs is helpful in the analysis and interpretation of the phenomenon.

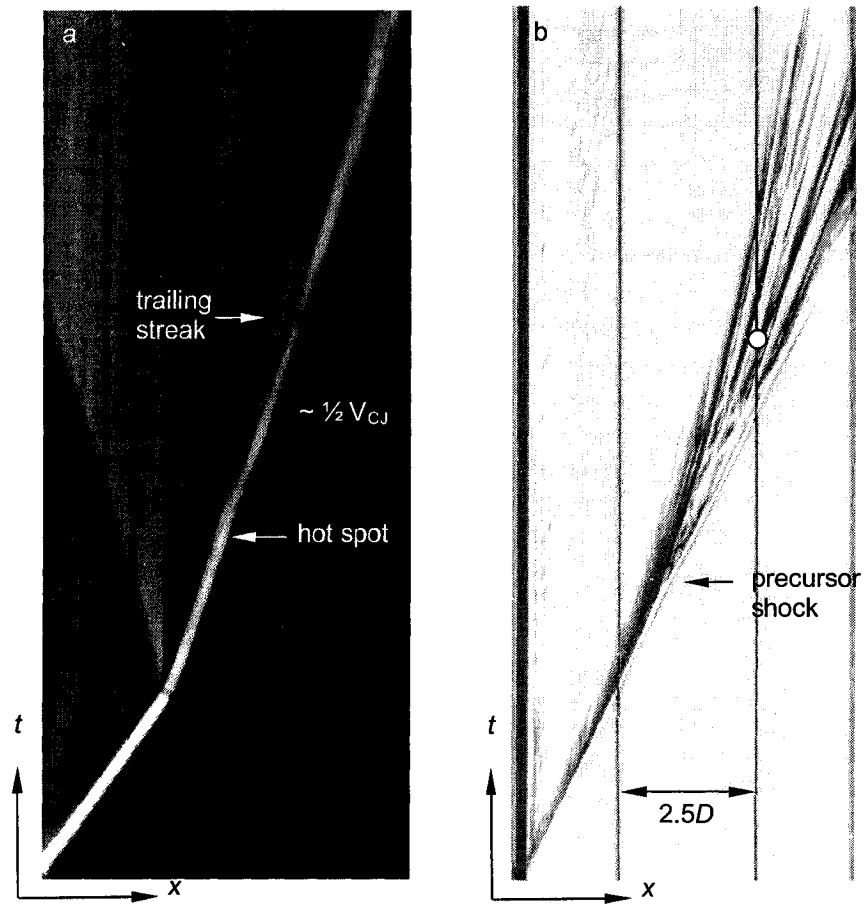

Figure 4.18. a) Self-luminous streak photograph of a CJ deflagration in stoichiometric acetylene-oxygen at P_o = 3 kPa (d = 1.6 mm & 69% blockage) and b) streak schlieren photograph of a CJ deflagration in stoichiometric acetylene-oxygen at P_o = 3 kPa (d = 5 mm & 80% blockage) .

In the self-luminous streak photograph, the luminous streak of the deflagration wave can be seen to travel at a relatively constant velocity of about 1200 m/s (about $\frac{1}{2}V_{CJ}$) for the entire field of view of the camera (about 9 tube diameters). Some hot spots, indicating intense localized reactions within the reaction zone, can be identified at the luminous front. In the accompanying streak schlieren photograph, a fan-like wave structure can be seen. The precursor shock coincides with the leading

edge of the wave structure and is measured to also propagate at about 1200 m/s. Similar to the results shown in Fig. 4.14, the reaction zone and the precursor shock wave are found in the photographs to propagate at roughly the same velocity.

The time of arrival of the reaction zone as measured by an ionization probe is indicated by the white dot in the streak schlieren photograph. It can be seen that the time of arrival measured by the ionization probe is located within the fan-like wave structure and most probably coincides with the back end of the reaction zone where ionization is the highest. This suggests that the majority of the chemical reactions take place within the extended reaction zone. However, black and white streaks (indicating varying densities) can be observed behind the reaction zone, which appear to coincide with the particle trajectories of burning reactants in various stages of reaction. Similar features can be seen in the self-luminous photograph where trailing luminous streaks recede from the main luminous front. This indicates that the deflagration wave is not comprised of a thin flame but rather an extended turbulent reaction zone. This is similar to the structure of a turbulent flame this is comprised of an extended reaction zone rather than a collection of laminar flamelets (Summerfield *et al.* 1955). It should be noted that turbulence in the reaction zone is comprised of both vorticity and transverse pressure fluctuations. The effect of an expansion wave can be seen in the trajectories of the streaks behind the main deflagration front: they become steeper with increasing distance from the deflagration front.

The expansion wave behind the deflagration front can be seen more clearly in the sequence of downstream pressure profiles shown in Fig. 4.19 for a hydrogen-oxygen-nitrogen mixture with $\beta = 5$. The arrival of the reaction front as measured by ionization probes is shown as the vertical dashed line. It can be seen that the reaction front arrives almost immediately behind the precursor shock wave in all three profiles, which indicates that the precursor shock and the reaction zone propagate at roughly the same velocity, similar to a CJ detonation. The theoretical arrival

interface is shown as the vertical dotted line in the first two traces. In the last pressure trace located at 5.7 tube diameter downstream of the perforated plate, the interface is not shown since it arrives much later in time.

In the first pressure trace located at 0.7 tube diameters downstream of the perforated plate, the pressure rise is rather sharp with a rise time of about 2 μs. The arrival of the reaction front follows shortly, and there is a gradual decrease in the pressure until the arrival of the interface. The interface lags closely behind the deflagration front (there is a time delay of about 30 μs between the precursor shock and the interface), and as a result, only high frequency fluctuations (500 kHz or a period of 2 μs) can be discerned between the precursor shock and the interface.

In the second pressure profile located at 3.7 tube diameters, the initial pressure rise across the precursor shock is similar to the first trace. Subsequent to the arrival of the reaction front, there is another sudden increase in pressure, which may be a result of the chemical energy released in the reaction zone. This is then followed by a decrease in pressure, which suggests that there is an expansion wave that follows the reaction zone to meet the back boundary at the interface (now following much farther behind). Therefore, it appears that for a high speed turbulent deflagration, rapid chemical reactions take place in an extended reaction zone that follows closely behind the precursor shock wave. The subsequent expansion of the combustion products seems to drive the deflagration front forward.

In the last pressure trace located at 5.7 tube diameters, it can be seen that although the initial pressure rise is not as high as that seen in the first two profiles, the constant volume explosion pressure (indicated by the horizontal dashed line) in the reaction zone is still maintained. This indicates that rapid chemical reactions are continually taking place in the reaction zone. Large fluctuations can also be observed within 40 μs of the arrival of the precursor shock, indicating that the pressure fluctuations are enhanced by fast chemical reactions. The interface now

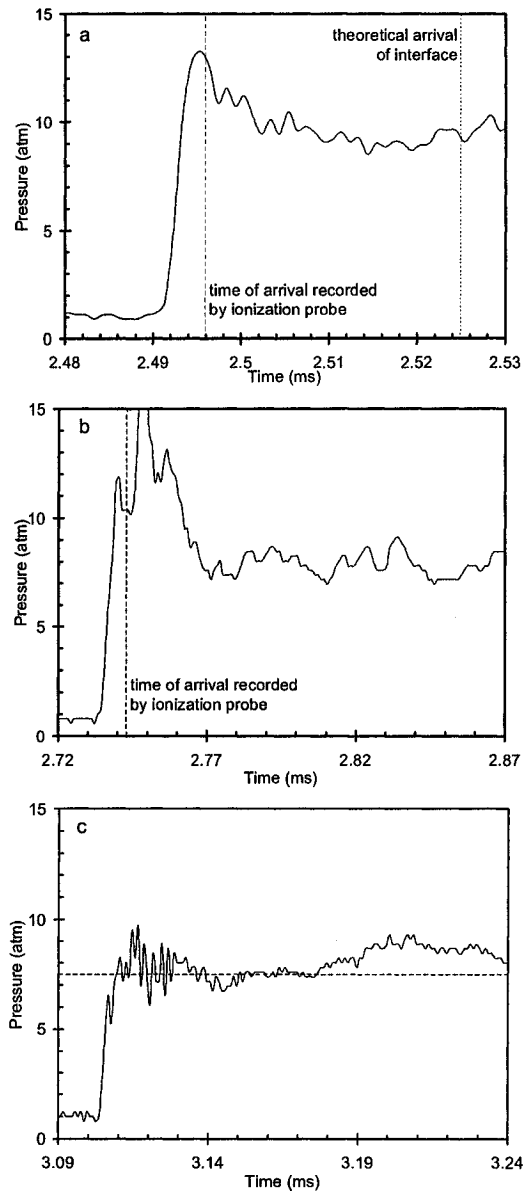

Figure 4.19. Pressure profiles of a CJ deflagration in stoichiometric hydrogen-oxygen-nitrogen ($\beta = 5$) at a) 0.7, b) 2.7 and c) 5.7 tube diameters downstream of the perforated plate ($P_o = 1$ atm; $D = 150$ mm; $d = 8$ mm & 64% blockage).

follows very far behind the front and does not appear to have any influence on the behaviour of the deflagration front itself.

It thus appears that a high speed turbulent deflagration–or a CJ deflagration–that propagates at $\frac{1}{2}V_{CJ}$ is comprised of a precursor shock wave followed very closely by an extended turbulent reaction zone. The deflagration front is driven forward by an expansion wave behind the reaction zone. This is reminiscent of the extended reaction zones of high speed turbulent deflagrations and quasi-detonations in obstacle filled tubes that were observed in previous studies (Teodorczyk 1988 & 1990, Chao & Lee 2003). These waves were also found to be driven by the expansion of the combustion products like a CJ detonation. However, unlike a CJ detonation, auto-ignition was achieved through turbulent mixing due to the shear layers and to the transverse waves generated by the obstacles.

In the same respect, the CJ deflagration waves that are observed in the present study are analogous to CJ detonations as they are energetically driven by the expansion of the combustion products in the reaction zone. In contrast to a CJ detonation, the extended reaction zone of a critical deflagration is not coupled to the leading shock wave. The strength of the leading shock is only about $M \approx 3$, and the temperature behind it is generally about 800 to 900 K. This corresponds to an induction time of the order of 1 s, which is insufficient to cause auto-ignition via adiabatic shock compression on the time scale of the experiment. Therefore, in contrast to the shock ignition mechanism for a detonation, the turbulent reaction zone of the CJ deflagration must provide its own ignition mechanism in order to achieve sufficiently fast reaction rates that can quickly build up the pressure (for example, to the constant volume explosion pressure) in the reaction zone. The subsequent expansion of the high pressure combustion products drives the deflagration front forward. Therefore, on the one hand, a CJ deflagration is driven by the expansion fan in its wake like a CJ detonation; on the other hand, the ignition and reaction mechanisms are not due

to shock heating from the precursor shock but perhaps to intense turbulence in the reaction zone (which is comprised of transverse pressure fluctuations in addition to vorticity).

4.4.1 Auto-Ignition via Rapid Turbulent Mixing

As the initial turbulence in the interface decays and as the interface recedes from the deflagration front, the plate generated turbulence can no longer be responsible for ignition at distances greater than a few tube diameters downstream of the perforated plate. Furthermore, since the present experiments are conducted in smooth tubes, there are no obstacles in the path of the critical deflagration that can generate compressible turbulence (i.e. transverse pressure fluctuations in addition to vorticity). Therefore, in order for the CJ deflagration velocity to be persist for such a long duration, it seems that the reaction zone itself must provide the mechanism by which turbulence can be generated and maintained.

The mixtures that have been tested so far in the present investigation are all considered to be "unstable" mixtures since they display irregular detonation cell patterns. This has been found to a characteristic of reactions rates (or, equivalently, the reaction zone length to the induction zone length as in the recent study of Ng *et al.* 2005) that are highly sensitive to temperature fluctuations. Due to the initial plate generated turbulence (the turbulent eddies and the transverse pressure fluctuations), there are regions or pockets at different temperatures that are created in the unburned mixture. The higher temperature regions have correspondingly fast reaction rates whereas the lower temperature regions have correspondingly slow reaction rates. As a result, local explosions (hot spots) occur in the high temperature regions. These local hot spot can be seen as bright spots in the reaction zone in self-luminous streak photographs (Fig. 4.18). This is similar to the "mild ignition"

mechanism discussed previously by Oppenheim et al. (1985). The energy released by the local explosion centres are incoherent in time and space, creating gasdynamic instabilities within the reaction zone.

The confinement of the tube also serves to maintain transverse pressure fluctuations as the transverse waves reflect from the tube walls. Furthermore, the coupling between the transverse pressure fluctuations and the chemical energy release can be achieved via Rayleigh's criterion where sound waves are amplified due to chemical energy release (Oran 1984). It has been shown for mixtures with high activation energies (i.e., unstable mixtures) that when the acoustic waves are coupled to the chemical kinetics, the fluctuations in the reaction rates become even more pronounced, which leads to the amplification of acoustic waves as energy is released (Clarke 1977, Choi & Majda 1989, and Toong 1972). As the transverse waves amplify and traverse the reaction zone, there is a mismatch of pressure and density gradients, generating vorticity through the baroclinic torque mechanism.

Therefore, the CJ deflagration is energetically driven and propagates by autoignition due to turbulent mixing. The initial turbulence from the perforated plate is maintained by the reaction zone itself since the mixture is sufficiently temperature sensitive. The transverse pressure fluctuations can be thus maintained and amplified in a confined tube, which sustains the propagation of the CJ deflagration for a long distance. This is similar to the idea of the "flame generated turbulence" that has been previously investigated for turbulent flames (Libby & Williams 1994).

4.5 Onset of Detonation

Essentially, a detonation propagates as a result of the proper resonant coupling between the transverse pressure waves and the chemical reactions. When the transverse waves are attenuated and the resonant coupling is destroyed, the CJ detonation fails

and a CJ deflagration is observed instead (Teodorczyk *et al.*, Dupré *et al.*, Radulescu & Lee). Therefore, in order for the CJ deflagration wave to transit back to a CJ detonation, the resonant coupling must be regained and the characteristic transverse wave structure of a detonation must be regenerated.

The successful coupling of transverse waves with the chemical energy release can be brought about by the classic "explosion within an explosion" mechanism of Oppenheim. A self-luminous streak photograph and a streak schlieren photograph depicting typical cases of successful onset of detonation are shown in Fig. 4.20. In both photographs, critical deflagration waves propagating at about $\frac{1}{2}V_{CJ}$ can be observed prior to the onset of detonation. The final onset originates at a point from a localized explosion that occurs somewhere in the turbulent reaction zone. The blast wave generated by this localized explosion then amplifies to form a "detonation bubble," which eventually expands and engulfs the precursor shock to form a fully-established detonation wave. Characteristic retonation waves (the blast wave from the local explosion propagating upstream into the burned products) that accompany the onset of detonation are evident in both photographs. As well, between the detonation front and the retonation wave, the reflection of the blast wave from the tube walls can be seen in both the self-luminous streak and the streak schlieren photographs.

A sequence of spark schlieren photographs taken at McGill University are shown in Fig. 4.21 to illustrate the genesis of the detonation following the reflection of a detonation upstream from porous media (which is equivalent to a perforated plate). In the first frame that is shown, a CJ detonation in stoichiometric propane-oxygen has already been reflected from the porous media. The combustion products emerge downstream through the space between each circle, and a precursor shock is driven ahead of the emerging detonation products. In the second frame 14.2 μs later, the emerging detonation products have coalesced and have formed a quasi-one-dimensional

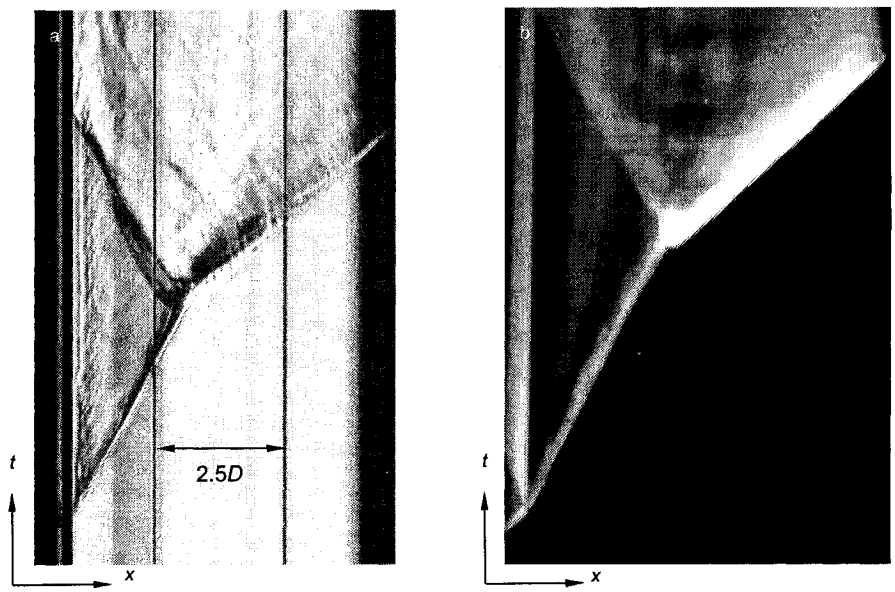

Figure 4.20. a) Streak schlieren photograph of the onset of detonation in stoichiometric acetylene-oxygen at $P_o = 3.5$ kPa ($d = 5$ mm & 80% blockage) and b) Self-luminous streak photograph of the onset of detonation in stoichiometric acetylene-oxygen at $P_o = 6$ kPa ($d = 1.6$ mm & 87% blockage).

interface. Ahead of the interface, a CJ deflagration propagates at a velocity of about 1100 m/s. The leading shock is followed closely by the reaction zone, and the two waves appear to propagate as together as a single CJ deflagration front with transverse waves trailing behind the front. The characteristic spacing between the transverse waves correspond to the dimension of the circles (or, equivalently, to the spacing between the holes of a perforated plate). In the third frame, local explosions can be seen to occur in the critical deflagration front. They eventually grow and amplify into a fully-developed detonation. By the last frame, a CJ detonation that propagates at about 2100 m/s can be seen. The interface appears to be almost stationary in the sequence of photographs and does not affect the propagation of the critical deflagration or the subsequent onset of detonation.

The direct initiation of a detonation via turbulent mixing was first demonstrated

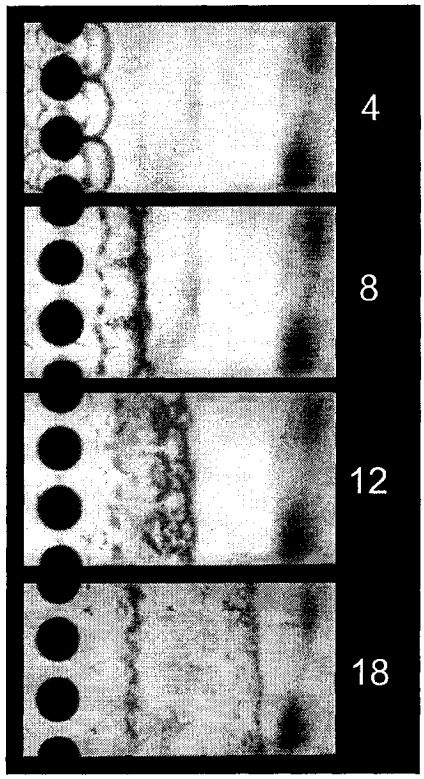

Figure 4.21. Sequence of spark schlieren photographs of the onset of detonation originating from a local explosion in the turbulent reaction zone of a critical deflagration wave (stoichiometric propane-oxygen at $P_o = 7.73$ kPa). Photograph taken at McGill University.

in the pioneering experiments of Knystautas et al. (1979), which inspired numerous subsequent studies of direct initiation by turbulent jet mixing. (Üngüt & Schuff 1989, Carnasciali *et al.* 1991, Inada *et al.* 1992, Dorofeev *et al.* 1996). The pioneering work of Knystautas et al. demonstrated for the first time that direct initiation does not necessarily require a sufficiently strong shock waves (to cause thermal dissociation and free radical production) in order to promote auto-ignition.

A sequence of pressure profiles are shown in Fig. 4.22 where the onset of detonation occurs just downstream of the second pressure transducer location. In the first pressure profile, the pressure ratio across the precursor shock can be seen to about 10.

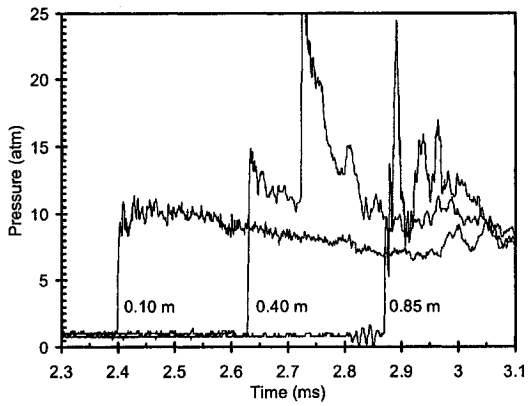

Figure 4.22. Pressure profiles leading to the onset of detonation in stoichiometric hydrogen-oxygen-nitrogen ($\beta = 4$; $D = 150$ mm); $d = 15$ mm & 63% blockage.

There are significant pressure fluctuations in the reaction zone ahead of the interface. By the second pressure trace, the precursor shock can be seen to have amplified, and the pressure ratio across the precursor shock is now greater at about 15. After a time delay of about 90 μs, a sudden increase in pressure can be observed. In this case, the onset of detonation occurred just downstream of the pressure transducer, and the second sudden pressure rise that is observed corresponds to the arrival of the retonation wave.

It is interesting to note that the onset of detonation does not always occur via a localized explosion centre. In Fig. 4.23, a streak schlieren photograph is shown where the onset of detonation appears to occur spontaneously ahead of the turbulent reaction zone. The genesis of the detonation is not accompanied by a bright hot spot or by a characteristic retonation wave. This suggests that, in this case, the onset of detonation does not occur via the classic local explosion that amplifies and drives a strong blast wave. Instead, the conspicuous absence of the retonation wave seems to indicate that pressure waves (with small density gradients compared to those across a detonation or a strong shock wave) are maintained and amplified through through the continual reflection from the tube walls and through resonance with

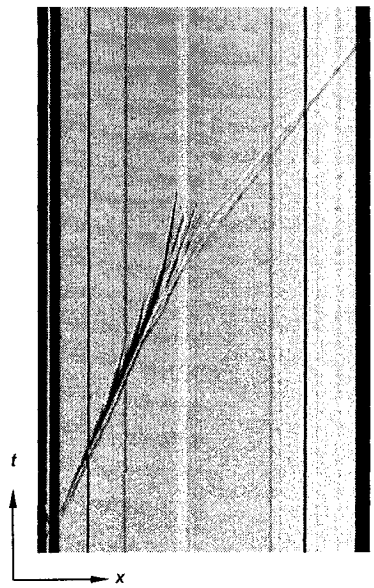

Figure 4.23. Streak Schlieren photograph of the progressive amplification of transverse waves that leads to the onset of detonation in stoichiometric acetylene-oxygen; $P_o = 2.75$ kPa; $D = 65$ mm; $d = 5$ mm & 80% blockage.

the chemical energy release as they traverse the reaction zone. At the onset of detonation, the eventual acoustic coupling with the reaction zone via the Rayleigh criterion is achieved through the gradual amplification of transverse pressure waves. This is similar to the amplification mechanism in galloping detonation where the low velocity phase re-accelerates to an overdriven detonation. This has been illustrated in the pressure traces of Moen *et al.* (1981).

4.5.1 Run-up to Onset

It can be seen that once the critical deflagration velocity (or the CJ deflagration velocity) is achieved, it must be maintained for a sufficient duration in order for the resonant coupling between the transverse waves and the chemical energy release to occur. Therefore, the run-up distance to onset (i.e., the distance from the perforated

plate to the onset of detonation) is an induction period during which the proper conditions for the onset of detonation are generated.

The run-up distance (RUD) to the onset of detonation for various test series are shown in Figs. 4.24a to c as a function of D/λ where D is the tube diameter and λ is the characteristic detonation cell size and a measure of the sensitivity of the mixture. In general, RUD's are shorter when perforated plates with larger holes and less blockage are used. However, it can also be seen from these figures that, for a given mixture sensitivity (denoted by D/λ since the tube diameter is fixed in each graph), the RUD is not entirely reproducible, which indicates that the incubation time required to achieve the appropriate resonant coupling between acoustic waves and chemical reactions for DDT varies from shot to shot.

For each perforated plate and tube dimension tested, it can be seen that the RUD increases slightly with decreasing sensitivity (or decreasing value of D/λ). At a critical value of D/λ (and, hence, a critical mixture sensitivity), the RUD increases abruptly, which seems to indicate that there may be a change in the mechanism responsible for the transition from deflagration to detonation.

For mixtures that are more sensitive than the critical value, the onset of detonation occurs within a few tube diameters (2 or 3 tube diameters) downstream from the plate. Within a couple of tube diameters from the perforated plate, the interface has not yet receded from the critical deflagration wave. Therefore, near the plate, there is essentially a mixing interface (or mixing zone) between the combustion products (from the upstream detonation) and the shocked unburned downstream mixture. The turbulent length scales and intensities in the mixing zone are controlled by the dimensions of the perforated plate (hole spacing, hole diameter, blockage of the plate). If the mixing conditions at the turbulent interface are appropriate, then the onset of detonation can occur from a localized explosion.

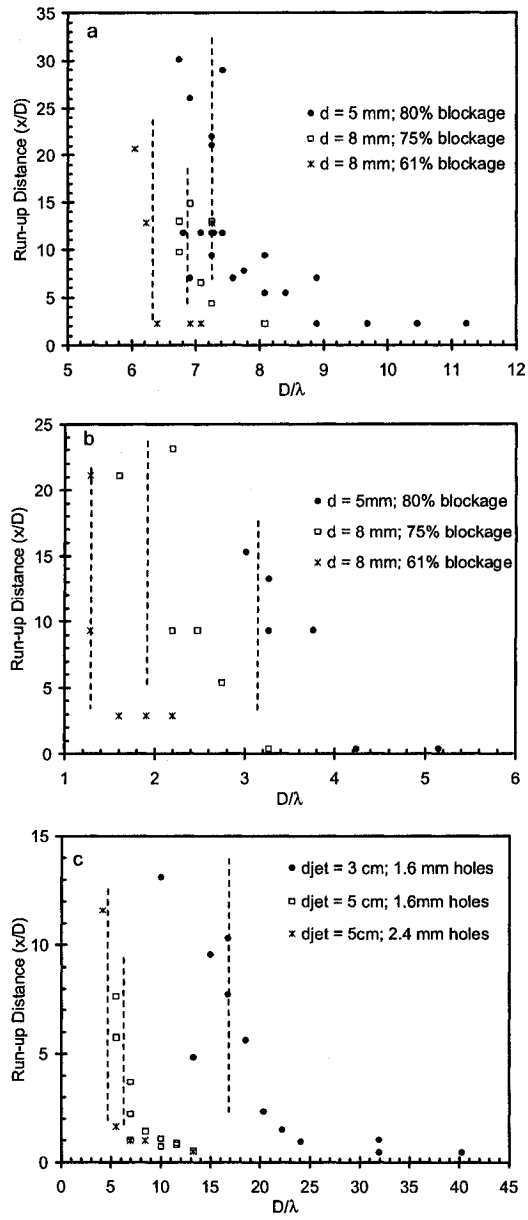

Figure 4.24. Run-up distance as a fucntion of D/λ in: a) stoichiometric acetylene-oxygen, b) stoichiometric propane-oxygen (both $D = 65$ mm) and c) stoichiometric acetylene-oxygen ($D = 50$ mm).

When the onset of detonation occurs far from the perforated plate (more than 2 to 3 tube diameters), the interface has receded completely from the critical deflagration wave. It is now unlikely that the turbulence from the perforated plate plays a role in the onset of detonation. Instead, the critical deflagration must rely on its own ignition mechanism, and the run-up distance to detonation becomes essentially an incubation period during which the instabilities in the reaction zone grow.

For the different fuel-air and fuel-oxygen-nitrogen mixtures that were tested, it appears that the onset of detonation always occurs relatively close to the perforated plate (within 4 tube diameters). This is in stark contrast to the experiments conducted with sensitive fuel-oxygen mixtures where the quasi-steady critical deflagration wave can propagate for very long distances prior to the onset of detonation. Although this may seem to suggest that there is a difference in behaviour between fuel-air and fuel-oxygen mixtures, it appears that small perturbations to the flow (i.e. the ionization probes) can trigger the onset of detonation to occur prematurely. The effect of an ionization probe on the onset of detonation is shown in Fig. 4.25 for a hydrogen-air mixture at $\phi = 1.4$. When ionization probes are placed 0.1, 0.2, and 0.3 m downstream of the perforated plate, the onset of detonation is observed to occur immediately after the first ionization probe. If the ionization probe at 0.1 m is removed such that the first ionization probe is now located 0.2 m downstream of the perforated plate, a quasi-steady deflagration wave can be seen to propagate at about $\frac{1}{2}V_{CJ}$ for about 2 tube diameters. The onset of detonation is delayed, and a fully-established detonation is now recorded by the ionization probe located at 3 tube diameters. If all the ionization probes are removed, a critical deflagration wave is observed to propagate at $\frac{1}{2}V_{CJ}$ for the entire test section. It can be seen that the critical deflagration wave is meta-stable and can be easily perturbed to trigger the onset of detonation.

There are also cases where the critical deflagration wave does not lead to the

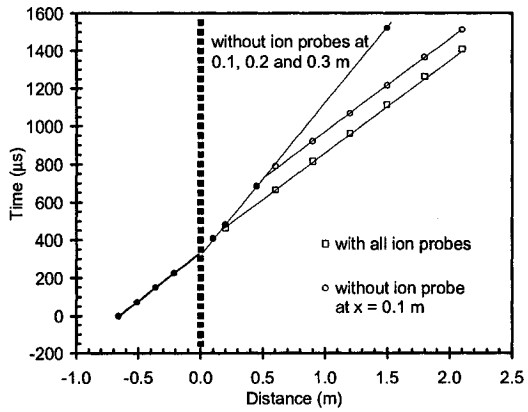

Figure 4.25. The effect of a small perturbation on the critical deflagration wave in hydrogen-air ($\phi = 1.4$; $D = 150$ mm; $d = 8$ mm & 64% blockage).

onset of detonation and propagates quasi-steadily at the $\frac{1}{2}V_{CJ}$ value for the entire length of the test section. It is not clear if the CJ deflagration eventually transits to a detonation or decays to a reacting interface as either the tube was not long enough or the field of view of the camera was not wide enough. A sequence of pressure traces shown in Fig. 4.26 for a stoichiometric propane-oxygen mixture at $P_o = 2.5$ kPa. The incident CJ detonation that was reflected upstream from the perforated plate is also shown for reference. It can be seen that in each successive pressure trace, the pressure rise of the deflagration front increases. Although the onset of detonation is not observed in this particular experiment, the deflagration wave is amplifying as it propagates downstream of the perforated plate, indicating that coupling between the pressure waves and the chemical reactions may eventually be reached. Given a longer test section, it appears that the critical deflagration wave may successfully transit to a detonation.

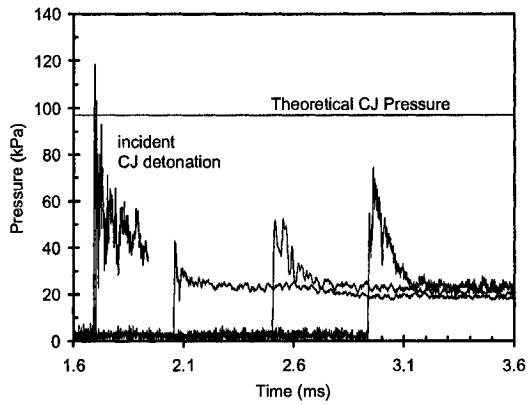

Figure 4.26. Pressure amplification in stoichiometric propane-oxygen at $P_o = 2.5$ kPa ($D = 65$ mm; $d = 5$ mm & 80% blockage).

4.5.2 Onset of Detonation in Stable Mixtures

Once the critical deflagration wave is established downstream of the perforated plate, the onset of detonation will not necessarily occur. The CJ deflagration velocity must be maintained in order for the transition to detonation to take place. Otherwise, the critical turbulent deflagration wave will decay and the onset of detonation will not be possible. Stable mixtures have regular detonation cell patterns with weak transverse waves, indicating that the reaction rates are insensitive to temperature perturbations (Radulescu *et al.* 2002, Ng *et al.* 2005). Therefore, once the turbulence from the perforated plate decays, the reaction zone should not be able to sustain and generate the instabilities that are required for the proper acoustic coupling with the chemical reactions (and, hence, for the propagation) of critical deflagration waves.

The successful onset of detonation is only observed in stable mixtures when it occurs near the perforated plate (within a few tube diameters) before the plate generated turbulence decays. Typical streak schlieren and self-luminous streak photographs are shown in Fig. 4.27. It can be seen that in both cases, the onset of detonation occurs within 2 tube diameters of the perforated plate. As well, in both

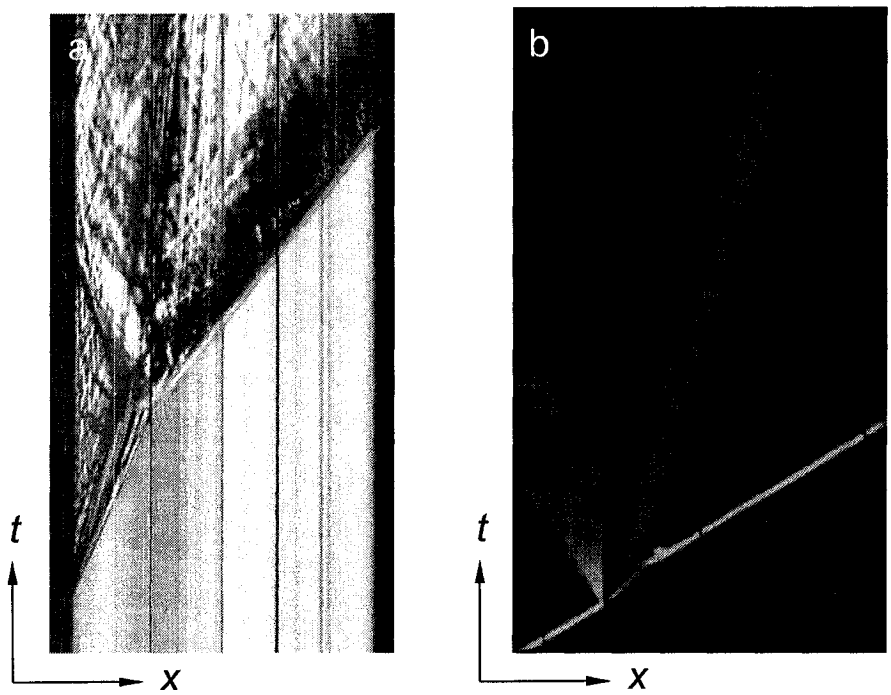

Figure 4.27. Photographs of the onset of detonation in stoichiometric acetylene-oxygen diluted with argon: a) streak schlieren photograph with 80% argon dilution ($P_o = 30$ kPa; $D = 65$ mm; $d = 5$ mm & 80% blockage)and b) self-luminous streak photograph with 75% argon dilution ($P_o = 18$ kPa; $D = 50$ mm; $d = 1.6$ mm & 69% blockage).

cases, it appears that the interface has not receded completely from the deflagration front, which suggests that the turbulence generated by the perforated plate is required to trigger the onset of detonation. Onset always appears to be accompanied by a retonation wave, which indicates that a strong local explosion is required to generate a sufficiently strong blast wave. This is perhaps similar to Oppenheim's "strong ignition" mechanism. If the power pulses from local explosions near the plate are coherent, then a sufficiently strong blast wave can be generated and then amplified into a fully-developed detonation.

If the CJ deflagration velocity cannot be maintained, the onset of detonation will not occur. A typical self-luminous streak photograph and a typical streak schlieren

photograph are shown in Fig. 4.28 for a stoichiometric mixture of acetylene-oxygen with 75% and 80% argon dilution, respectively. In the self-luminous photograph, it appears that the interface ignites a reaction zone that propagates at about $\frac{1}{2}V_{CJ}$ for a very short distance of less than a tube diameter. After a few tube diameters, the reaction zone dies out and there is no more evidence of luminosity from the reaction zone in the self-luminous streak photograph. In the streak schlieren photograph, the interface can be seen to drive a precursor shock wave. Although there appears to be regular wave activity ahead of the interface and behind the precursor shock, the transverse pressure fluctuations are insufficient to cause auto-ignition. In contrast to unstable mixtures where acoustic waves are amplified by energy release, the acoustic waves in mixtures with low activation energies (i.e., stable mixtures) can become attenuated due to chemical energy release (Clarke, Choi & Majda, Toong). As the transverse pressure fluctuations become attenuated, the intense turbulence from the perforated plate cannot be maintained and, thus, the fast reaction rates that are required to quickly pressure the reaction zone cannot be maintained. As a result, the reaction zone decays and chemical reactions occur due to turbulent transport at the interface.

A sequence of two downstream pressure traces are shown for an unsuccessful case of detonation onset in a stable mixture of stoichiometric acetylene-oxygen with 80% argon dilution (P_o = 15 kPa) in Fig. 4.29. In the first pressure trace located at 0.5 tube diameters downstream of the perforated plate, the pressure rise is relatively fast with a rise time of about 4 μs. The pressure increases to an average of about 100 kPa. There high frequency pressure fluctuations between the precursor shock and the arrival of the interface (denoted by the vertical dashed line) that correspond to a period of about 2 μs. In the second pressure trace located at 1.3 tube diameters downstream of the perforated plate, it can be seen that the precursor shock is beginning to decay. The rise time is much slower at about 50 μs. Also, the average pressure rise is slightly lower around 80 kPa.

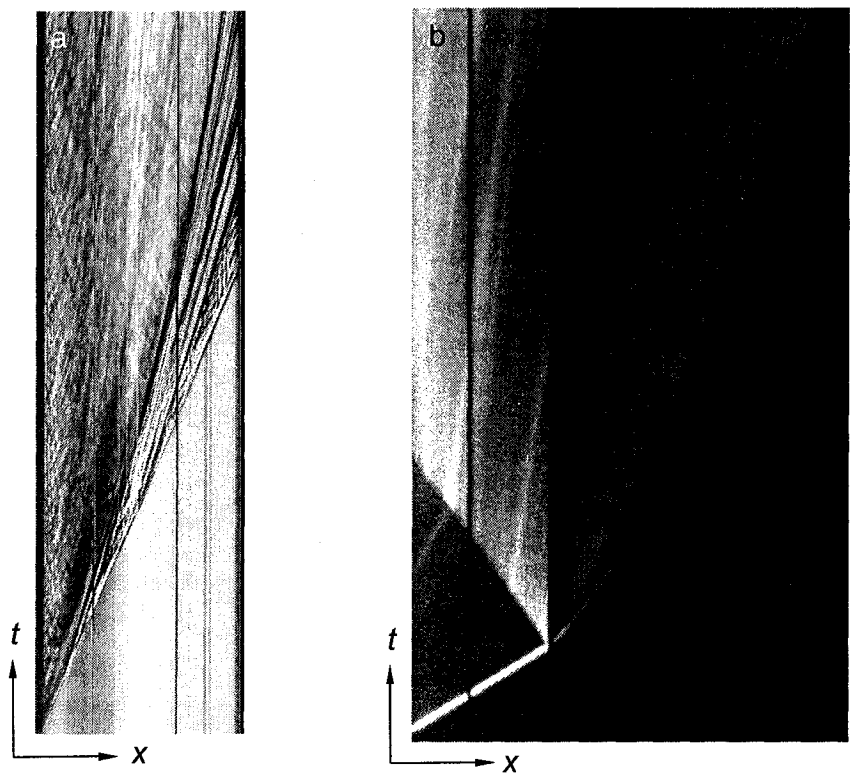

Figure 4.28. Unsuccessful onset of detonation in stoichiometric acetylene-oxygen diluted with argon: a) streak schlieren photograph with 80% argon dilution (P_o = 30 kPa; D = 65 mm; d = 5 mm & 80% blockage)and b) self-luminous streak photograph with 75% argon dilution (P_o = 18 kPa; D = 50 mm; d = 1.6 mm & 69% blockage).

4.5.3 Critical Conditions for Onset

It has been argued by Lee (1986) that the criterion for successful transition from deflagration to detonation may coincide with the detonability limits, which is the most conservative criterion for DDT. If the initial and boundary conditions of a particular experiment are outside the detonability limits, it should not be possible for DDT to occur at all. Kogarko and Zel'dovich (1948) proposed the detonability limits to be $\pi D \approx \lambda$ where πD corresponds to the lowest acoustic mode of the tube and λ is the characteristic detonation cell size of the mixture (representing the

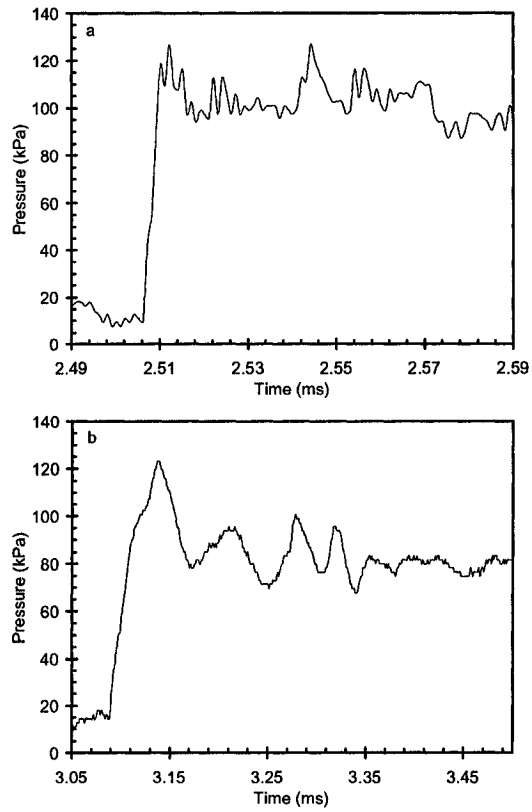

Figure 4.29. Pressure profiles for stoichiometric acetylene-oxygen with 80% argon dilution at a) 0.5 and b) 1.3 tube diameters downstream of the perforated plate (D = 65 mm; d = 8 mm & 75% blockage).

periodicity of the chemical reactions). Although a precise quantitative correlation cannot be formulated from the present data, the results indicate that, in general, $D > \lambda$ is required for the successful onset of detonation to occur. This implies that the tube dimension compared to the chemical length scale provides the basis for a critical correlation for successful onset. This correlation appears to describe correctly the necessary conditions for the final onset of detonation if one considers that the ultimate condition for transition from a critical deflagration wave requires that the acoustic wave fluctuations and the chemical energy release to be resonantly coupled.

Chapter 5

Concluding Remarks

It can be concluded from the present experimental investigation that the criterion required for DDT in a smooth tube is a deflagration wave that propagates at the maximum possible deflagration velocity of a CJ deflagration. Theoretically speaking, the CJ deflagration velocity is independent of boundary conditions and is controlled only by the energetics of the given mixture like a CJ detonation due to the sonic condition behind the reaction zone. Experimentally, the CJ deflagration velocity is observed within a narrow range between 800 to 1200 m/s (depending on the given mixture) and is obtained regardless of tube characteristics, turbulence scales and intensities, as well as the thermodynamic and chemical properties of the combustion products that are transmitted downstream. Therefore, similar to a CJ detonation, a CJ deflagration is driven by the expansion of the combustion products behind the wave.

However, unlike a CJ detonation, the leading shock of a CJ deflagration is too weak to auto-ignite the mixture via adiabatic shock compression. Instead, the rapid burning of the mixture behind the precursor shock wave must be due to turbulent mixing between the combustion products and the shocked unburned mixture that is

entrained into the extended turbulent reaction zone of the critical deflagration. In the present experimental configuration, the turbulence is initially provided by the perforated plate but decays rapidly downstream. Therefore, in order for a critical deflagration wave to propagate for an extended distance (of more than a few tube diameters) in a smooth tube, the deflagration itself must provide its own turbulence generating mechanism to achieve rapid combustion and thus rapid pressurization of the reaction zone (such that the subsequent expansion of the combustion products can drive the front forward). In unstable mixtures where the reaction rates are extremely sensitive to temperature fluctuations, the initial plate generated turbulence (i.e., vorticity and pressure fluctuations) can be maintained through chemical instabilities and the coupling of the transverse pressure fluctuations with the reaction zone. On the other hand, in stable mixtures that are less sensitive to temperature fluctuations, the initial turbulence cannot be maintained downstream and the initially high speed deflagration front will decay to sub-critical velocities.

It is now well-established that self-propagating detonations in most explosive mixtures require the resonant coupling between the transverse wave fluctuations and the chemical energy release. The results of the present study indicate that these transverse waves can be developed from the amplification of the pressure fluctuations in the turbulent mixing zone of a CJ deflagration, thereby effecting the onset of detonation. The amplification process follows the Rayleigh criterion for the phase relationship between pressure and reaction rate fluctuations and requires a sufficiently long duration in order achieve resonant coupling. Transverse pressure fluctuations are continually reflected from the tube wall, and as they repeatedly traverse the reaction zone, they become further amplified by the chemical energy release. This mechanism is similar to that of a galloping detonation where transverse pressure fluctuations amplify in the low velocity phase until the buildup to an overdriven detonation occurs. It should be noted that the progressive amplification of transverse pressure fluctuations is a gradual process and can only be achieved in a confined tube

where pressure fluctuations can be maintained by reflection from the tube walls. An alternative mechanism of the onset of detonation can be due to a local explosion in the turbulent reaction zone that rapidly amplifies via the SWACER mechanism into a detonation. In this case, the onset of detonation is accompanied by a characteristic retonation wave from the blast wave of the local explosion.

It can also be concluded from this study that the tube dimension is an important criterion for successful DDT. Since transverse waves must be generated and coupled to the chemical reactions, the tube dimension must be sufficiently large compared to the chemical length scale of the mixture (i.e., $D/\lambda > 1$). The present results confirm this criterion. A more precise quantitative correlation for the successful transition from a CJ deflagration to a CJ detonation may involve the detonability limits. For a given mixture, the limiting tube diameter for a detonation to propagate was found to be $\pi D \approx \lambda$. For the onset of detonation to occur, it is clear that the detonation limit must be satisfied. If a self-sustained detonation cannot propagate in a given tube geometry, then the onset of detonation also cannot be obtained.

Contributions to Original Knowledge

Although it has been identified implicitly in previous studies on DDT, the critical deflagration velocity required for the onset of detonation in smooth tubes has not been explicitly studied before. Therefore, the main contribution of the present work is the demonstration that a critical deflagration wave propagating at a velocity of the order of the CJ deflagration velocity is required for the onset of detonation.

Experimentally, the CJ deflagration velocity is not controlled by turbulent transport rates (which depend on boundary conditions) but depends on the energetics of the mixture instead. Therefore, like a CJ detonation, a critical CJ deflagration wave is driven by the expansion of the combustion products. In contrast to a CJ detona-

tion where auto-ignition results from shock heating, the ignition mechanism of a CJ deflagration is controlled by rapid turbulent mixing and requires intense turbulence in the reaction zone for rapid combustion.

It is also established in the present investigation that the sustained propagation of a CJ deflagration in a smooth tube is achieved when the turbulence (vorticity and pressure fluctuations) in the reaction zone is maintained by temperature sensitive mixtures via "flame generated turbulence." The transverse waves that are required for a self-sustained detonation to propagate can be generated via amplification of the pressure fluctuations in the turbulent reaction zone of a CJ deflagration via the Rayleigh criterion, thereby achieving the onset of detonation when the resonant coupling between the transverse waves and the chemical energy release is established.

This study also provided a basis for the future development of a quantitative criterion for successful DDT that should involve the tube dimension in relation to the chemical length scale (e.g., $\pi D \approx \lambda$) to describe the resonant coupling between the chemical energy release and the transverse pressure fluctuations.

References

[1] Arienti, M. & Shepherd, J. E. (2005) The role of diffusion at shear layers in irregular detonations. *4th Meeting of the US Sections of the Combustion Institute*, Philadelphia, PA, March 20-23

[2] Atkinson, R., Bull, D. C. & Shuff, P. J. (1980) Initiation of Spherical detonation in hydrogen/air. *Combust. Flame* **39**, 287-300

[3] Bakken, J., Slungaard, T., Engebretsen, T. & Christensen, S. O. (2003) Attenuation of Shock Waves by Granular Filters. *Shock Waves* **3**, 33-40

[4] Bartenev, A. M. & Gelfand, B. E. (2000) Spontaneous initiation of detonations. *Prog. Energy Combust. Science* **26**, 29-55

[5] Berger, M. J. & Oliger, J. (1984) Adaptive mesh refinement for hyperbolic partial differential equations *J. Comput. Phys.* **53**, 484-512

[6] Berthelot, M. & Vieille, P. (1882) Sur la vitesse de propagation des phénomènes explosifs dans les gaz. *C. R. Acad. Sci. Paris* **94**, 101-108

[7] Chao, J. & Lee, J. H. S. (2003) The propagation mechanism of high speed turbulent deflagrations. *Shock Waves* **12**, 277-289

[8] Chapman, W. R. & Wheeler, R. V. (1926) The propagation of flame in mixtures of methane and air. Part IV. The effect of restrictions in the path of the flame. *J. Chem. Soc.* **37**, 2138-2147

[9] Carnasciali, F., Lee, J. H. S. & Knystautas, R. (1991) Turbulent jet initiation of detonation. *Combust. Flame* **84**, 170-180

[10] Choi, Y. S. & Majda, A. (1989) Amplification of small-amplitude high-frequency waves in a reactive mixture. *SIAM Review* **31**, 401-427

[11] Chue, R. S., Clarke, J. F. & Lee, J. H. S. (1993) Chapman-Jouguet deflagrations. *Proc. R. Soc. Lond. A* **441**, 607-623

[12] Clarke, J. F. (1977) Chemical amplification at the wave head of a finite amplitude gasdynamic disturbance. *J. Fluid Mech.* **81**, 257-264

[13] Courant, R. & Friedrichs, K. O. (1948) Supersonic Flow and Shock Waves. Wiley-Interscience, New York

[14] Crank, J. (1975) *The Mathematics of Diffusion.* Oxford Press, U.K.

[15] Dharmavaram, S., Hanna, S. R. & Hansen, O. R. (2005) Consequence analysis–using a CFD model for industrial sites. *Process Safety Prog.* **24**, 316-327

[16] Desbordes, D., Manson, N. & Brossard, J. (1983) Influence of walls on pressure behind self-sustained expanding cylindrical and plane detonations in gases. *Prog. Astro. Aero.* **87**, 302-317

[17] Dorofeev, S. B., Bezmelnitsin, A. V., Sidorov, V. P., Yankin, J. G. & Matsukov, I. D. (1996) Turbulent jet initiation of detonation in hydrogen-air mixtures. *Shock Waves* **6**, 73-78

[18] Dorofeev S. B. (2002) Flame acceleration and DDT in gas explosions. *J. Phys. IV France* **12**, 3-10

[19] Dosanjh, D. S. (1955) Some Comments on "A theoretical and experimental study of shock tube flows. *J. Aero. Sci.*, 797-799

[20] Dupré, G., Peraldi, O., Lee, J. H. & Knystautas, R. (1988) Propagation of detonation waves in an acoustic absorbing walled tube. *Prog. Astro. Aeronaut.* **114**, 248-263

[21] Eder, A. & Brehm, N. (2001) Analytical and experimental insights into fast deflagrations, detonations, and the deflagration-to-detonation transition process. *Heat and Mass Transfer* **37**, 543-548

[22] Edwards D. H., Jones, T. G. & Price, B. (1963) Observations on oblique shock waves in gaseous detonations. *J. Fluid Mech.* **17**, 21-32

[23] Edwards, D. H., Jones, A. T. & Phillips, D. E. (1976) The location of the Chapman-Jouguet surface in a multiheaded detonation waves. *J. Physics D* **9**, 1331-1342

[24] Edwards, D. H. & Morgan, J. M. (1977) Instabilities in detonation waves near the limits of propagation. *J. Physics D* **10**, 2377-2387

[25] Ergun, S. (1952) Fluid flow through packed columns. *Chem. Eng. Prog.* **48**, 89-94

[26] Fay, J. A. (1962) The structure of detonation waves. *Proc. Combust. Inst.* **8**, 30-40

[27] Frank, W. J. (1957) Interaction of a shock wave with a wire screen. *Univ. Toronto Inst. Aerophysics UTIA Technical Notes* **13**

[28] Inada, M., Lee, J. H. & Knystautas, R. (1992) Photographic study of the direct initiation of detonation by a turbulent jet. *Prog. Astro. Aero.* **153**, 253-269

[29] Khokhlov, A. M. & Oran, E. S. (1999) Numerical simulation of detonation initiation in a flame brush: the role of hot spots. *Combust. Flame* **119**, 400-416

[30] Knikker, R., Dauptain, A., Cuenot, B. & Poinsot, T. (2003) Comparison of computational methodologies for ignition of diffusion layers. *Combust. Sci. Technol.* **175**, 1783-1806

[31] Knystautas, R., Lee, J. H., Moen, I. & Wagner, H. Gg. (1979) Direct initiation of spherical detonation by a hot turbulent gas jet. *Proc. Combust. Inst.* **17**, 1235-1245

[32] Knystautas, R., Lee, J. H. S., Peraldi, O. & Chan, C. K. (1986) Transmission of a flame from a rough to a smooth-walled tube. *Prog. Asto. Aero.* **106**, 37-52

[33] Kogarko, S. M. & Zeldovich, Ya. B. (1948) On detonation of gas mixtures. *Doklady Akademii Nauk SSSR* **63**, 553-556

[34] Laffitte, P. (1923) Sur la formation de l'onde explosive. *Acadimie des Sciences* **176**, 1392-1395

[35] Lee, J. H., Soloukhin, R. I. & Oppenheim, A. K. (1969) Current views on gaseous detonation. *Astro. Acta* **14**, 565-584

[36] Lee, J. H., Knystautas, R. & Yoshikawa, N. (1978) Photochemical initiation of gaseous detonation. *Astro. Acta.* **5**, 971-982

[37] Lee, J. H. S. & Moen, I. O. (1980) The mechanism of transition from deflagration to detonation in vapour cloud explosions. *Prog. Energy Combust. Sci.* **6**, 359-389

[38] Lee, J. H. S. & Guirao, C. (1981) Gasdynamic effects of fast exothermic reactions. *Fast Reactions in Energetic Systems*, R. F. W. C. Capellos, D. Reidel Publishing Company, 245-313

[39] Lee, J. H., Knystautas, R. & Chan, C. K. (1984a) Turbulence flame propagation in obstacle-filled tubes. *Proc. Combust. Inst.* **20**, 1663-1672

[40] Lee, J. H. S., Knystautas, R. & Freiman, A. (1984b) High speed turbulent deflagrations and transition to detonation in H2-Air mixtures. *Combust. Flame* **56**, 227-239

[41] Lee, J. H. S. (1986) The propagation of turbulent flames and detonations in tubes. In *Advances in Chemical Reaction Dynamics*, Edited by Rentzepis, P. M. & Capellos, C., 346-378

[42] Lee, J. H. S. & Higgins, A. J. (1999) Comments on criteria for direct initiation of detonation. *Phil. Trans. R. Soc. Lond. A* **357**, 3503-3521

[43] Lee, J. J., Dupré, G., Knystautas, R. & Lee, J. H. S. (1995) Doppler interferometry study of unstable detonations. *Shock Waves* **5**, 175-181

[44] Libby, P. A. & William, F. A. (1994) *Turbulent Reactive Flows*, Academic Press, New York

[45] Macdonald, I. F., El-Sayed, M. S., Mow, K. & Dullien, F. A. L. (1979) Flow through porous media – the Ergun equation revisited. *Ind. Eng. Chem. Fundam.* **18**, 199-208

[46] Mallard, F. E. & Le Chatelier, H. (1883) Recherches experimentales et theoriques sur la combustion des mélanges gaseux explosifs. *Ann. Mines* **8**, 274-568

[47] Medvedev, S. P., Frolov, S. M. & Gelfand, B. E. (1990) Attenuation of shock waves by screens of granular material. *Inst. Chem. Phys.* **58**, 924-928

[48] Meyer, J. W., Urtiew, P. A. & Oppenheim, A. K. (1970) On the inadequacy of gasdynamic processes for triggering the transition to detonation. *Combust. Flame* **14**, 13-20

[49] Meyer, J. W. & Oppenheim, A. K. (1971a) Coherence theory of the strong ignition limit. *Combust. Flame* **17**, 65-68

[50] Meyer, J. W. & Oppenheim, A. K. (1971b) On the shock-induced ignition of explosive gases. *Proc. Combust. Inst.* **13**, 1153-1164

[51] Moen, I. O., Donato, M., Knystautas, R. & Lee, J. H. (1981) The influence of confinement on the propagation of detonations near the detonability limits. *Proc. Combust. Inst.* **18**, 1615-1622

[52] Nettleton, M. A. (2002) Recent work on gaseous detonations. *Shock Waves* **12**, 3-12

[53] Ng, H. D., Radulescu, M. I., Higgins, A. J., Nikiforakis, N. & Lee, J. H. S. (2005) Numerical Investigation of the instability for one-dimensional Chapman-Jouguet detonations with chain-branching kinetics. *Combust. Theory. Model.* **9**, 385-401

[54] Oppenheim, A. K. (1985) Dynamic features of combustion. *Phil. Trans R. Soc. A* **315,** 471-508

[55] Oran, E. (1984) Chemical kinetic-fluid dynamic interactions in detonations. *Chemistry of Combustion Processes* 151-173

[56] Peraldi, O., Knystautas, R. & Lee, J. H. S. (1986) Criteria for transition to detonation in tubes. *Proc. Combust. Inst.* **21**, 1629-1637

[57] Popat, N. R., Caitlin, C. A., Arntzen, B. J., Lindstedt, R. P., Hjertager, B. H., Solberg, T., Saeter, O. & Van den Berg, A. C. (1996) Investigations to improve and assess the accuracy of computational fluid dynamic based explosion models. *J. Hazardous Materials* **45**, 1-25

[58] Radulescu, M. I. & Lee, J. H. S. (2002) The failure mechanism of gaseous detonations - Experiments in porous wall tubes. *Combust. Flame* **131**, 29-46

[59] Radulescu, M. I., Ng, H. D., Lee, J. H. S. & Varatharajan, B. (2002) The effect of argon dilution on the stability of acetylene-oxygen detonations. *Proc. Combust. Inst.* **29**, 2825-2831

[60] Reichenbach H. (1963) Messungen des druckverlaufs nach hindernissen in gängen. Ernst Mach Insitut. Freiburg, Germany

[61] Saint-Cloud, J. P., Guerraud, C., Brochet, C. & Manson, N. (1972) Some properties of very unstable detonations in gaseous mixtures. *Astro. Acta* **17** 487-498

[62] Settles, G. S. (2001) Schlieren and Shadowgraph Techniques. Springer-Verlag, Berlin and New York

[63] Shchelkin, K. I. (1940) Effect of roughness of the surface in a tube on origination and propagation of detonation in gases. *J. Exp. Theor. Physics* **10**, 823-827

[64] Shepherd, J. E. & Lee, J. H. S. (1992) On the transition from deflagration to detonation. in *Major Research Topics in Combustion*, ICASE/NASA LaRC Series, Edited by Hussaini, M. Y., Kumar, A. & Voigt, R. G., 439-487, Springer-Verlag, New York

[65] Shepherd, J. E., Teodorczyk, A., Knystautas, R. & Lee, J. H. S. (1991) Shock waves produced by reflected detonations. *Prog. Astro. Aero.* **134**, 244-264

[66] Skews, B. W. (2005) Shock wave interaction with porous plates. *Experiments in Fluids* **39**, 875-884

[67] Solouhkin, R. I. (1974) Ignition and detonation processes in the interaction of shock waves with perforated plates. *Acta Astro.* **1**, 249-258

[68] Summerfield, M., Reiter, S. H., Kebely, V. & Mascolo, R. W. (1955) The structure and propagation mechanism of turbulent flames in high speed flow. *Jet Propulsion* **25**, 377-384

[69] Taylor, G. I. & Tankin, R. S. (1958) Gas dynamical aspects of detonation. in *Gasdynamics of Combustion and Detonation*, Edited by Emmons, H.W., 622-686, Princeton University PRess, Princeton

[70] Teodorczyk, A., Lee, J. H. S. & Knystautas, R. (1988) Propagation mechanism of quasi-detonations. *Proc. Combust. Inst.* **22**, 1723-1731

[71] Teodorczyk, A., Lee, J. H. S. & Knystautas, R. (1990) The structure of fast turbulent flames in very rough, obstacle-filled channels. *Proc. Combust. Inst.* **23**, 735-741

[72] Teodorczyk, A. & Lee, J. H. S. (1995) Detonation attenuation by foams and wire meshes lining the walls. *Shock Waves* 4, 225-236

[73] Toong, T. Y. (1972) Chemical effects on sound propagation. *Combust. Flame* **18**, 207-216

[74] Toro, E. F. (1999) *Riemann Solvers and Numerical Methods for Fluid Dynamics*, Springer-Verlag, Berlin

[75] Ünglüt, A. & Shuff, P. J. (1989). Deflagration to detonation transition from a venting pipe. textitCombust. Sci. Technol. **63**, 75-87

[76] Urtiew, P. A. & Oppenheim, A. K. (1965) Onset of detonation. *Combust. Flame* **9**, 405-407

[77] Urtiew, P. A. & Oppenheim, A. K. (1966) Experimental observations of the transition to detonation in an explosive gas. *Proc. R. Soc. Lond. A* **295**, 13-28

[78] Vasil'ev A. A. (2006) Estimation of critical conditions for the detonation-to-deflagration transition. *Combust. Expl. and Shock Waves* **42**, 205-209

[79] Westbrook, C. K. & Urtiew, P. A. (1982) Chemical kinetic prediction of critical conditions in gaseous detonations. *Proc. Combust. Inst.* **19**, 615-623

[80] Zel'dovich, Ya. B., Librovich, V. B., Makhviladze, G. M. & Sivashinsky, G. I. (1970). On the development of detonation in a non-uniformly preheated gas. *Astro. Acta* **15**, 313-321

[81] Zel'dovich, Ya. B. (1980) Regime classification of an exothermic reaction with nonuniform initial conditions. *Combust. Flame* **39**, 211-214

[82] Zel'dovich, Ya. B., Borisov, A. A., Gelfand, B. E., Frolov, S. M. & Mailkov, A. E. (1988) Nonideal detonation waves in rough tubes. *Prog. Astro. Aero.* **144**, 211-231

[83] Zloch, N. (1976) Shock attenuation in beds of granular solids. *Arch. of Mech.* **28**, 817-825